INTRACELLULAR DELIVERY USING FLUOROPHORE-CPP CONJUGATES AND LIGHT: MECHANISMS AND IMPLICATIONS

A Dissertation

by

NANDHINI MUTHUKRISHNAN

Submitted to the Office of Graduate and Professional Studies of
Texas A&M University
in partial fulfillment of the requirement for the degree of

DOCTOR OF PHILOSOPHY

Chair of Committee,	Jean-Philippe Pellois
Committee Members,	Gregory Reinhart
	Ryland Young
	Siegfried Musser
Head of Department,	Gregory Reinhart

May 2014

Major Subject: Biochemistry

ABSTRACT

Cell-penetrating peptides (CPPs) can induce translocation of conjugated macromolecules across the plasma membrane of live cells. The major route of uptake of these CPPs by cells is through endocytosis. However, intracellular cytosolic delivery efficiency of these reagents is inefficient because CPP-cargo conjugates typically remain trapped inside endosomes. As a result, macromolecules are unable to reach their cytosolic targets and exert biological function. The fluorophore-CPP conjugate (Fl-CPPs) where the prototypical CPP TAT is conjugated to the fluorophore TMR gets entrapped inside endosomes of live cells upon incubation. Interestingly, irradiation of the endosomally contained TMR-TAT with moderate doses of light induces release of Fl-CPPs into the cytosol. However, the mechanism of this phenomenon is not clear. Also, the endosomal release of TMR-TAT is accompanied by loss of plasma membrane integrity, membrane blebbing, and cell-death. I investigated the molecular basis of the photo-induced endosomolytic activity of Fl-CPPs and the mechanisms behind Fl-CPP mediated cell death.

I reported that Fl-CPPs act as photosensitizer molecules that can destroy membranes such as endosomal membranes, membranes of simpler model systems RBCs and liposomes. I showed that the CPP moiety of Fl-CPPs binds to negatively charged phospholipids of target membranes and brings the attached fluorophore into close proximity of the membrane. Upon irradiation of Fl-CPPs, reactive oxygen species (ROS) such as singlet oxygen and superoxide are produced that cause oxidation of membrane lipids. In addition, CPPs have a latent ability to cause damage of photo-oxidized lipid membranes. Thus, CPPs and singlet oxygen generators act in synergy to cause photolysis of membranes. I further establish structure activity relationship of Fl-CPPs to understand how structure of Fl-CPPs impact synergistic activity on membranes. These factors should therefore be considered for the development of effective delivery agents.

I also explored mechanisms behind cell death that accompanied TMR-TAT mediated PCI. I showed that the lysis of endocytic organelles by TMR-TAT caused a rapid increase in the concentration of calcium in the cytosol followed by accumulation of calcium in the mitochondria. Ruthenium red and cyclosporin A, inhibitors of calcium import in mitochondria and of the mitochondria permeability transition pore were able to inhibit cell death.

DEDICATION

I would like to dedicate this work to my parents for their immense support during the course of my Ph.D. study.

ACKNOWLEDGEMENTS

I would like to express my sincere gratitude to Dr. Jean-Philippe Pellois, my advisor, for his guidance and support throughout my Ph.D. His constant motivation has made it possible for me achieve this goal. I would like to sincerely acknowledge my committee members Dr. Gregory Reinhart, Dr. Ryland Young and Dr. Siegfried Musser for their contributions and helpful comments to my study. I extend my gratitude and appreciation to all the former and current members of the Pellois laboratory for their support and encouragement.

I am truly grateful to my parents and sister for their advice and support without which this work would not have been possible.

NOMENCLATURE

ATCC	American Type Culture Collection
CPP	Cell-Penetrating peptide
DMEM	Dulbecco's Modified Eagle Media
DMSO	Dimethyl sulfoxide
EGTA	Ethylene glycol tetraacetic acid
Fl-CPP	Fluorophore-cell-penetrating peptide
FITC	Fluorescein isothiocyanate
GSH	Glutathione
HIV	Human immunodeficiency virus
HP	Hematoporphyrin
HPD	Hematoporphyrin derivative
HPLC	High performance liquid chromatography
L-15	Leibovitz's 15
NBT	Nitro blue tetrazolium
ND	Neutral density
PBS	Phosphate buffered saline
PCI	Photochemical internalization
PDT	Photodynamic therapy
PM	Plasma membrane
PTD	Protein transduction domain
RB	Rose Bengal
RBC	Red blood cell
RNO	p-dimethylnitrosoaniline
ROS	Reactive oxygen species
sh-RNA	short hairpin RNA
SPPS	Solid phase peptide synthesis

TAT	Trans activator of transcription
TMPD	N,N,N',N'-tetramethyl-p-phenylenediamine
TMR	5(6)-carboxytetramethylrhodamine
TPC	5-[4-Carboxyphenyl]-10,15,20- triphenyl-2,3-dihydroxychlorin

TABLE OF CONTENTS

LIST OF FIGURES

Page

Page

1. INTRODUCTION AND LITERATURE REVIEW

1.1 Intracellular delivery of macromolecules: Significance

Delivery of therapeutic macromolecules such as proteins, nucleic acids and small molecules inside the cell cytosol is highly significant for applications in medicine as well as biochemical research. The rationale behind aiming for cytosolic delivery is that the therapeutic targets of these macromolecules are located mainly in the cytosolic space of a cell. Transport of macromolecules inside cells however, is hindered by a highly selective plasma membrane. The plasma membrane (PM) is hydrophobic in nature and hence acts as a barrier to all extracellular molecules except for hydrophobic moieties and small hydrophilic molecules. This PM barrier has to be overcome in order to achieve successful translocation of macromolecules from the extracellular region to intracellular space. Methods such as electroporation and microinjection have been applied to introduce molecules inside cells for decades. Their usage however is limited due to their low efficiency and associated cytotoxicity issues. Recent approaches for intracellular delivery extensively use cell-penetrating peptides (CPPs) that have the ability to non-invasively translocate across the plasma membrane.

1.2 Cell-penetrating peptides: Intracellular delivery tools

Cell-penetrating peptides (CPPs) possess the ability to carry cell-impermeable molecules inside live cells(1-3). One of the first CPPs that were reported to display cellular transduction activity was TAT, a peptide derived from the HIV-1 TAT protein(4). A protein called Tat (Trans activator of transcription) was derived from HIV(4, 5) and was shown to translocate across cell membranes into non-infected cells and induce transcription of viral genes resulting in rapid propagation of HIV infection. A short stretch of amino acids within the protein sequence (later named as the TAT peptide) was found to be sufficient for promoting translocation of the biologically functional TAT protein across membranes(6). Translocation by the TAT peptide was

independent of presence of receptor molecules(7) and was induced by simple incubation with cells(8).

Typically, cell penetrating peptides (CPPs) are short peptide sequences usually containing around 10-30 amino acids. CPPs can be either cationic or amphipathic molecules. The TAT peptide is a typical example of a cationic CPP(1). It consists of 6 arginines and 2 lysine residues, making it highly positively charged, and hence capable of interacting with a negatively charged plasma membrane. CPPs such Penetratin, and VP22 also come under this category(9, 10). Synthetic CPPs such as polyarginines were designed based on characteristics observed with the TAT peptide(11, 12). CPPs such as MPG, MPG, Pep-1, MAP, and PPTG1(13-15) and transportan are examples of amphipathic CPPs(16).

CPPs have been shown to successfully cause cellular uptake of cargos such as DNA, siRNA, proteins (upto 120 kDa), fluorophores, liposomes, nanoparticles both *in vivo* and *in vitro*(17, 18, 8, 19-22). For instance, the amphipathic fusion peptide of HA2 subunit of influenza hemaglutinin, GALA peptide analogs and histidine-rich CPPs have been used to deliver poly-L-lysine/DNA conjugates, cationic lipids and polymers due to their endosomolytic ability(23). CPPs have also been known cause delivery of siRNAs into cells(22, 24, 25). Usually, siRNAs are covalently linked to CPPs in a manner that the complex formed has a net positive charge in order to mask the negative charge of the nucleic acid and facilitate uptake(26). Non-covalent strategies however, seem to induce more efficient delivery of siRNA in a variety of cell lines(27, 28). siRNA delivery using CPPs have been shown to efficiently target cell-cycle protein, cyclin B and as a result block tumor growth(29). Upon association of TAT peptide with an RNA-binding motif, in vivo blocking of the epidermal growth factor (EGF) factor has been shown(30). Intracellular delivery of proteins has also been achieved although with limitations of size and biochemical properties. For instance, delivery of biologically active β- galactosidase protein (120 kDa) across the blood brain barrier was achieved by fusing the enzyme with the TAT peptide(18). Thus, efficient delivery of macromolecules could be achieved

upon association of the macromolecules to protein transduction domain or cell-penetrating peptides.

1.3 Mechanisms of CPP uptake

Although CPPs are a highly successful and extensively applied class of intracellular delivery tools, on a molecular level, the exact mechanism(s) by which CPPs and CPP-cargo conjugates are internalized by cells is unknown. The mechanistic details remain poorly understood and are till date, highly debatable(31). It is however known that naturally derived peptides such as TAT or Antennapedia internalize into cells efficiently, without inducing membrane destabilization effects or cytotoxicity. Lack of mechanistic understanding of CPP uptake could be attributed to limitations of biochemical assays mainly cell-fixation during experimentation that gives rise to artifacts(32-34).

Early studies reported that CPP internalization used an energy-independent direct membrane translocation mechanism as Antennapedia entered cells at lower temperatures(35). Later studies using inhibitors however suggested that an endocytic mechanism might also be involved in the uptake of CPPs(36, 37). Another study showed that the translocation efficiency of CPPs synthesized from D- amino acids and containing reverted sequences was similar or more when compared to corresponding CPPs prepared from L-amino acids and without sequence reversal(38, 11). This suggested that cellular internalization of CPPs did not require or involve membrane surface receptors. Due to the limitation of cell-fixation protocols, a complete re-evaluation of membrane translocation mechanisms was done using live-cell experiments(34). Results from live-cell experiments showed that in addition to direct translocation of CPPs across plasma membranes, additional endocytic mechanisms such as caveolae-mediated endocytosis(39, 40), clathrin-mediated endocytosis(41) and macropinocytosis(42, 43) were involved in CPP internalization into cells. An important role of heparan sulfate proteoglycans (HSPGs) present on the cell surface has also been suggested for CPP uptake(44) as binding of CPPs to HSPGs could promote CPP

interaction with the plasma membrane of cells in turn inducing translocation. Mechanisms involving translocation of CPPs due to direct interaction with membrane phospholipid moieties have also been suggested(31). CPPs have also been shown to destabilize the plasma membrane and lead to the influx of molecules such as Ca2+ inside cells(15). Interestingly, Ca^{2+} can trigger the plasma membrane repair response(45). It has therefore been suggested that the plasma membrane translocation of CPPs might be masked by this membrane repair response(45). The mode of uptake however is suggested to depend on various factors including nature of cargo attached, type of cell line, CPP concentration and times of incubation with cells(36, 46).

1.3.1 Direct translocation of CPPs across plasma membrane

Four different models were proposed to explain uptake of CPPs into cells by direct plasma membrane translocation (Fig. 1-1). These include the Inverted micelle model, Carpet model, Barrel-stave model and a Toroidal pore model.

Inverted Micelle model

The inverted micelle model was proposed considering results from uptake of Antp peptide by cells(35). As per this model, it was suggested that the interaction of CPPs with cellular membranes induces disturbance of lipid bilayers in turn forming inverted hexagonal structures. The interior hydrophilic chamber of these structures entrap the CPPs until an inverse process causes destabilization of the hexagonal structure and release of entrapped CPPs into the cells interior(35). Additional data from NMR studies support the formation of inverted structures(47). Even though the inverted micelle model might explain the translocation of small hydrophilic CPPs, it is, however, not compatible with translocation of CPP-cargo conjugates of high molecular weight (energy barrier presented by hydrophobic lipid bilayers)(31).

Barrel-stave and Toroidal Pore model

In both the barrel-stave and the toroidal pore models, the CPP is suggested to insert into the plasma membrane and further oligomerization of the inserted CPPs would result in the formation of ring shaped structure that act as transient pores(31). In the barrel stave model, it is proposed that CPPs form amphipathic α-helical structures upon

insertion into membranes. The hydrophobic face of helix will then interact with the aliphatic chains of membrane phospholipids while the interior of the pore is hydrophilic(48-51). The toroidal pore alternatively involves interaction of the CPPs with the polar head groups of membrane phospholipids resulting in major rearrangement of the lipid bilayer(51, 52).

Carpet Model

In this model, translocation of CPPs occurs as a result of destabilization of the plasma membrane due to reorganization of the membrane phospholipids when CPP associates to the membrane. The destabilization is transient(48, 49, 52, 51).

The models for direct translocation of CPPs across the plasma membrane barrier are significantly different even though they share many common features. For instance, according to the inverted micelle model, CPPs do not come in contact with the hydrophobic lipid bilayers(35) and always remain bound to the plasma membrane unlike the barrel stave or the toroidal pore models. Also, significant reorganization of membrane phospholipids occurs in the toroidal pore and the carpet model but not for the barrel stave model(52). CPP interactions with membranes form concave surfaces in the inverted micelle model and convex surfaces in the toroidal pore model. Finally, while the pore models suggest formation of well-defined structure, the carpet model suggests a highly disorganized structure formation(51). None of the direct translocation models are however compatible with translocation of high molecular weight cargo since no cytotoxicity is observed in case of internalization of CPP-cargo conjugates.

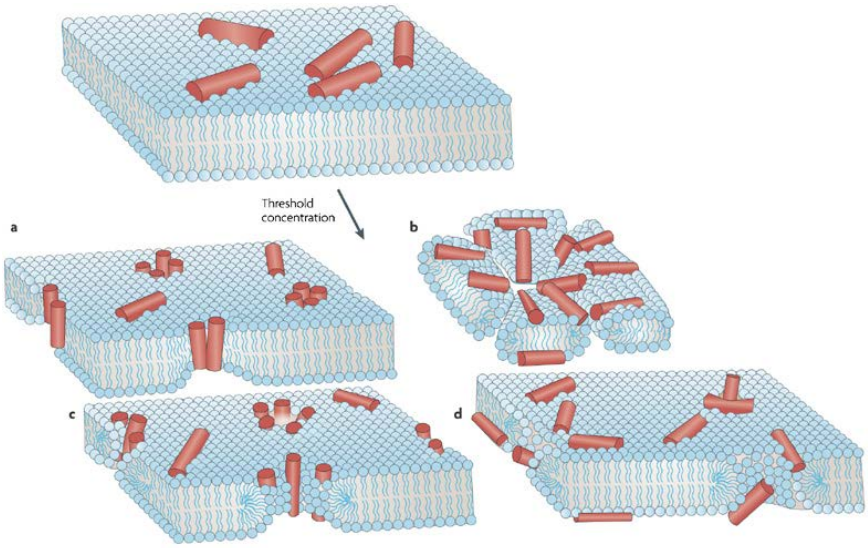

Figure 1-1. Different models proposed for direct penetration of CPPs. Reprinted with permission from (53), "Antimicrobial peptides: linking partition, activity and high membrane-bound concentrations" by Melo, M. N., Ferre, R. and Castanho, M. A., 2009. *Nat Rev Microbiol* **7**, 245-50, Copyright 2009 by Nature Publishing Group

CPPs are proposed to enter cells through a direct membrane translocation mechanism. Different proposed models are (a) Barrel-stave model; CPPs insert into lipid bilayer perpendicularly (b) Carpet model; CPPs are adsorbed on the membrane parallel to the lipid bilayer and above a threshold concentration disrupt the membrane (c) Toroidal pore model; CPPs insert into the membrane perpendicularly and induce a membrane curvature (d) Disordered toroidal pore; this model involves formation of less-rigid peptide conformations and orientations.

1.3.2 Endocytic mechanisms of CPP internalization

Endocytosis of cargo molecules can be mainly divided into (i) phagocytosis, which occurs only in macrophages and (ii) pinocytosis, which includes macropinocytosis, clathrin-mediated endocytosis, and caveolae-mediated endocytosis(54-56).

Multiple approaches have been used to test the involvement of the various endocytic pathways in CPP uptake some of which are; (i) CPP uptake at 4ºC, (ii) CPP uptake in the presence of selective endocytosis pathway inhibitors, (iii) testing co-localization of CPPs with molecules known to internalize by specific pathways (transferrin) or with molecular markers of endocytic pathways (EEA1, Caveolin-1), (iv) overexpression of dominant negative mutants of specialized pathways proteins (dynamin). Studies suggested that unconjugated TAT peptide entered cells using clathrin-mediated endocytosis(41). GST-TAT-GFP fusion protein used caveolae mediated endocytosis(40) while TAT-HA2 fusion protein was internalized mainly by macropinocytosis(43, 42, 57, 58).

In a study comparing cellular uptake of Antp, TAT and nona-arginine R9 peptides, it was shown that multiple endocytic pathways were involved for each peptide(36). The magnitude of uptake by the different endocytic pathways however differed between peptides(36). This difference could be attributed to observed cytotoxicity effects(59), usage of different cell lines, peptides concentrations and incubation times. Cellular uptake studies of different CPPs conjugated to PNA molecules suggested that while cationic CPP conjugates preferably internalized by macropinocytosis, amphipathic CPP conjugates entered cells via clathrin-mediated endocytosis(60).

Although, CPP mediated endocytic uptake is typically efficient, it appears that the endosomolytic activity of CPPs is, in contrast, very poor. For instance, CPPs conjugated to small organic fluorophores or fluorescent proteins display a punctate distribution inside cells consistent with endosomal entrapment when observed by fluorescence microscopy(61-63). Often, no cytosolic signal is observed, indicating that the CPP-cargo has not reached the cytosol(64). Consistent with this notion, CPPs conjugated to biologically active cargos often fail to display significant cellular activities(65). (In contrast, reagents that disrupt endosomes have been shown to dramatically improve the cellular delivery and biological activity of CPP-cargos(66).) In

order to optimize delivery, a current challenge is therefore to increase the endosomolytic activity of CPPs.

1.4 Proposed mechanism of TAT mediated delivery

Today, the most accepted model for TAT uptake is macropinocytosis. This model involves 3 steps; a) Interaction of CPP with plasma membrane, b) entry of CPPs by endocytosis or micropinocytosis, c) endosomal escape of CPP into the cytosol.

1.4.1 Interaction with plasma membrane

CPPs are usually positively charged peptides containing basic residues such as arginines and lysines. TAT (GRKKRRQRRR), for instance, contains 6 arginines and 2 lysines. It has been shown that the positively charged residues of TAT are highly essential for its membrane transduction activity(12). The presence of positively charged residues can give rise to electrostatic interactions with negatively charged groups present on the plasma membrane. Bidentate hydrogen bonding can occur between the guanidinium groups of positively charged arginine residues on the CPP and the phosphate, sulfate and carboxylate anionic groups present on the plasma membrane(67, 11, 2). The ammonium cations on lysine residues of CPPs can also interact with plasma membrane anions by forming a hydrogen bond. Both guanidinium and ammonium groups have a single positive charge however, charge solely is not sufficient to determine strength of binding in case of CPPs(68). Under conditions of the assays, the degree of protonation is higher for the more basic guanidinium group of arginine residues(68). Also, arginine residues have a high affinity for the anionic heparan sulfate proteoglycans present on the outer leaflet of plasma membrane.

1.4.2 Entry of CPPs by endocytosis

CPPs can be internalized by passive fluid-phase endocytosis or by binding to cell-surface components that are being internalized in a piggyback manner(56). Heparan sulfate proteoglycans (HSPGs) have been implicated in this activity(69, 70). While positively charged CPPs undeniably interact with the negatively charged heparan sulfate (HS), the question of whether this interaction directly triggers macropinocytosis remains

unanswered. A model has been proposed where the CPP reaches the inner leaflet of the plasma membrane while the attached cargo remains trapped on the external side of the membrane. Under such circumstances, TAT has been shown to induce actin rearrangement in model systems, indicating a possible mechanism of macropinocytosis induction(71). The most direct evidence for the importance of endocytosis comes from experiments involving the delivery of biologically active cargos. For example, TAT-Cre conjugate is able to penetrate cells and activate expression of a luciferase or GFP reporter upon recombination of a plasmid containing the loxP sequence(71, 58). In the presence of amiloride and cytochalasin-D, inhibitors of macropinocytosis, activation of the reporter by TAT-Cre is greatly reduced(71). Other examples include CPP-mediated delivery of a peptide nucleic acid (PNA) complex, which is able to induce splice correction of an aberrant splice site in a luciferase reporter gene(72). Here again, the CPPs TAT, penetratin, and transportan appear to require endocytosis to allow delivery of the PNA. In the presence of chloroquine, a lysosomotropic agent, the splice correction efficacy increased 4-fold. On the contrary, inhibition of endocytosis by lowering the temperature to 4ºC decreased the splice correction efficacy significantly(72). These experiments reveal that direct plasma membrane translocation does not contribute significantly to delivery and that endocytosis is a required step. They also suggest that endosomal escape must take place. How and to what extent CPPs can mediate endosomal escape remains, however, unclear.

Upon endocytosis, TAT peptide along with the attached or co-incubated cargo is internalized into intracellular compartments called endocytic vesicles. The endocytic vesicles undergo multiple stages of maturation converting from early endosomes to multi-vesicular bodies to late endosomes. Finally, the late endosomes fuses with organelles called lysosomes that contain enzymes which will degrade the internalized TAT or TAT-cargo complex. For successful delivery, cargo needs to be released from endocytic vesicles before being subjected to degradation in lysosomes. Along the endocytic pathway, there is a gradual drop in the intraluminal pH (Fig. 1-2) of the endocytic vesicles from 6-6.5 in the early endosomes to 4.5 in the lysosomal

compartments(73). The vacuolar H^+ ATPase proton pump is widely accepted to be responsible for acidification of endocytic vesicles by pumping protons into their lumen(74). Other proton translocation mechanisms such as ion transporters and channel on the endosomes might also be involved in establishing and maintaining the pH of endocytic vesicles(75, 76). Perturbation of the endosomal acidification process with chemicals such as chloroquine (membrane-permeable weak base) or bafilomycin (inhibitor of the endosomal H^+ pump) can inhibit the transport of cargo through the endocytic pathway(73).

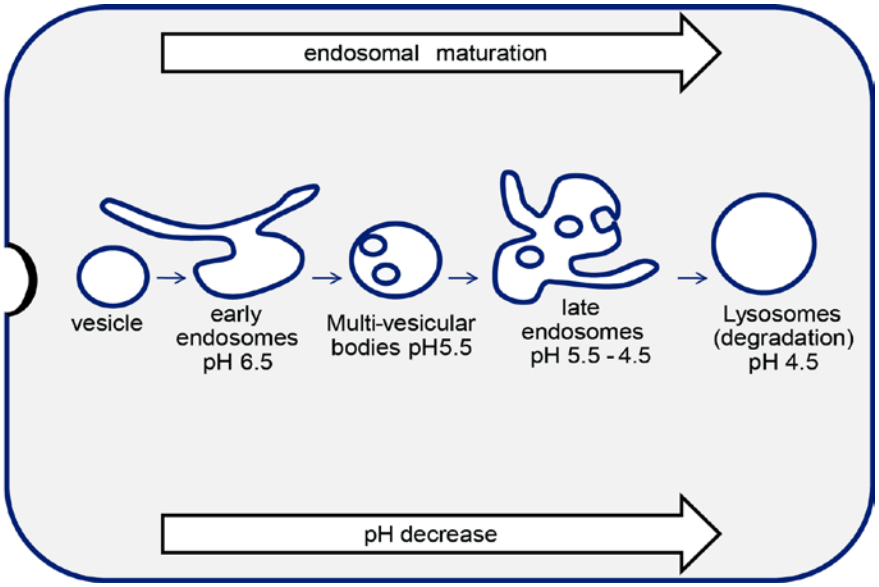

Figure 1-2. pH gradient in the endosomal pathway

1.4.3 Endosomal escape of CPPs into cell cytosol

The endosomal escape of entrapped macromolecules from inside endocytic vesicles into the cytosol is crucial for macromolecules to reach their cytosolic targets and function biologically. To date, these mechanisms remain poorly defined. Part of the challenge associated with understanding how CPP-cargos escape from the endocytic pathway is that efficiency of endosomal escape is often poor. Cargos that typically require fewer copies to elicit a biological response certainly demonstrate that endosomal escape takes place (as is the case for TAT-Cre). However, cargos that require more copies inside cells for activity often fail to show significant biological effects. Several assays have been developed to assess the endosomal escape efficiency of CPPs. Fluorescence-based methods have revealed that CPPs conjugated to fluorescent cargos typically remain localized within the endocytic pathway(77). Mass spectrometry approaches have also confirmed these results, though estimates vary widely depending on the conditions used(78-82). Maybe the most telling examples are not those in which delivery worked, but the applications where no cytosolic delivery is detected(83-86). For instance, TAT has been conjugated to a ubiquitin cargo designed to be cleaved by cytosolic de-ubiquitinating enzymes upon escape from endosomes. However, upon incubation with cells, endocytosis was detected but cleavage of ubiquitin was not(86). It was therefore concluded that the protein did not access the cytosol to any detectable extent.

While many mechanisms have been proposed to explain plasma membrane translocation(87), fewer have been offered to explain endosomal escape. First, it should be noted that mechanisms that imply the disruption of lipid bilayers are not only applicable to plasma membrane translocation but also to endosomal escape. A mechanism that has been proposed to explain how CPPs could translocate across the plasma membrane of cells involves the negatively charged phospholipid phosphatidylserine. Positively charged CPPs are known to bind negatively charged phospholipids such as phosphatidylserine(88, 89). This phospholipid is, however, found mainly in the inner leaflet of the plasma membrane of mammalian cells(90, 91). The

outer leaflet of the plasma membrane bilayer is, in contrast, composed of zwitterionic phospholipids for which CPPs have little affinity(92, 93). Nevertheless, it was proposed that CPPs and phosphatidylserine, positioned on either side of the lipid bilayer, might together form the equivalent of a membrane capacitor. This capacitor theoretically generates a membrane potential high enough to create a reversible electropore on a membrane(94). This model also agrees with experimental data that has found a relatively enhanced ability of oligoarginine peptides to deliver cargo molecules across membranes when compared to oligolysine peptides(95). The membrane capacitor model suggests that oligoarginines could bind the negatively charged phosphate groups in phospholipids better than oligolysines and forms a more stable CPP-phosphatidylserine capacitor. Because the phosphatidylserine lipid asymmetry is presumably maintained within the endocytic pathway, such mechanisms could take place inside endosomes(90). If this is true, a key question lies in determining how a CPP might permeabilize an endosome without acting first on the plasma membrane. A possible answer to this question could involve the difference in how CPPs access these different bilayers. As previously stated, positively charged CPPs interact with HSPGs present on the cell surface(96). The abundance of HS at the plasma membrane might therefore contribute to reducing the concentration of CPP directly in contact with lipids. During endocytosis, HSPGs are presumably internalized with CPPs(41, 97, 98). HSPGs therefore continue to have an inhibitory effect on the membrane disruption activity of CPPs(99). However, HSPGs are gradually hydrolyzed during maturation within the endocytic pathway(44). HS hydrolysis and release from the membrane of endosomes could in turn favor the interaction between CPPs and endosomal lipid bilayer(98).

Several lines of evidence suggest that CPPs could disrupt the lipid bilayer of endocytic organelles more readily than that of the plasma membrane. For instance, positively charged CPPs preferentially bind negatively charged phospholipids over neutral ones(100, 101) [36, 80]. Interestingly, the intraluminal lipid bilayers of late endosomes appear to be uniquely enriched in the negatively charged phospholipid bis(monoacylglycero)phosphate (BMP), also known as lysobisphosphatidic acid

(LBPA)(102, 103). Recently, TAT was shown to induce the leaky fusion of liposomes containing BMP(104). TAT induces lipid mixing and membrane leakage in a BMP concentration-dependent manner and these activities were also greater at pH 5.5 than at physiological pH. This is important because pH 5.5 is characteristic of the acidic pH found in the lumen of late endosomes. The involvement of BMP in CPP-mediated delivery has not been demonstrated yet. However, cellular assays in which progression through the endocytic pathway is blocked with dominant negative Rab proteins have also suggested that TAT and polyarginine peptides only escape from the endocytic pathway upon reaching late endosomes(78). Together, these results strongly suggest that BMP is a target for CPPs and that fusion between the limiting membrane of late endosomes and that of intraluminal vesicles is involved in the escape of CPP-cargo to the cytosolic space of cells.

1.5 Limitations of CPP-mediated delivery

Cell-penetrating peptides are novel and attractive intracellular tools, however, there are limitations. Primarily, endosomal release of entrapped CPP or CPP-cargo conjugates is highly inefficient. Better strategies are required to facilitate cytosolic release of entrapped cargo from endosomes. Also, endosomal vesicles and lysosomes contain degradative enzymes such as proteases that might breakdown the CPP and as a result inhibit further cytosolic delivery. This limitation could be overcome by using D-amino acids for synthesizing peptides since D-CPPs are resistant to proteolytic degradation. In addition to the above a number of other factors limit the applicability of CPPs.

Studies were performed investigating the translocation of TAT and penetratin in different cell lines, SK-BR-3 (breast carcinoma), IMR-90 (fetal lung fibroblast), H9 (lymphoid) and U937 (monocytic) cells(105). TAT and penetratin showed poor uptake in these cell lines suggesting that CPP uptake might be different in different cell types and might also depend on cell-specific membrane components or composition of phospholipids on the lipid bilayer(105). Similarly, Confocal laser scanning microscopy showed that TAT-fluorescein conjugate failed to enter MDCK cells but accumulated at

the basal side(106). It has also been suggested that oral and dermal routes of delivery using CPPs might be inefficient due to low permeability reasons(107).

Several studies suggest that CPP delivery might be limiting in *in vivo* applications. For instance, TAT-EGFP fusion protein was unable to efficiently reach muscle cells upon injection using subcutaneous or intra-arterial injections(108). TAT-EGFP however showed binding to components of the extracellular matrix which might be hindering the transduction process. In a different study, the TAT peptide affected the intracellular delivery of a lysosomal enzyme β-glucuronase (expressed from viral vectors)(109). Intracellular delivery of liposomes using TAT and penetratin was reported to be proportional to the number of copies of CPPs attached to the liposomal surface, however the cytotoxicity was unaffected(110). Overall, these reports suggest that different experimental set ups including type of cell lines used, cellular differentiation states, enzymatic activity, metabolic activity and use of *in vivo* and *in vitro* experiments might affect the tranlocation ability and delivery efficiency of CPPs.

1.6 Photochemical internalization

Photochemical internalization (PCI) is another strategy that has been used to achieve intracellular delivery of macromolecules. PCI uses compounds called photosensitizers in combination with light to cause endosomal release. Photosensitizers are compounds that can produce reactive oxygen species (ROS) upon excitation with light. These photosensitizers are usually lipophilic and thus can associate with cellular membranes such as the endosomal membranes. ROS produced upon light irradiation can damage endosomal membranes by reacting with membrane components and result in membrane permeabilization. Light can therefore be used as a trigger to induce the lysis of endosomes when these organelles are loaded with photosensitizers (Fig. 1-3). This photo-induced delivery strategy was termed photochemical internalization (PCI) by Berg and co-workers, who introduced this concept in 1999(111). PCI has been successfully applied to the cytosolic delivery of immunotoxins, oligonucleotides and other therapeutic agents such as bleomycin and doxorubicin inside cells using PCI both *in vitro* and *in vivo*(112, 113). The photosensitizers that are commonly used are sulfonated

tetraphenylporphyrins (TPPS2a or TPPS4a), sulfonated aluminum phthalocynanines (AlPcS2a) and chlorins (TPCS2a)(114, 45, 111, 115, 116).

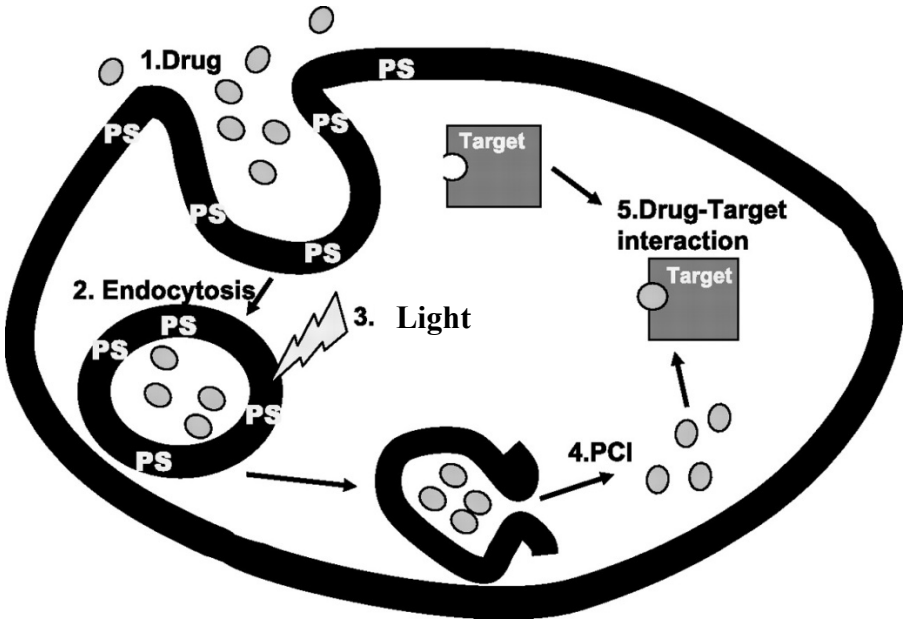

Figure 1-3. **Scheme of principle involved in photochemical internalization.** Reprinted with permission from (117), "Photodynamic therapy with an endocytically located photosensitizer cause a rapid activation of the mitogen-activated protein kinases extracellular signal-regulated kinase, p38, and c-Jun NH2 terminal kinase with opposing effects on cell survival" by Weyergang, A., Kaalhus, O. and Berg, K., 2008. *Mol Cancer Ther* **7**, 1740-50, Copyright 2014 by AACR journal

The extracellular hydrophilic cargo molecule (1) is endocytosed into the cell and is transported to an endocytic vesicle while the hydrophobic photosensitizer is localized to the membranes (2). Light irradiation excites the photosensitizer molecule localized on the endosomal membrane and causes membrane disruption (3). This results in the release of entrapped cargo into the cytosol (4) where it can interact with its target (5).

1.6.1 CPP-mediated photochemical internalization

In 2004, two groups made the observation that fluorescently labeled CPPs could also escape from endosomes upon irradiation with visible light. Arginine-rich CPPs labeled with fluorescein were released from endocytic compartments upon irradiation with laser light at 488 nm. Similar endosomal release was observed when the peptide was labeled with Alexa-Fluor 633, incubated with cells and irradiated with 633 nm laser light(118). This phenomenon has also been demonstrated when the CPPs are conjugated to proteins. For instance, the protein p53 labeled with the CPP R11 and with the fluorophore FITC was observed to accumulate in endosomes upon incubation with cells. Repeated fluorescence imaging at 480 nm by confocal laser scanning microscopy, however, led to a redistribution of the FITC conjugate into the cytosolic and nuclear compartments of cells(119). The use of fluorescently labeled CPPs for PCI has been extended to the cytosolic delivery of RNA molecules. Ohtsuki and co-workers have fused an RNA binding protein U1A to the TAT peptide(25). This TatU1A construct was labeled with Alexa-Fluor 546 or cyanine fluorophores at its C-terminus. The fluorescently labeled TatU1A construct could bind small hairpin RNA (shRNA) containing a U1A binding sequence and carry its cargo into the endocytic pathway of cells(25). Irradiation with light corresponding to the excitation wavelength of the fluorophores led to release of shRNA from endosomes into cytosol as measured by the cytosolic redistribution of fluorescence as well as by gene silencing mediated by the delivered shRNA. It was therefore shown that gene expression could be spatially and temporally controlled using light irradiation(120).

In addition to the fluorophores cited previously (i.e. xanthenes, Alexa fluors, cyanines), CPP-photosensitizer conjugates have also been tested. For instance, aluminum phthalocyanine (AlPcS2a) has been attached to TAT to photo-induce endosomal release and cytosolic delivery(121). Better uptake of the photosensitizer 5-[4-Carboxyphenyl]-10,15,20-triphenyl-2,3-dihydroxychlorin (TPC) was also seen when conjugated to oligoarginine R7(122). The irradiation wavelength required to induce endosomal escape has to match the excitation spectra of the fluorophore and so far, light

in the range of 480 to 670 nm has been successfully used(111, 116, 123, 112, 114, 64, 115, 118). When irradiation is performed on a confocal laser scanning microscope, the fluorophores have to be subjected to multiple light exposures to achieve significant endosomal release. Consequently, cytosolic redistribution typically happens on a time scale of minutes.

1.6.2 Mechanisms of CPP-mediated photochemical internalization

The molecular mechanisms of CPP-mediated PCI are not completely understood. While it is clear that PS-CPP conjugates might induce endosomal lysis by generation of ROS(124), the fact that Fl-CPPs might be photolytic can seem surprising. Indeed, the fluorophores used to synthesize Fl-CPP conjugates are widely used for various cell biology applications and they typically do not damage cellular membranes(125, 126). However, fluorophores, like photosensitizer molecules, can act generate reactive oxygen species upon light excitation. This can occur in two different ways using namely Type I and Type II photosensitization reactions respectively(127).

ROS production by photosensitization

In a typical photosensitization reaction, the photosensitizer (Sen) molecule absorbs a photon upon light irradiation and gets excited to one or more higher energy states. The excited photosensitizer molecule (Sen*) then undergoes a series of internal reactions that produce reactive oxygen species, which can result in chemical alternation of a substrate molecule commonly proteins, lipids and DNA. A simplified scheme representing a photosensitization reaction is shown in Figure 1-4.

Type I photosensitization

In a Type I reaction, the excited photosensitizer (Sen*) reacts with the substrate molecule directly and as a result produces a radical ion by a one-electron transfer reaction in both the photosensitizer molecule and the substrate. Commonly, a substrate cation (Substrate+) and a photosensitizer anion (Sen-) are formed as substrate donates an electron(128). Further, upon reaction with molecular oxygen, both the substrate and photosensitizer radicals produce oxygenated products or ROS. In this reaction, the photosensitizer gets oxidized and cannot be recovered. Alternatively, however, the

photosensitizer anion (Sen-) can transfer its extra electron directly to molecular oxygen to produce a superoxide radical (O^2-). Here, the photosensitizer molecule is regenerated(128, 127).

Type II photosensitization

In a Type II reaction, the excited photosensitizer (Sen*) transfers its excess energy to the ground state molecular oxygen, in turn exciting oxygen to a singlet state. This results in formation of singlet oxygen radicals(128, 127). Here the photosensitizer (Sen) returns to ground state and is regenerated. Singlet oxygen is an excited state radical that can promptly react with substrates to generate oxidized products(129).

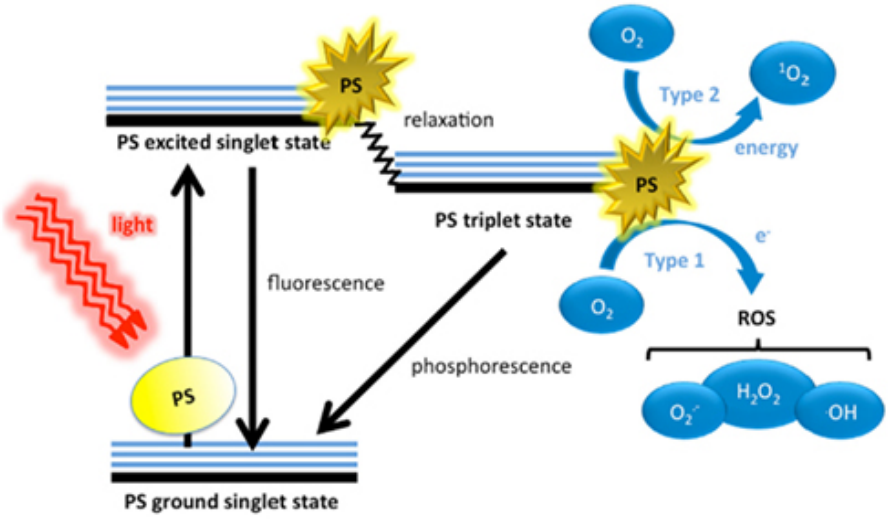

Figure 1-4. Scheme for the production of ROS by a photosensitizer. Reprinted with permission from (128), "Concepts and principles of photodynamic therapy as an alternative antifungal discovery platform" by Dai, T., Fuchs, B. B., Coleman, J. J., Prates, R. A., Astrakas, C., et al., 2012. *Front Microbiol* **3**, 120, Copyright 2014 by Frontiers journal

Types of reactive oxygen species- Superoxides, Hydroxyl and Singlet oxygen

As a result of Type I photoreactions, products containing uneven number of electrons are formed which are typically highly reactive in nature. Superoxides and hydroxyl radicals are produced by the Type I reactions(127). These radicals can cause damage to substrates by reacting with them. Malachite Green, for instance is a known photosensitizer molecule that causes damage to biological molecules by production of hydroxyl radicals(130). The type I reactions are favored by high concentration of substrates as they involve a direct interaction between the excited photosensitizer (Sen*) and the substrate. These reactions are common at low oxygen concentrations since oxygen might compete with the substrate molecule for interaction with photosensitizer(127).

Excited singlet oxygen radical is formed as a result of transfer of energy from an excited photosensitizer to molecular oxygen in a type II photoreaction(128). Most excited photosensitizers undergo a process called intersystem crossing whereby they transition to a slightly lower energy level called the triplet state(131). Excited photosensitizers tend to have a longer lifetime and are likely to undergo an energy transfer reaction at this stage. Singlet oxygen radicals typically have a very low lifetime of 3-4.5 μs in water and in most biological environments(132). Singlet oxygen radicals can readily react with biological molecules such as lipids and proteins and thus, they have low diffusion ability unlike molecular oxygen(129). Hence type II reactions occur mostly within short distances from the place of formation of the singlet oxygen. This distance is estimated to be around 0.02 μm(132) and Type II photoreactions are likely to occur under conditions of high oxygen concentration and low substrate concentrations.

Interestingly, the small diffusion distances of the singlet oxygen and hydroxyl radical suggest that localization of the photosensitizer molecule plays an important role in the type of damage caused upon light irradiation. For instance, a lipophilic photosensitizer would accumulate in the membrane lipid bilayer. Singlet oxygen in the lipid bilayer has a lifetime double of that in an aqueous environment(132).

Recent evidence suggests that the photolytic activity of the Fl-CPP TMR-TAT requires the production of reactive oxygen species such as superoxide and singlet oxygen. The singlet oxygen inhibitor crocetin has, for instance, been shown to reduce the light-induced endosomal escape of TMR-TAT inside cells(133). However, singlet oxygen quenchers such as α-tocopherol inhibit photolysis of RBCs(133). Also, lytic damage by TMR-TAT is inhibited in the presence of tiron, a superoxide quencher. Together, these results support the notion that Fl-CPPs produce singlet oxygen and superoxide radicals inside endosomes upon light irradiation(134, 135). Using liposomes as membrane model systems, it has been shown that Fl-CPPs such as TMR-TAT bind to negatively charged phospholipids on the membranes. This binding is suggested to be necessary for the photolytic activity shown by TMR-TAT(135). Also, ROS produced by TMR-TAT can cause oxidation of lipids. Interestingly, arginine-rich CPPs showed more binding and lytic activity than lysine-rich CPPs, suggesting that the arginine residues of the CPPs are responsible for the lytic activity of TMR-TAT(134). The production of ROS by TMR-TAT and modulation of lytic activity shown by alteration of CPP sequences implies that in addition to ROS generation, the CPP moiety of Fl-CPPs contribute directly to Fl-CPP mediated photo-destruction of membranes(134, 135). Studies show that a synergy between ROS produced by fluorophores and the CPP exists during photo-induced lysis by Fl-CPP conjugates(134, 135).

1.6.3 PCI- associated cytotoxicity issues

A potential limitation of PCI and CPP-mediated PCI in particular is the phototoxicity associated with these methodologies. Due to the lipophilic and membrane associative nature of most photosensitizer molecules, irradiation can result in damage of the cell's plasma membrane. The photosensitizers used for PCI can cause cell death when exposed to sufficient light(136). The light dose applied to achieve endosomal release must therefore carefully be controlled so as to avoid cell death during delivery(136). Several reports have shown that CPP-mediated PCI can be accomplished without killing cells(118, 25). However, R7-TPC causes apoptosis and necrotic cell

damage at low and high concentrations, respectively(122). PCI of TMR-TAT was also always accompanied by rapid plasma membrane blebbing and loss of membrane permeability resulting in cell death. The reasons for the cytotoxicity that results due to photochemical internalization of Fl-CPP conjugates have not been explored till date and are unknown.

It was proposed that Fl-CPPs once released from the endosomes into the cytosolic space of a cell might target and lyse other intracellular organelles as Fl-CPPs are shown to associate with membranes(133). However, when TMR-TAT was microinjected directly into the cells cytosol and irradiated, cell killing was not observed. Another conjugate TMR-S-S-TAT was used with a rationale that it would mimic TMR-TAT inside endosomal vesicles but lose its lytic activity in the cytosolic reducing environment. The endosomal release of TMR-S-S-TAT surprisingly resulted in cell death similar to that observed with TMR-TAT. This led to the conclusion that TMR-TAT or Fl-CPPs are not significantly cytotoxic in the cell cytosol but that the endosomal release process itself was involved in the cell killing.

Release of Lysosomal Contents during PCI

It has been shown that hydrophobic photosensitizers such as sulfonated tetraphenyl porphines ($TPPS_n$) localize to acidic lysosomal compartments of cells(137), also referred to as suicidal bags of a cell. The lysosomes contain a more than fifty proteases and hydrolases that can degrade biomolecules of a cell(138, 139). Studies showed that upon irradiation of cells treated with TPPS4, lysosomal enzymes such as P-N-acetyl-D-glucosaminidase and cathepsins were released into the cytosol of the cell(137). However, further experiments suggested that these enzymes were not cytotoxic to cells due to photochemical inactivation of the enzymes and inhibition by certain cysteine cathepsin inhibitors present in the cytosol of the cell(137). This led to the conclusion that cells undergoing PCI can survive a partial lysosomal disruption. It is however difficult to estimate in the case of Fl-CPP mediated PCI, the extent of lysosomal content release into the cell cytosol. It is reported that a significant delay exists between lysosomal lysis and cell death if proteases and hydrolases are involved. In

the case of TMR-TAT, there is no delay between the endosomal escape and observation of cell death(133). It is thus possible that the cell death mediated by Fl-CPPs such as TMR-TAT is caused due to release of toxic molecules rather than hydrolytic enzymes.

Lysosomes are also a storehouse of large amounts of iron as a result of degradation of iron containing mitochondrial components and ferritin(138). Iron exists as Fe(II) inside lysosomes as a result of the acidic and reducing environment in lysosomes(138). Fe(II) is a catalyst for Fenton reactions, which can yield highly reaction hydroxyl radicals(138). It is thus possible that lysosomal disruption during Fl-CPP mediated PCI might result in the release of Fe(II) which in turn produces hydroxyl radicals and induces cell damage.

Lysosomes and late endosomal compartments contain a high concentration of calcium ions which could be release as a result of TMR-TAT photo-endosomolysis. The reported concentration of Ca^{2+} in the lysosomes is approximately 600 μM(140). In a typical mammalian cell, the Ca^{2+} concentration in the cytosol is maintained at 100 nM. Disturbance in the calcium homeostasis within a cell is suggested to be dangerous to the cell and is implicated in apoptotic cell death pathways(141-143). A well-documented link exists between calcium and cell death(141).

Calcium and Cell death

Calcium homeostasis plays an important role in the maintenance of a cell's important functions. One of the main cell death pathways, apoptosis, is reported to be induced by the loss of Ca^{2+} homeostatic control. This homeostatic control can be regulated positively or negatively upon alterations in the Ca^{2+} distribution within a cell's intracellular compartments. An initial study showed that entry of high concentration of Ca^{2+} into myocytes resulted in cardiac pathology that followed Ischaemia(144). Overstimulation of certain receptors(145) and treatment with cytotoxic agents(146, 143) also caused a lethal influx of Ca^{2+} into the cells cytosol. A detailed scheme depicting intracellular Ca^{2+} distribution, fluxes and how the regulation of calcium concentrations in each compartment occurs through pumps and channels is shown in Figure 1-5(141). Ca^{2+} homeostasis disruption is also suggested to alter cell proliferation and differentiation in

addition to apoptosis. A number of processes that require Ca^{2+} are linked to molecules called Caspases that are known apoptosis executioners. Studies show that activation of Ca^{2+} and Mg^{2+}dependent endonucleases produced a DNA fragmentation pattern in thymocyte nuclei(147, 148) which is typical of apoptosis. Also, apoptosis induced in thymocytes by glucocorticoid treatment required extracellular Ca^{2+} in the media(149). Recent studies show that sequestering excess Ca^{2+} from cytoplasm to intracellular pools such as the endoplasmic reticulum or mitochondria is sufficient to activate cell death pathways(141).

Treatment of human embryonic kidney (HEK) cells that stably expressed hSK4-type K_{Ca} channels with a RNase Sa mutant led to an drastic changes in K_{Ca} membrane currents within 48 h resulting in apoptosis(150). The RNase Sa from *Streptomyces aureofaciens* was mutated at the surface aspartate and glutamate residues to positively charged lysines (D1K, D17K, D25K, E41K, E74K) giving the mutant a cationic character(151). This case of cell death induction upon treatment with cationic mutant RNase could be related to the cell death effects seen upon treatment of cells with highly cationic TMR-TAT.

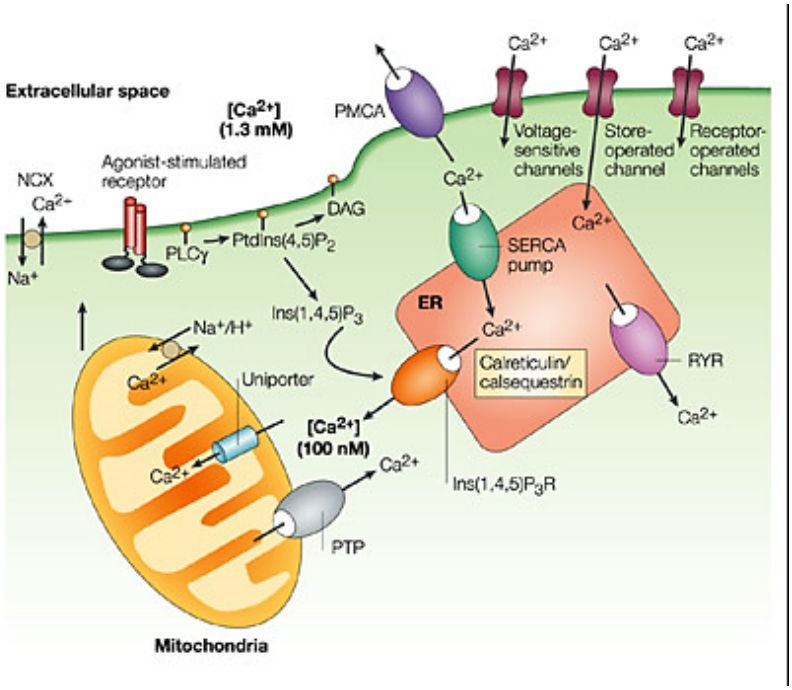

Figure 1-5. Distribution and regulation of Ca^{2+} in a mammalian cell. Reprinted with permission from (141), "Regulation of cell death: the calcium-apoptosis link" by Orrenius, S., Zhivotovsky, B. and Nicotera, P., 2003. *Nat Rev Mol Cell Biol* **4**, 552-65, Copyright 2014 by Nature Publishing Group

The regulation of Ca^{2+} import into cells through the plasma membrane is regulated by several receptor-operated, voltage-gated and store-operated channels. Inside the cell, Ca^{2+} is sequestered to either the ER or the mitochondria. ER Ca^{2+} concentrations are approximately 100-800 μM. ER Ca^{2+} pool is regulated by the SERCA pumps, inositol-1,4,5-trisphosphate receptors, ryanodine receptors and by Ca^{2+} -binding proteins (calreticulin, calsequestrin)(152). The mitochondria can uptake Ca^{2+} electrophoretically through a uniport transporter and can release it via reversal of the uniporter, Na+/H+-dependent Ca^{2+} exchange, or by opening the mPTP.

Link between Endoplasmic Reticulum, Ca^{2+} and Cell death

The ER is an important storehouse of Ca^{2+} and contains upto 800 μM of free Ca^{2+}. The ER plays a role in folding, modifying and sorting of the newly synthesized proteins of mammalian cells. Any discrepancies in the normal functioning of the ER, an overload or loss of Ca^{2+} in the ER can lead to ER stress and lead to changes in protein folding. Two pathways namely the unfolding protein response (UPR) pathway and the ER overload response (EOR) pathway are known to regulate protein folding in the ER(153). But ER stress can lead to activation of apoptotic pathways via the UPR and EOR pathways(154). Further, disturbances in the intracellular Ca^{2+} pool of the ER can initiate cleavage and activation of an enzyme called pro-caspase-12 by m-CALPAIN(155). Upon activation by m-CALPAIN, caspase 12 can act on other caspases that can induce apoptotic pathways. An intricate coordination exists between the two proteases families, Calpains and caspase with respect to activation of cell death apoptotic pathways involving ER stress(155). Alterations in ER Ca^{2+} pools affects the Sarcoplasmic reticulum Ca^{2+} ATPase pump and the Ins(1,4,5)P_3 receptors present on the ER membrane, which are in turn directly linked to activation of caspases(155).

Another key study shows that release of Ca^{2+} from the ER pool is associated with an uptake of Ca^{2+} into the mitochondria(156). The mitochondria are suggested to recruit a dynamin-like protein which in turn mediated the disruption of mitochondrial membrane(157). Consequently, the mitochondria can release an apoptotic activator molecule called Cytochrome C into the cytosol of cells(157).

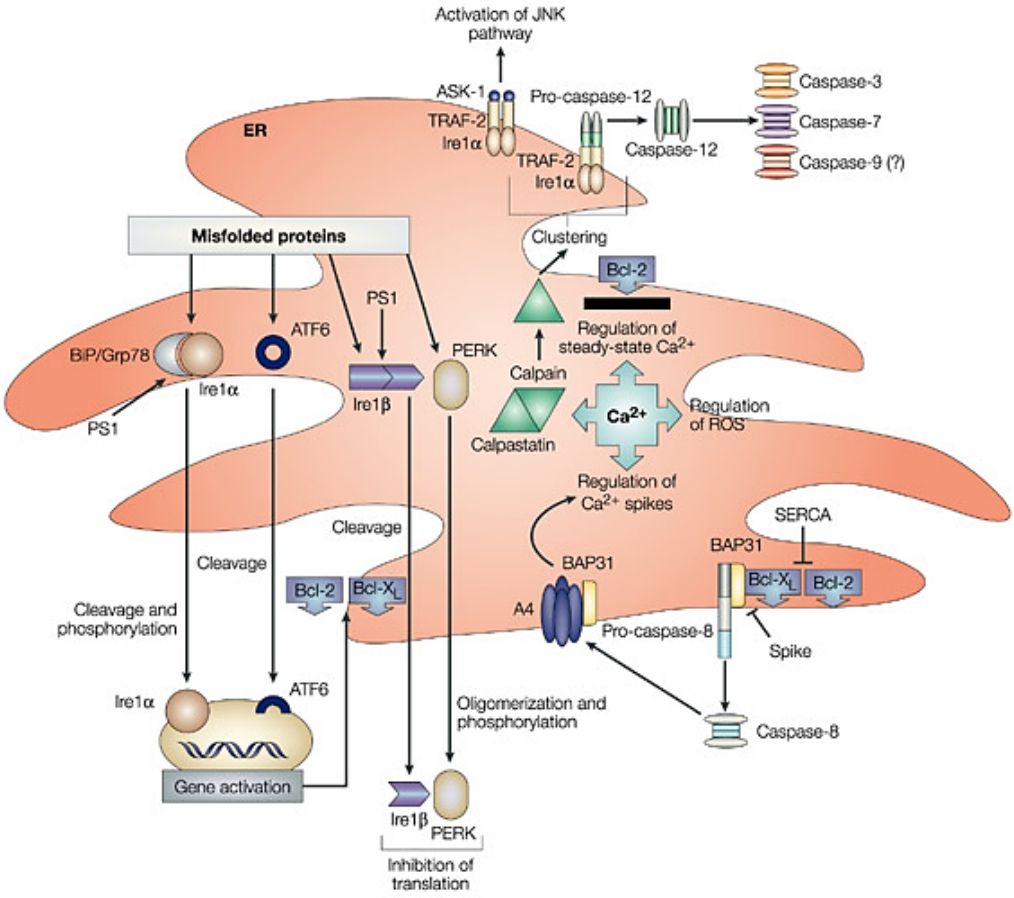

Figure 1-6. Role of Ca^{2+} in ER stress and Ca^{2+} regulation. Reprinted with permission from **(141)**, "Regulation of cell death: the calcium-apoptosis link" by Orrenius, S., Zhivotovsky, B. and Nicotera, P., 2003. *Nat Rev Mol Cell Biol* **4**, 552-65, Copyright 2014 by Nature Publishing Group

A change in the Ca^{2+} concentration in the ER (four arrows in the middle of the figure) can activate of Ca^{2+}-dependent enzymes (calpains) and reactive oxygen species (ROS) production. The Ca^{2+} concentration in the ER lumen is regulated by SERCA pumps, inositol-1,4,5-trisphosphate receptors, ryanodine receptors and by Ca^{2+} -binding proteins (calreticulin, calsequestrin)(152) and Bcl-2 proteins.

Link between Mitochondria, Ca^{2+} and Cell death

Mitochondrial compartments are also important storehouses of Ca^{2+} in mammalian cells. Ca^{2+} is present upto xx mM in the mitochondria. It has been shown to be an active participant in the intracellular Ca^{2+} compartmentalization process(158). The mitochondria are able to uptake Ca^{2+} electrophoretically from the cytosolic space through a uniporter transporter and also release it through several different routes. A detailed scheme involving all these different routes of calcium uptake and release is shown in Figure 1-6. An energy-dissipating Ca^{2+} cycle exists in the mitochondria whereby Ca^{2+} uptake is coupled to numerous exchange systems. Under physiological conditions, the concentration of Ca^{2+} in the mitochondria is low. Also the affinity of the uniporter for Ca^{2+} is low. But, the mitochondria are able to accumulate large amounts of Ca^{2+} under pathological conditions when there is an overload of intracellular Ca^{2+} in the cell(159). The excess Ca^{2+} upon uptake of phosphate by the mitochondria, gets precipitated inside the the mitochondrial matrix as insoluble hydroxyapatite(160). Novel indicators that detect Ca^{2+} concentrations in specific compartments of a cell have been used to explore other roles of mitochondria in the cell(161). Previously, it was believed that the mitochondrial Ca^{2+} uptake was a mechanism to protect a cell from situations of Ca^{2+} overload. But now, it is evident that Ca^{2+} fluxes are integral parts of a cells Ca^{2+} signaling pathways(162). Since the affinity of the uniporter for Ca^{2+} is low, the mitochondrial is located in close proximity to the ER facilitate rapid uptake of Ca^{2+} by the mitochondria(163). Also, Ca^{2+} hotspots are established very close to the release channels(163) which enables mitochondria to take up Ca^{2+}. The rapid influx of Ca^{2+} into the mitochondria of cell can stimulate the Ca^{2+} -sensitive dehydrogenases in the matrix resulting in the stimulation of mitochondrial energy metabolism(163).

Permeability Transition Pore

Ca^{2+} uptake into the mitochondria activates cell death pathways by a mechanism that involves the OMM (outer mitochondrial membrane) and releasing pro-apoptotic mitochondrial proteins(164). This mechanism also involves the opening of an inner mitochondrial membrane permeability transition(164). Here, a protein complex in called

the permeability transition pore (PTP) located between the inner mitochondrial membrane (IMM) and the outer mitochondrial membrane (OMM) is involved(165). This complex comprises of a Voltage-dependent anion channel (VDAC), an adenine nucleotide translocator (ANT), mitochondrial cyclophilin D and other proteins(166, 167, 165).

The mPTP is voltage-gated chaneel and activated when the Ca^{2+} concentration in the mitochondria is high, under conditions of oxidative stress ie. high ROS concentration, or low transmembrane potential(165). The mPTP rapidly opens and closes under the above conditions. Subsequently, the mPTP opens persistently allowing the release of Ca^{2+} and also components of the mitochondrial matrix (MW <1500 Da)(168). Agents such as Ca^{2+} ionophores, thapsigargin or neurotoxins can trigger apoptosis through the Ca^{2+} mediated mitochondrial PTP activation(169-171). Inhibitors of the mPTP such as cyclosporin A can prevent the opening of the pore(168, 172). Also Ruthenium red, an inhibitor of Ca^{2+} uptake by mitochondria can prevent apoptosis by inhibiting mPTP opening(173). Opening of the mPTP results in the escape of cytochrome C and other pro-apoptotic factors fromt eh mitochondria and might result in mitochondrial swelling and OMM rupture. However, the mPTP can reseal itself in an attempt to recover even after the loss of cytochrome C and other proteins from the matrix(174). Ceramide, an apoptotic inducer was shown to induce apoptosis by facilitating a Ca^{2+} -induced mPTP opening(175). However, the overexpression of Bcl-2 protein is shown to increase the overall capacity of the mitochondria for Ca^{2+}, but still prevent the mPTP opening and cytochrome C release(176, 177).

In an alternate pathway, Ca^{2+} is known to interact with an anionic phospholipid called cardiolipin uniquely present in the IMM. Cytochrome C is bound to the IMM via cardiolipin(178). It is indicative through studies that the dissociation of cytochrome C from cardiolipin is the first and foremost step to facilitate release of cytochrome C from the mitochondria into the cytosol(178). This cleavage of cytochrome C occurs through peroxidation of cardiolipin, resulting in its decreased affinity for cytochrome C(178, 179). Ca^{2+} is known to bind to cardiolipin and cause reduced lipid mobility and protein

aggregates(180). This results in increased formation of ROS by the mitochondrial respiratory chain, leading to promotion of oxidation of membrane phospholipids and proteins.

Ca^{2+} might also activate certain protein kinases or phosphatases such as calcineurin, Ca^{2+}/calmodulin-dependent protein phosphatase leading to modulation of gene expressions that activates apoptosis(181). Several Ca^{2+}-dependent enzymes scuh as endonucleases are reported to be involved in apoptotic DNA degradation(182-185). Ca^{2+} overload in the cytosol has been reported to activate phospholipase A2 (PLA2). As a result of PLA2 activation, arachidonic acid and other polyunsaturated fatty acids are released and metabolized by lipoxygenases or cyclooxygenases, resulting in ROS generation(186). Also PLA2 activation induces membrane alterations by generating lysophosphatides(186).

In the case of cell death induced by endosomal escape of Fl-CPPs such as TMR-TAT, it was reported that TMR-TAT by itself did not target other membranes following cytosolic distribution using microinjection experiments(187). It was shown that the endosomal process itself was however required for the cell death to occur. Further studies using indicators of Ca^{2+} ions such as Fluo-4, it is evident that a high amount of free Ca^{2+} is released into the cytosol along with the release of TMR-TAT from the endocytic vesicles(187). The excess Ca^{2+} was shown to originate from intracellular sources such as lysosomes and endosomes as TMR-TAT co-localized with Ca^{2+} containing vesicles of the cell and could also cause release of co-incubated molecules upon light irradiation into the cytosol(187). The staining of mitochondria with Ca^{2+} indicator following Ca^{2+} overload in the cytosol suggested that the mitochondria was involved in the cell death caused by TMR-TAT release. Subsequent studies with inhibitors of calcium uptake into mitochondria and mitochondrial permeability transition pore (mPTP), ruthenium red and cyclosporin A showed inhibition of cell death even after delivery of TMR-TAT into the cell cytosol(187). Overall, these observations suggested that TMR-TAT mediated cell death mechanism involved overload of cytosol with Ca^{2+} released upon TMR-TAT endosomal escape and subsequent mPTP activation.

1.7 The goal of my study

It has been shown that attaching small fluorophore molecules such as Alexa-Fluor or fluorescein to cell-penetrating peptides (CPP) like TAT or polyarginine facilitates endocytic uptake of the conjugates and light irradiation further causes the Fl-CPP conjugates to release from endocytic vesicles into cytosolic space. The focus of my work was to study and understand the molecular mechanism(s) behind the light mediated release of Fl-CPP conjugates from endocytic vesicles into the cells' cytosol. My study focused on understanding the implications of the light induced intracellular delivery strategy with respect to cytotoxicity. I also sought to establish a structure activity relationship for the Fl-CPPs. Overall, this study will aid in the development of novel Fl-CPP tools to achieve efficient intracellular delivery of macromolecules.

2. TMR-TAT, A NOVEL PHOTO-ENDOSOMOLYTIC FLUOROPHORE-CPP CONJUGATE

2.1 Introduction

In this section, I show that the prototypical cell-penetrating peptide TAT when labeled with an innocuous fluorophore 5(6)-carboxytetramethylrhodamine (TMR), escapes from the endosomes upon light irradiation. The mechanism of this endosomal escape by the Fl-CPPs is however unknown. I investigate the molecular basis of this photo-induced endosomolytic activity of Fl-CPP conjugates. Interestingly, I also observed that the endosomal release of TMR-TAT conjugate is accompanied by a membrane blebbing effect and cell death. Fl-CPP mediated photolytic activity with red blood cell membrane models is also tested. Finally, I test the hypothesis that the photolytic activity of Fl-CPPs is a result of the production of singlet oxygen upon light irradiation by Fl-CPPs.

2.2 Results

2.2.1 Irradiation of TMR-TAT contained in endosomes results in endosomal release

The effect of light irradiation on cells with endocytosed TMR-TAT was first investigated. HeLa cells were incubated in the presence of TMR-TAT (3 μM) for 1 h at 37°C. After washing the cells, the sample was placed on a microscope and the cellular distribution of the peptide was assessed by fluorescence imaging. The peptide initially showed a punctate intracellular distribution consistent with their accumulation within endocytic organelles (TAT typically requires higher concentrations than the one used here to penetrate the cytosolic space of cells directly) (Fig. 2-1)(36). Fluorescence excitation of the cells on the microscope, however, rapidly caused the release of the fluorescent peptides from endosomes into the cytosol. As shown in Fig. 2-1, the escape from individual endosomes was observed after only a few hundred milliseconds of light

exposure at 560 nm. Within seconds, the content of many endosomes was released into the cell and the peptides were distributed throughout the cell. The peptide also accumulated at the nucleoli, a known effect of TAT(188). Significantly, photo-induced endosomal release was accompanied by dramatic blebbing of the plasma membrane and cell shrinkage (Fig. 2-2). The irradiated cells also became permeable to the cell-impermeant dye SYTOX® Blue, indicating that their plasma membranes were compromised and that the cells underwent rapid necrosis (Fig. 2-2 shows the morphological changes cells undergo after irradiation in details while Fig. 2-3 illustrates that this phenomenon occurs for all irradiated cells). The viability of non-irradiated cells was, in contrast, not affected by TMR-TAT (Fig. 2-4); the cytotoxicity of the peptide was found to be negligible in the absence of light at concentrations up to 25 μM (supporting information Fig. 2-5).

A retro-inverso version of the TAT peptide also referred to as riTAT was conjugated to TMR to obtain TMR-ri-TAT. The rationale behind synthesizing this conjugate was that the retro-inverso peptides are resistant to protease degradation. TMR-R9 and TMR-riTAT had similar photo-endosomolytic and photocytotoxic activities as TMR-TAT, indicating that an arginine-rich composition might be sufficient for these activities (Fig. 2-2 and 2-6). Like TMR-TAT, TMR-K9 was endocytosed by cells (higher concentration was used to get equal or greater amount of material inside

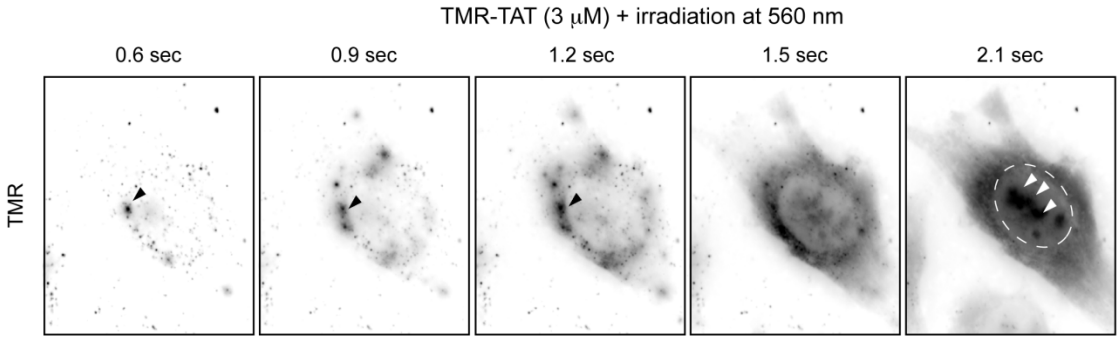

Figure 2-1. Photolytic effects of TMR-TAT after endocytosis in HeLa cells.

Light irradiation causes escape of TMR-TAT from endocytic organelles into the cytosol. HeLa cells were incubated with TMR-TAT (3 μM), washed, and irradiated at 560±20 nm through a 100X objective on a wide-field microscope. Images were acquired in a time-lapse experiment with a light excitation of 300 ms and an interval of 2 sec. The time displayed on the images represents the total light exposure time. The TMR fluorescence signal is represented as inverted monochrome (black= fluorescent signal, white= no signal). The TMR signal, initially in a punctate distribution, can be seen to diffuse away from individual endocytic organelles upon irradiation (black arrows). The perimeter of the nucleus is highlighted by a dashed line in the last image and the signal from TMR-TAT presumably accumulated at nucleoli is indicated with white arrows.

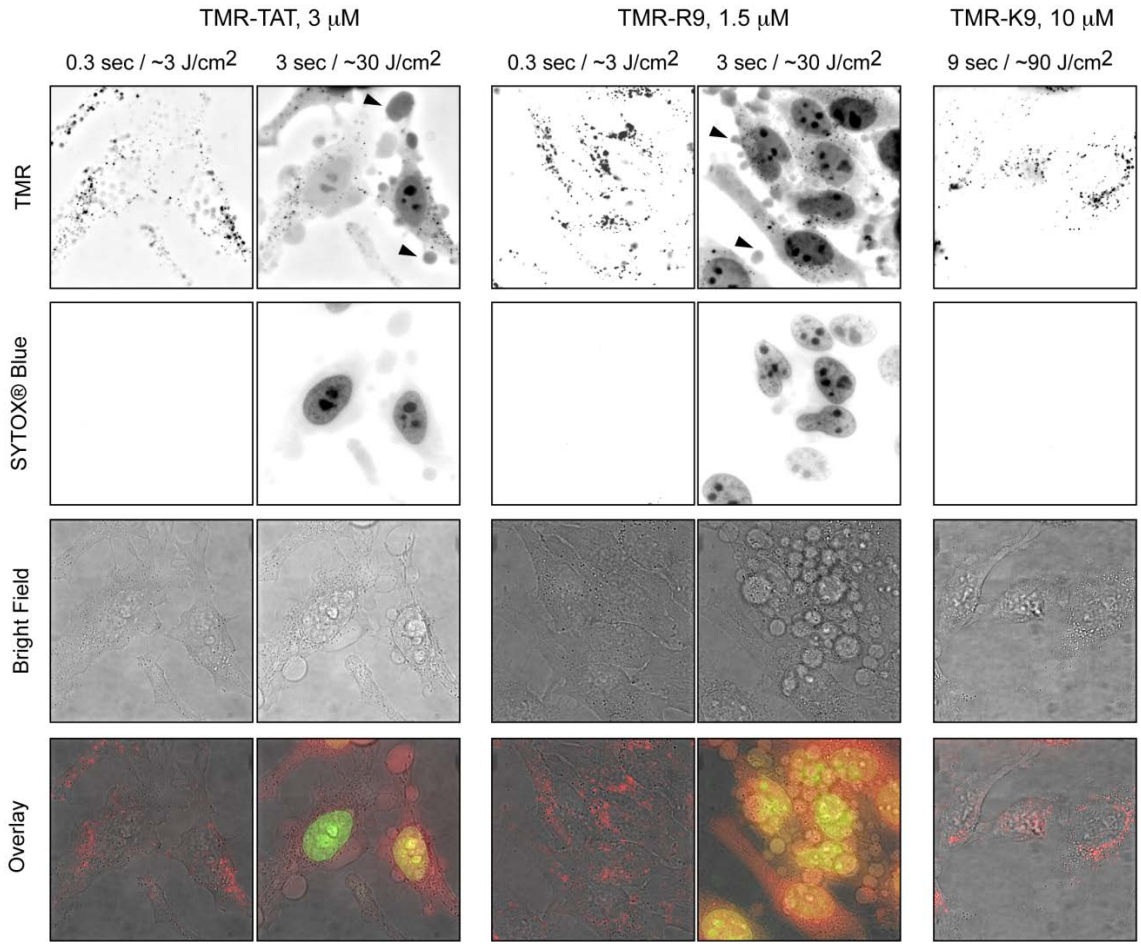

Figure 2-2. Comparison of photolytic effects of TMR-TAT, TMR-R9 and TMR-K9

The TAT peptide (GRKKRRQRRR), R9 (RRRRRRRRR) and the K9 (KKKKKKKKK) peptides were conjugated to fluorophore TMR on their N-terminus to obtain TMR-TAT, TMR-R9 and TMR-K9 respectively. Upon incubation with HeLa cells, uptake by endocytosis is observed. Photosensitization of TMR-TAT or TMR-R9 endocytosed by cells causes plasma membrane damage and cell death. In contrast, cells containing TMR-K9 remain viable and the punctate distribution of TMR-K9 is not affected by the light irradiation under the conditions tested. The fluorescence signals of TMR and SYTOX® Blue are represented as inverted monochrome or pseudo-colored red and green in the overlay image, respectively.

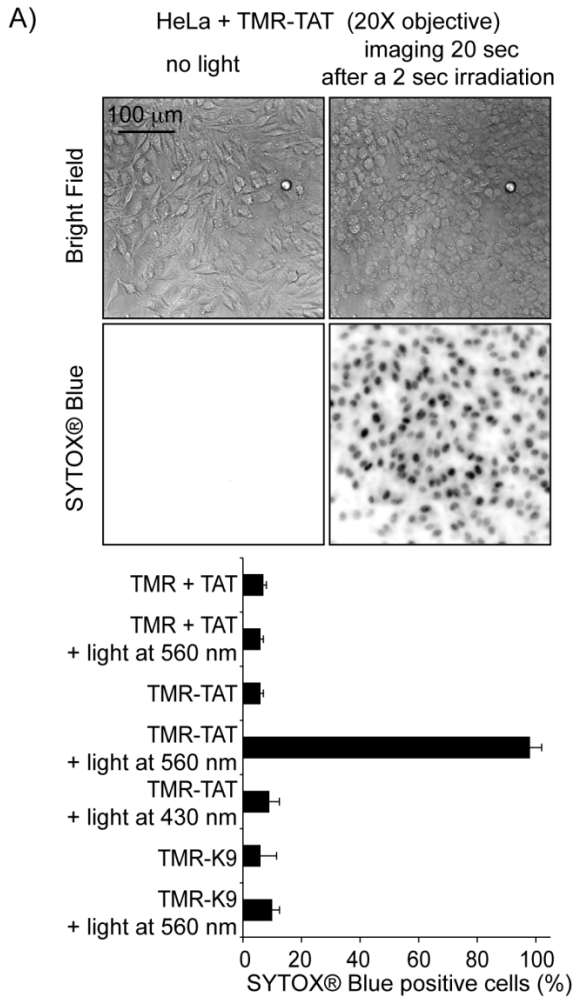

Figure 2-3. Photolytic and photocytotoxic effects of TMR-TAT in red blood cells

Irradiation of TMR-TAT endocytosed by cells causes plasma membrane blebbing and permeabilization (SYTOX® Blue staining) within 20 sec after 2 sec irradiation at 560 nm (the radiant exposure is approximately 40 J/cm^2). Cell destruction is observed in more than 95% of the cells irradiated at 560 nm. In contrast, no photocytoxicity is observed when cells treated with TMR-K9 (10 μM) or TMR (3 μM) and TAT (3 μM) are irradiated under similar conditions. Cells incubated with TMR-TAT but irradiated at 430 nm are not destroyed (excitation wavelength of SYTOX® Blue but not of TMR, radiant exposure was also approximately 40 J/cm^2). The histogram represents the average percentage of cells stained by SYTOX® Blue after peptide and light treatment (the number of cells examined was at least 3000) and the error bars represent the standard deviation (experiments were reproduced at least 3 times).

endosomes, Fig. 2-2 and 2-7). However, irradiation of cells containing TMR-K9 caused no endosomal release or cell death under the same conditions of irradiation as TMR-TAT (Fig. 2-2). TMR alone was not endocytosed to a detectable level and irradiation post-incubation did not cause cell death (data not shown). Together these data suggest that the presence of CPPs like TAT or R9 is important for the observed photo-induced endosomal lysis and cell-death. In addition, these activities cannot be solely attributed to the endocytosis of the TMR-CPP conjugates as TMR-K9 did not have any observable effects despite similar endocytic uptake. No endosomal release and no cell death were observed when TMR-TAT-treated cells were exposed to light of wavelengths not absorbed by TMR (e.g. 436 or 470 nm). Moreover, irradiation of cells incubated with unlabeled TAT and irradiated at the TMR excitation wavelength did not die (Fig. 2-3). This suggests that excitation of the fluorophore is required to achieve photosensitization and that TAT and light alone do not induce endosomal release or cell death (Fig. 2-3). Irradiation of cells co-incubated with both TAT and TMR did not result in cell death, suggesting that conjugation of TMR to TAT is required for this effect. Finally, the photo-induced activities of TMR-TAT could be reproduced in other cell lines, such as COLO316 and COS7, indicating that the effects observed are not specific to HeLa cells (Fig. 2-4 and 2-8).

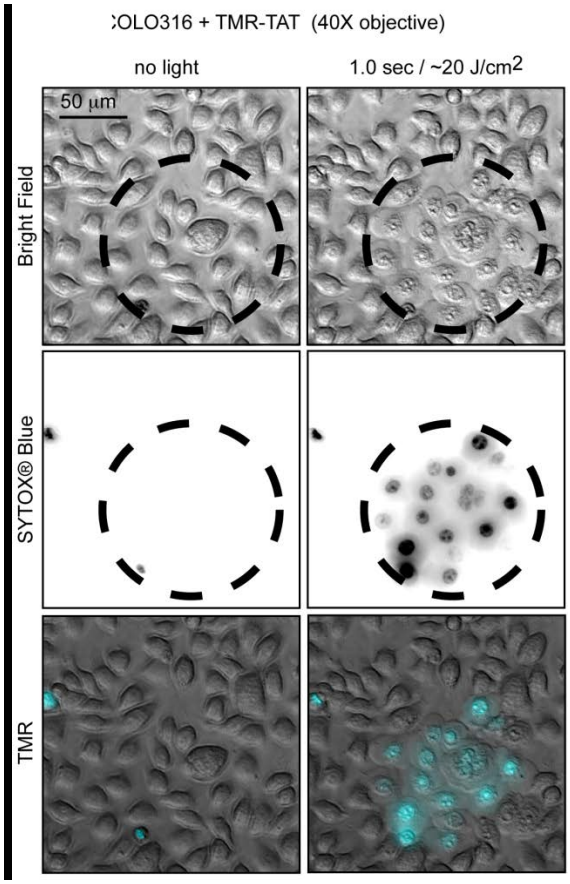

Figure 2-4. Photolytic and photocytotoxic effects of TMR-TAT in COLO316 cells

The cytotoxic effect of TMR-TAT is limited to irradiated areas. COLO316 cells were incubated with TMR-TAT (3 μM) for 1 h. The cells were washed with fresh media and endocytosis of TMR-TAT was confirmed by fluorescence microscopy. The cells within the circled area were exposed to light at 560 nm. Morphological changes and SYTOX® Blue staining (inverted monochrome or pseudo-colored cyan) are only observable in the irradiated area.

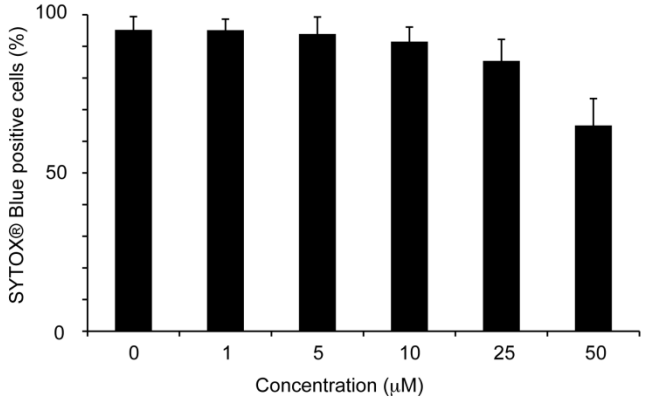

Figure 2-5. Toxicity of TMR-TAT toward HeLa cells in the absence of light.

TMR-TAT was incubated at different concentrations as indicated, with HeLa cells for 1 h in L-15 at 37°C. Cells were washed with fresh L-15 and incubated for an additional 4 h. Cells were then treated with L-15 containing DAPI and SYTOX® green. DAPI stains the nucleus of all cells while SYTOX® green only stains the nucleus of dead cells. Cells were imaged by fluorescence microscopy using the DAPI and FITC filters to detect DAPI and SYTOX® green, respectively. For each experiments, five representative images were acquired using the 20X objective and the percentage of dead cells were calculated from the ratio of cells stained by SYTOX® green divided by the number of cells stained by DAPI. The reported data is the average of 3 experiments (3×5 images, $\geq$ 1000 cells/experiments) and the error bar represents the standard deviation.

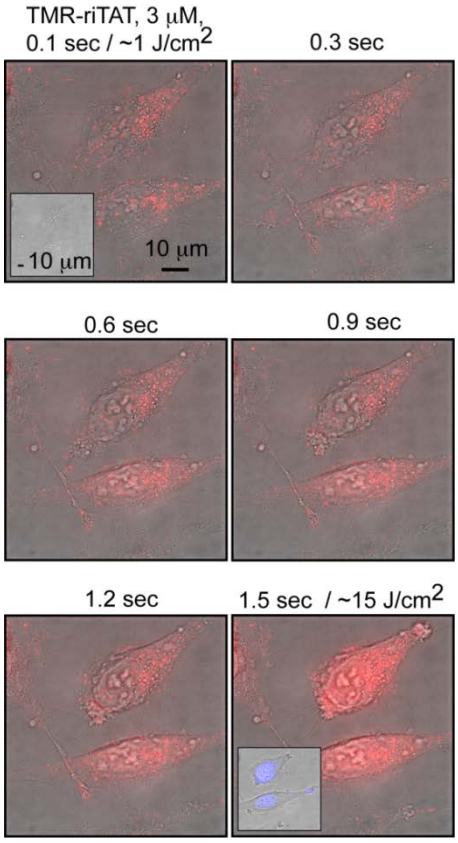

Figure 2-6. Photosensitization of TMR-riTAT endocytosed by HeLa cells.

HeLa cells were incubated with TMR-riTAT (3 μM) for 1 h and washed with fresh L-15 media. Cells were then incubated with L-15 containing 1 μM SYTOX® Blue to detect cells with compromised plasma membranes. Cells were observed using a 100X objective using bright field and fluorescence imaging (RFP filter to detect TMR-riTAT, pseudocolored red, and CFP filter to detect SYTOX® Blue, pseudo colored blue). The images are the overlay of TMR and bright field images and the insert images are the overlay of SYTOX® Blue and bright field images. At a low exposure dose, TMR-riTAT is distributed in a punctate manner within cells and cells are impermeable to SYTOX® Blue. As with TMR-TAT, TMR-riTAT is however quickly redistributed thought the cell as light exposure is increased. As this takes place, the cell shrinks and membrane blebs form. The nuclei of cells are also stained by SYTOX® Blue, indicating that the plasma membrane integrity is compromised.

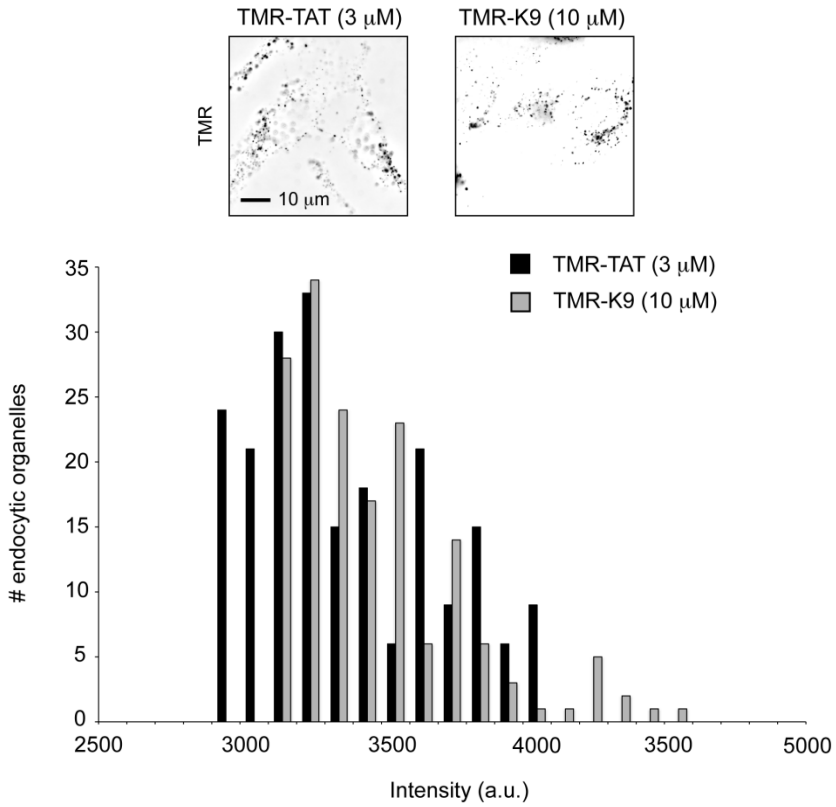

Figure 2-7. Comparison of the fluorescence intensity of endosomes containing TMR-TAT or TMR-K9.

Imaging was performed in both cases with identical conditions. The fluorescence intensities of all endocytic organelles was measured the Slidebook software. These data show that the amount of TMR-K9 (incubation at 10 μM) present in endocytic organelles is typically equal or greater than that of TMR-TAT (incubation at 3 μM) (TMR-K9 however requires a greater concentration in the incubation media to achieve this result). These results therefore indicate that the reduced activity seen with TMR-K9 when compared to TMR-TAT is not due to the fact that less material is present inside endocytic organelles.

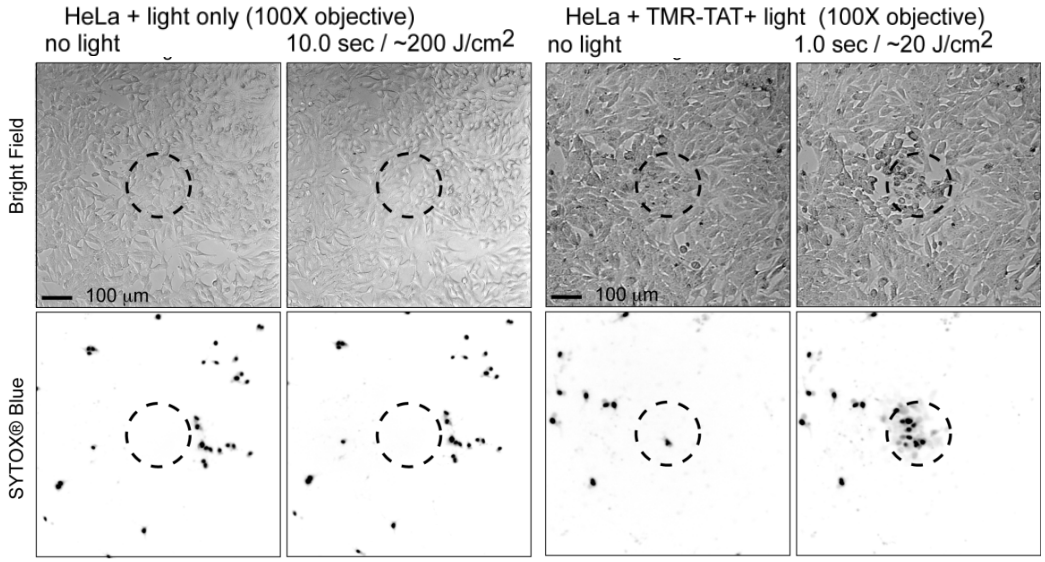

Figure 2-8. Light irradiation alone does not cause cell-death. TMR-TAT induces cell-death upon light irradiation in HeLa or COS-7 cells (contd.)

A) The conditions of light irradiation used in Fig. 2-3 do not affect cell viability. HeLa cells were prepared as in Fig. 2-7 except that TMR-TAT was omitted during the 1 h incubation in L-15. Cells were observed using a 10 X objective using bright field and fluorescence imaging (CFP filter to detect SYTOX® Blue). The cells within the circled area were exposed to light at 560 nm for 10 sec (10 × the exposure time used in Fig. 2-7). Cells were then imaged 5 min after irradiation to allow for SYTOX® Blue staining. Nuclei stained by SYTOX® Blue are represented as black dots in the inverted monochrome image. In contrast to Fig. 2-7, the cells within the irradiated area do not become stained with SYTOX® Blue after exposure to light.

B) Similar experiment as in A) but with cells incubated with TMR-TAT.

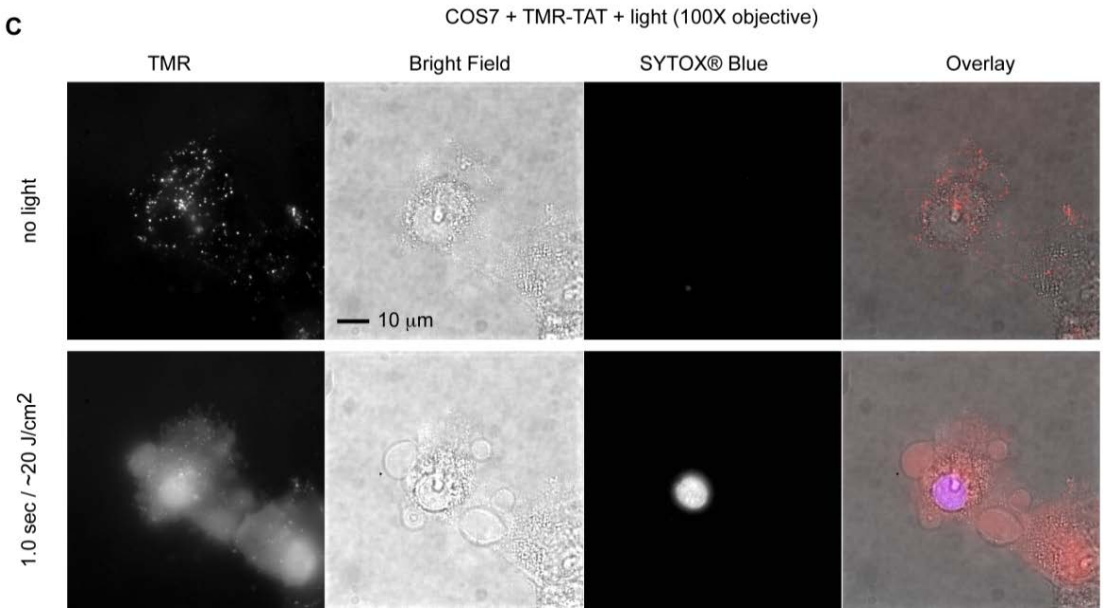

Figure 2-8. Continued

C) Photosensitization of TMR-TAT endocytosed by COS-7 cells. Experimental conditions were identical to those of Fig. 2-8. Cells were observed using a 100X objective using bright field and fluorescence imaging (RFP filter to detect TMR-TAT, pseudocolored red, and CFP filter to detect SYTOX® Blue, pseudo colored blue). As with HeLa cells, TMR-TAT is distributed in a punctate manner within cells at a low exposure dose and cells are impermeable to SYTOX® Blue. TMR-TAT is however quickly redistributed thought the cell as light exposure is increased. After 1 sec of irradiation, membrane blebs are formed on the cell surface, and the nuclei of cells are stained by SYTOX® Blue.

2.2.2 Degradation of TAT within endosomes abolished endosomal escape

The previous experiments suggest that TMR and TAT have to be conjugated to one another to achieve the light-induced endosomal release and the observed cell-death (Fig. 2-3). To confirm these results, the activities of TMR-TAT and TMR-riTAT were compared as a function of the time spent within the endocytic pathway. One would expect that TMR-TAT would accumulate within late endosomes and lysosomes over time and that the TAT moiety might be degraded by proteases present in these organelles. If TAT is required for the lytic activity of TMR-TAT, degradation of the peptide should therefore abolish the activity of the compound. On the other hand, riTAT should be resistant to proteolysis and its lytic activity should not be dependent on the incubation time. HeLa cells were treated with TMR-TAT or TMR-riTAT for 1 h to allow for endocytosis. The cells were then washed and incubated for an additional 1, 4, or 8 h in L-15 media to allow for the accumulation of the endocytosed peptides into late endosomes and lysosomes. The cells were then observed under the microscope and treated with light as described in the previous paragraph. As expected, incubation time did not appear to have an effect on the activity of TMR-riTAT as both rapid endosomal release and cell-death were observed under all conditions tested (Fig. 2-9). In contrast, while endosomal release and cell-death were observed when cells treated with TMR-TAT were incubated for 1 h, these effects were reduced or completely abolished at the 4 and 8 h time points, respectively (Fig. 2-9). Together, these results indicate that it is TMR-TAT that participates in the activities observed and not molecular species that might be obtained by degradation of the peptide within the endocytic pathway.

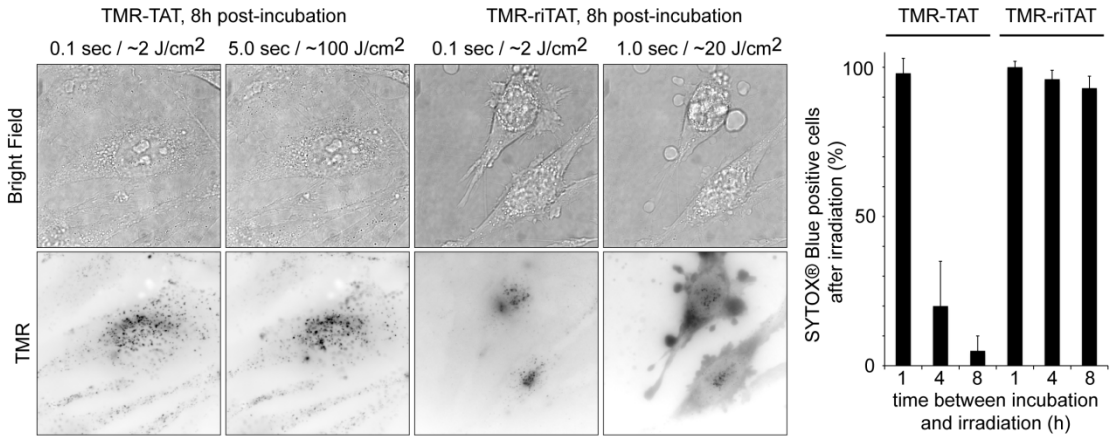

Figure 2-9. Degradation of TMR-TAT in endocytic organelles abolishes photo-induced endosomal release and photocytotoxicity.

HeLa cells were incubated with TMR-TAT or TMR-riTAT (3 μM) for 1 h, washed, and incubated at 37°C for an additional 1, 4 or 8 h. Irradiation of cells incubated with TMR-riTAT led to the cytosolic distribution of the TMR fluorescence signal, plasma membrane blebbing (as seen in the bright field image) and permeabilization (represented in histogram) under all tested conditions. In contrast, these photo-induced effects are dramatically reduced for TMR-TAT as the time between peptide incubation and irradiation is increased. The histogram represents the average percentage of cells stained by SYTOX® Blue after peptide and light treatment (the number of cells examined is at least 3000) and the error bars represent the standard deviation (experiments were reproduced at least 3 times).

2.2.3 TMR-TAT endosomal release results in plasma membrane blebs and cell death

The disruption of lysosomes by photosensitizers or lysosomotropic compounds has been shown to induce cell-death(139, 189, 137). It is therefore possible that the endosomal release observed in the experiments of Fig. 2-1 might be necessary to cause cell death. To investigate whether this is the case, I examined if light-induced cell-death could be observed when the peptides were only localized at the plasma membrane of cells. For these experiments, HeLa cells were first incubated with the peptides (3 μM) at 4 °C to block endocytosis. Cells were then irradiated with the peptides still present in the media (the peptide is not retained at the plasma membrane when cells are washed). As shown in Fig. 2-10, cells incubated with TMR-TAT underwent dramatic cytoplasmic extrusion, membrane blebbing, shrinkage and cell death (SYTOX® Blue staining) upon light irradiation. Cells were then washed and observed by fluorescence imaging. Live cells in areas that were not irradiated did not contain fluorescent endosomes, demonstrating that the cells in this assay did not internalize the peptides. Cells incubated with either TMR-K9 or TMR alone at similar concentrations (determined by TMR absorbance) did not die under the same conditions of irradiation. On the other hand, the membrane damage and cell death obtained after TMR-TAT photosensitization were also observed when hematoporphyrin (HP) or hematoporphyrin derivative (HPD) were used (Fig. 2-10B). HP (or porphyrin impurities present in commercially available HP) and hematoporphyrin derivative are relatively hydrophobic photosensitizers that cause membrane damage and cell killing upon light irradiation(129). Considering that singlet oxygen is expected to cause damage in close proximity to where the photosensitizer is located, accumulation of HP and HPD into membranes is believed to be critical to their photodynamic action on membranes. The similar destruction of membranes observed between HP and TMR-TAT suggests that TAT positions TMR in close proximity to membranes. In contrast, TAT-K9 would fail to induce a significant photocytotoxic effect because it doesn't localize at the membranes in the same manner. Because TMR-TAT is excluded from the intracellular space in these experiments, these results also suggest that

photosensitization of TMR-TAT at the plasma membrane is sufficient to induce membrane blebbing, SYTOX® Blue permeation, and cell death. In other words, endocytic uptake of TMR-TAT by cells is not required to achieve light-induced cell-death as long as the peptide is localized at the plasma membrane.

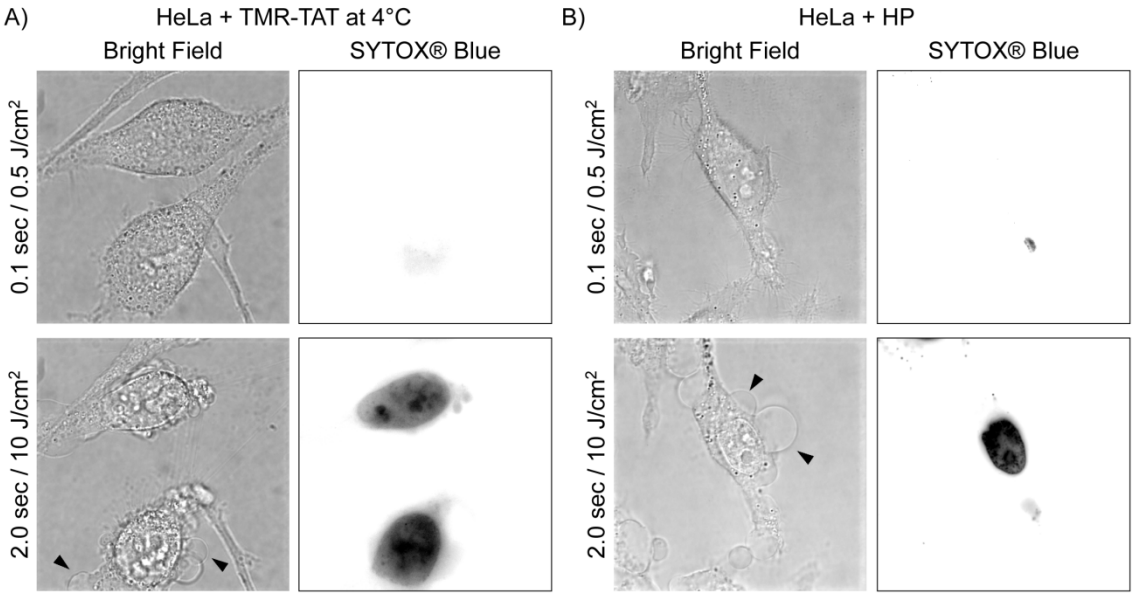

Figure 2-10. Photosensitization of extracellular TMR-TAT causes plasma membrane blebbing, plasma membrane permeabilization, and cell shrinkage.

A) HeLa cells were incubated with TMR-TAT (3 μM) at 4°C to block endocytosis of the peptide. Images represent the bright field image and the fluorescence image of SYTOX® Blue (inverted monochrome).

B) The effects of photosensitization of hematoporphyrin (HP) on cell morphology are similar to those obtained by photosensitization of TMR-TAT. HP was incubated with HeLa cells for 1 h, washed with fresh L-15 media, and irradiated at 560 nm. Black arrows in A) and B) highlight the membrane blebbing observed during light exposure.

To further confirm that the fluorescent peptides are acting on membranes when irradiated, the effect of TMR-TAT, TMR-R9, and TMR-riTAT on the membrane of red blood cells (RBCs) was examined. RBCs do not typically endocytose extracellular material to significant levels(190, 191). As a result, the effects of the peptides on the plasma membrane can be examined specifically and quantitatively. Damage to the membrane of RBCs and cell lysis can be easily monitored and quantified by bright field microscopy(192). RBCs were incubated with TMR-TAT and TMR-riTAT (1-5 μM, control experiments indicated that TMR-TAT and TMR-riTAT do not penetrate RBCs under these conditions, Fig. 2-11). No lysis was observed in the absence of irradiation of TMR (white light was used for bright field imaging, but this has no effect on the cells). Many RBCs however, adopted a crenated morphology upon incubation with the peptides (Fig. 2-12A). Crenation is indicative of a disturbance in the RBCs' membrane, an effect often observed for amphiphilic compounds, suggesting that the peptide might partially partition in the lipid bilayer(193, 194). When observed by fluorescence imaging (at low light intensity to avoid photosensitization of TMR), the peptide's fluorescence was diffusely distributed in the media (Fig. 2-11). Together, these results indicate that the fraction of peptide that might interact with the RBC membranes is small in comparison to the fraction of peptide which partitions in solution. RBCs that had been unaffected by incubation with TMR-TAT for a prolonged period of time in the absence of light (10 min) started lysing immediately upon excitation with light (Fig. 2-12A). Formation of cell ghosts could be clearly identified by bright field imaging as RBCs leaked and lost their optical contrast (Fig. 2-12A). The number of lysed ghosts was proportional to the radiant exposure (Fig. 2-11). The ghosts formed initially had a spherical shape with a diameter approximately equal to that of non-irradiated spherical and intact RBCs. Extended exposure to light however caused a dramatic shrinking of the membrane, suggesting that damage to the lipid bilayer might continue well after lysis has occurred (Fig. 2-11). Consistent with the results observed with HeLa cells, TMR alone had no lytic effect on RBCs even after prolonged light exposure (Fig. 2-12B). TMR-K9 was 5-fold less efficient than TMR-TAT and TMR-riTAT in causing photohemolysis,

suggesting again that some key features of TAT contribute to the potentiation of TMR photosensitization.

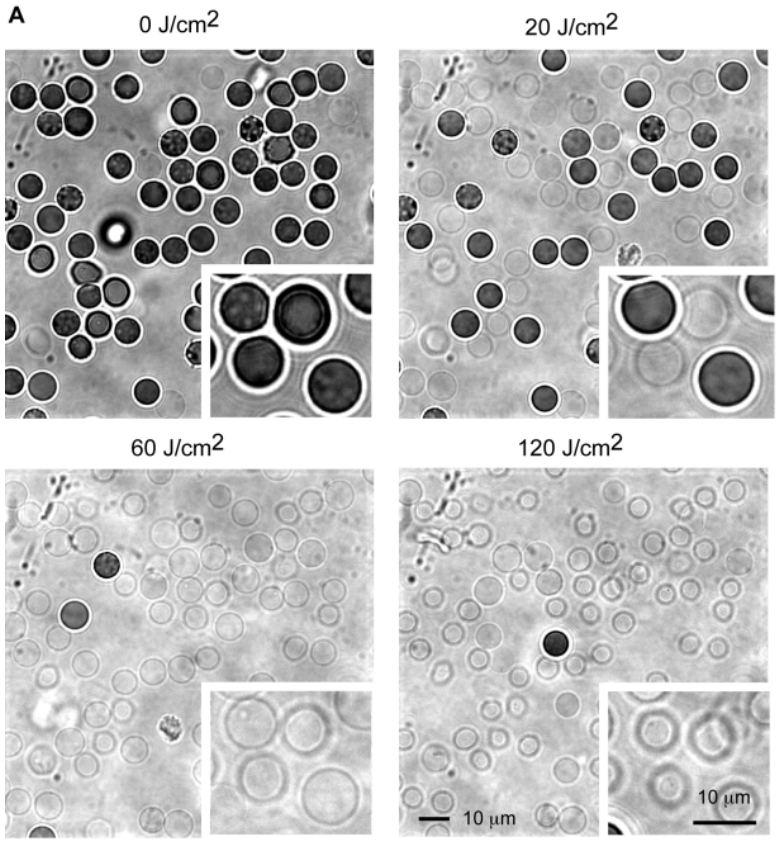

Figure 2-11.

A) Photohemolysis of RBCs with TMR-TAT. Short exposure of RBCs incubated with TMR-TAT (3 μM) to 560 nm causes lysis and formation of ghost cells as observed by bright field imaging. Lysis of more than 90% of the cells can be achieved when light exposure is increased. Initially, the ghosts formed appear to have a constant diameter as shown in the images corresponding to exposure at 20 J/cm^2 and 60 J/cm^2. As light exposure is increased, the ghosts shrink to a much smaller diameter (120 J/cm^2 image). This shrinkage was not observed when the ghosts formed by irradiation with 60 J/cm^2 of light were incubated without additional light irradiation (data not shown). These results suggest that light irradiation causes damages to membranes well after lysis as occurred.

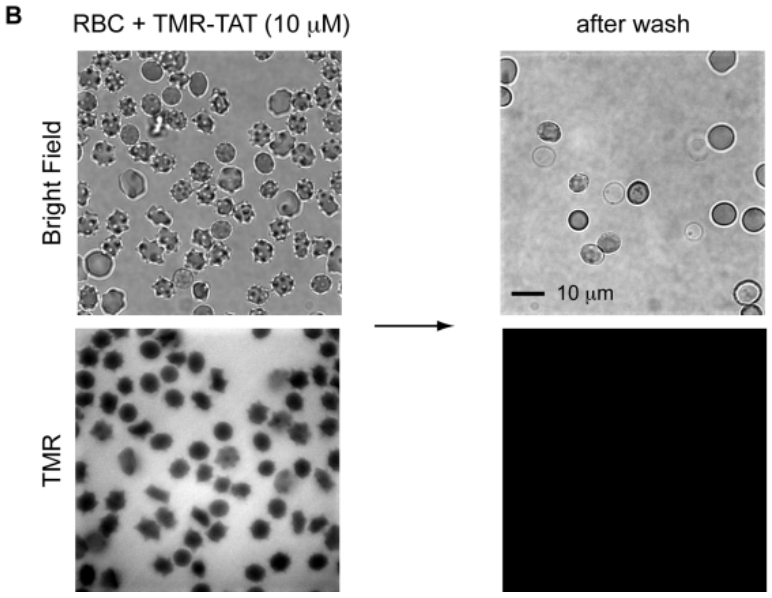

Figure 2-11. Continued

B) TMR-TAT does not appear to penetrate RBCs. RBCs were incubated with TMR-TAT (10 μM) in PBS for 1 h. The RBCs were then spun down at low speed and the supernatant was removed from the pelleted cells. Cells were rapidly washed with cold PBS (4°C) and spun down twice. Images are the bright field and TMR confocal fluorescence images before and after washing of the RBCs. During incubation, the interior of RBCs display a dark contrast when compared to the fluorescent peptide present in solution. After washing the cells, no appreciable TMR fluorescence could be detected. It is important to note that RBCs have a weak auto-fluorescence signal in the TMR channel. The contrast in the image represented was therefore adjusted to display a signal that would be above this auto-fluorescence background. In addition, light irradiation of the washed cells did not lead to photohemolysis. Together, these results suggest that TMR-TAT does not penetrate RBCs to a large extent.

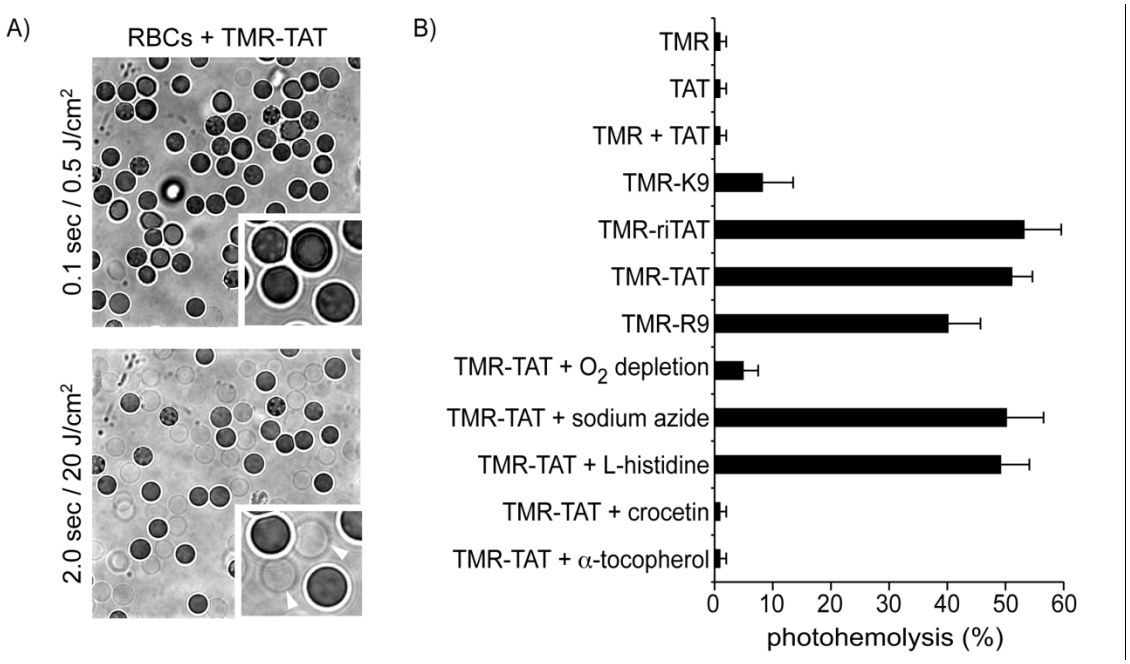

Figure 2-12. Photosensitization of TMR-TAT causes the lysis of red blood cells by the production of singlet oxygen in their membrane.

A) RBCs incubated with TMR-TAT (2 μM) have either a concave or crenated morphology initially. Irradiation of the sample at 560 nm causes formation of spherical cell ghosts (highlighted with white arrows in inserts) that lose their contrast in bright field images as the cells lyse.

B) Percentage of lysed RBCs as a function of the compounds present in the media. TMR and TMR containing peptides were used at 2 μM. All experiments were performed by irradiating the samples at 560 nm for 400 ms (~8 J/cm^2). The data in the histogram represents the average of 4 experiments and the error bars correspond to the standard deviation. No lysis was observed for any of the samples in the absence of light.

2.2.4 Mechanism of cell death involves ROS generation

To determine whether oxygen is involved in the light-induced lysis of RBCs mediated by TMR-TAT, oxygen was removed from the cell culture by degassing the incubation media with nitrogen. Under these conditions, the photohemolysis of RBCs exposed to TMR-TAT was greatly reduced (Fig. 2-12B). Co-incubation of TMR-TAT or TMR-riTAT (3 μM) with up to 50 mM sodium azide or L-histidine, two hydrophilic $^1O_2$ scavengers, caused no detectable decrease in photohemolysis(195). In contrast, addition of crocetin (50 μM), an amphiphilic carotenoid that inhibits $^1O_2$ formation, led to a dramatic reduction in photohemolysis (Fig. 2-12B)(196). A similar effect was observed upon addition of α-tocopherol acetate (60 μM), a lipophilic $^1O_2$ quencher known to accumulate in membranes and to inhibit lipid peroxidation(197, 198). A possible explanation for these observations might therefore be that crocetin and α-tocopherol acetate are able to quench singlet oxygen present in the hydrophobic environment of the membrane while other quenchers are not (Fig. 2-12B). In order to test whether $^1O_2$ is also involved in the phototoxicity observed within HeLa cells, cells were incubated with crocetin or α-tocopherol acetate prior to incubation with TMR-TAT and during light irradiation. In the case of α-tocopherol acetate, photo-induced endosomal release and cell death were still observed (data not shown). The photosensitization of TMR-TAT was, however, delayed. This is consistent with this quencher being consumed during the experiment because of its reaction with $^1O_2$. In contrast, crocetin inhibits $^1O_2$ formation without being degraded. When using crocetin, endosomal release of the peptide could be observed; although at a lesser extent than when crocetin is not present (e.g. many fluorescent endosomes remain present during the experiment, Fig. 2-13). However, cell-death was not observed under these conditions; cells did not display membrane blebbing and did not become permeable to SYTOX® Blue (Fig. 2-13). In addition, photobleaching of TMR-TAT was observed when light exposure was increased. It is difficult to determine why crocetin did not inhibit endosomal release. On the other hand, this experiment suggests that the lysis of endocytic organelles is not sufficient to cause cell death. Overall, these results suggest that singlet oxygen is involved in the membrane

disruption and cell death induced by light irradiation of TMR-TAT. They also suggest that the singlet oxygen responsible for membrane damage is generated directly in the lipid bilayer, since hydrophilic quenchers have no effects.

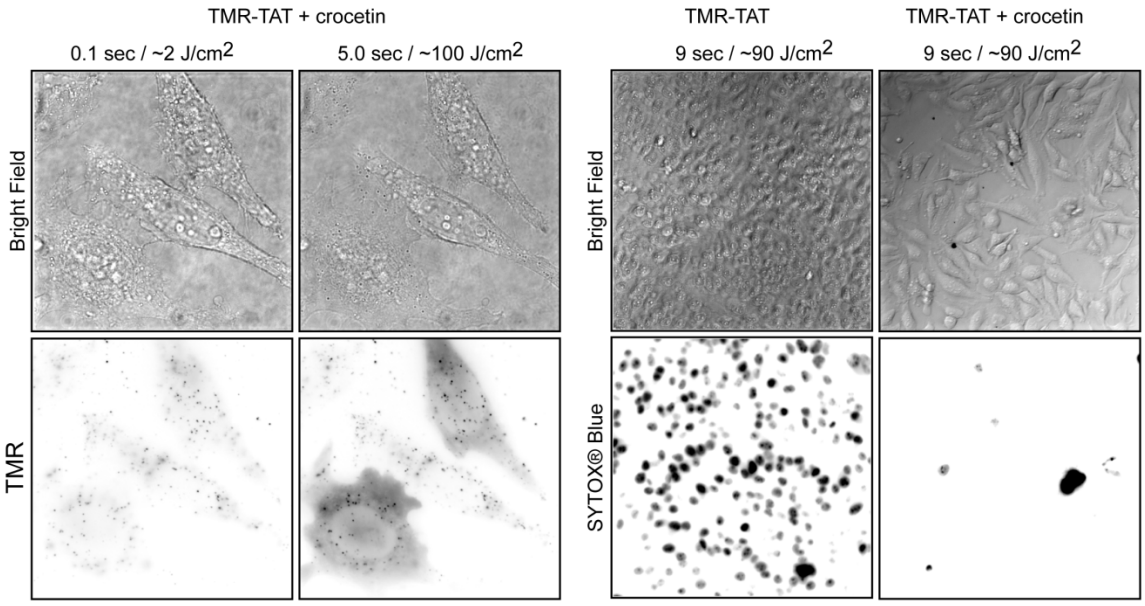

Figure 2-13. Crocetin inhibits photosensitization of TMR-TAT.

TMR-TAT (3 μM) was incubated with crocetin (50 μM) and HeLa cells for 1 h. Cells were washed with fresh L-15, placed on the microscope, and irradiated at 560 nm for the times indicated. The left panel represents cells imaged with the 100X and illustrates that endosomal release of TMR-TAT appears reduced by crocetin but not abolished. However, endosomal release is not accompanied by membrane blebbing or SYTOX® Blue staining (no signal detected, not shown) as seen when crocetin is omitted (right panel, cells are imaged with 20X objective).

2.3 Discussion

Upon light irradiation of TMR-TAT, the endosomal membrane is rapidly and efficiently disrupted. However, in my experiments, this result is also accompanied by the simultaneous destruction of cells. The peptide therefore played the role of a photosensitizer, a molecule that can induce damage of cellular components upon excitation with light. While multiple cellular events might take place as a result of illumination of the compound in a mammalian cell, the damage to cellular membranes other than that of endosomes such as RBC membranes and the plasma membrane suggests that the photocytotoxic effect is due to TMR-TAT. TMR-TAT, for instance was able to lyse the plasma membrane of HeLa cells as well as the membrane of RBCs upon light irradiation. The photocytotoxicity of the peptide also appears to involve the formation of singlet oxygen upon light irradiation. Singlet oxygen is short-lived (lifetime < 4 μs) and diffuses across only very short distances (singlet oxygen would travel a distance of ~ 220 nm in water during three lifetimes and presumably much less when reacting with biomolecules inside a cell)(132).To my knowledge, the singlet oxygen quantum yield of TMR has not been determined. However, triplet quantum yields ranging from 0.001 to 0.003 have been reported(199, 200). Because formation of the fluorophore's triplet state is required for $^1O_2$ formation, the singlet oxygen quantum yield of TMR should therefore be very low. Consequently, TMR would not be expected to act as an efficient photosensitizer. Indeed, TMR and TMR-K9 were essentially non-cytotoxic to cells under the conditions tested. Yet, TMR-TAT can reproduce some of the photo-induced effects obtained with hematoporphyrin, a prototypical photosensitizer with a singlet oxygen quantum yield of approximately 0.5(201, 129). TAT, therefore, appears to greatly enhance the phototoxicity of TMR. One possible explanation for this phenomenon might be related to how TAT interacts with membranes. TAT is known to bind heparan sulfate proteoglycans on the surface of cells and interactions with these species are important for the endocytosis of the peptide(202-205). The surface of RBCs is, however, depleted in heparan sulfate proteoglycans(206, 207). The photolysis achieved with RBCs would therefore suggest that binding to heparan sulfate

proteoglycans is not required for efficient photosensitization and that other membrane interactions are involved. Interestingly, TAT has also been shown to bind to the negatively charged head groups of phospholipids and to float on lipid bilayers at the water/lipid interface(208). While the peptide does not appear to be strongly associated with cellular membranes in my fluorescence assays, it is, however, possible that a fraction of TMR-TAT resides close to or at the lipid bilayer as indicated by the crenation of erythrocytes. TAT might then position TMR in a membrane environment that the soluble TMR or TMR-K9 do not access. Interestingly, the membrane affinity of lipophilic porphyrin-based photosensitizers is thought to be an important feature of their photocytotoxicity(129, 209). It has been proposed, for instance, that singlet oxygen generated in membranes reacts with membrane proteins or unsaturated lipids to form hydroperoxides according to the ene reaction(132). This damage to membrane constituents is sufficient to cause membrane lysis and cell death(210, 211). In addition, degradation of the formed lipid hydroperoxides might initiate the auto-catalyzed oxidation of neighboring lipids and cause a propagation of the damage done to the lipid bilayer through a chain reaction(197, 212). A similar phenomenon might take place for TMR-TAT. While singlet oxygen might be produced in low yield upon irradiation, it might nonetheless be produced in a membrane environment more susceptible to damage. Overall, these experiments suggest that singlet oxygen might be generated in a hydrophobic environment. The amphiphilic crocetin and the hydrophobic α-tocopherol acetate inhibits the photocytotoxicity of TMR-TAT, but soluble singlet oxygen quenchers such sodium azide, L-histidine, and glutathione do not. The membrane blebbing of HeLa cells and the shrinkage of RBCs further support the notion that the cell membranes and their constituents are being damaged. It is clear that photosensitization of TMR initiates these effects. Yet it is possible that TAT, beyond targeting TMR to critical cellular environments, might also play a direct role in the destruction of membranes. TAT is, for instance, able to cross lipid bilayers and, while the exact mechanisms involved in this process remain unclear, this activity is thought to involve the formation of transient pores in lipid bilayers(87, 213). TAT could therefore

aggravate the initial damage done by singlet oxygen. Elucidating whether this is the case will be the object of further studies.

The peptide had many desirable properties: photo-induced endosomal release required only short illumination with light of moderate intensities (as opposed to long irradiation time with intense lasers), this phenomenon happened in all irradiated cells, and a large fraction of the material endocytosed was released into the cytosolic space. On the other hand, photo-induced endosomal release could not be achieved without cell-death occurring either simultaneously or with a short delay. The photocytoxicity associated with TMR-TAT constitutes a significant problem when one considers using this peptide in the context of photo-induced delivery of macromolecules into live cells. Addition of crocetin to the media might help solve this problem as crocetin inhibited the photocytotoxicity of TMR-TAT. However, the efficiency of endosomal release was also reduced by this treatment. In order to maximize the potential of this delivery approach, a future challenge will be to identify efficient photo-endosomolytic peptides that do not cause cell-death. Future investigations into the exact mechanisms by which TMR-TAT functions should help in the rational design of such compounds.

Despite being a problem for delivery applications, the photocytotoxicity of TMR-TAT might have interesting applications in Photodynamic therapy (PDT)(214). PDT is a form of treatment that uses light to kill cells. PDT is used for the treatment of various cancers as well as for the management of diseases such as acne, macular degeneration, and arthritis(215-218). In a typical PDT protocol, a patient is treated with a photosensitizer, and tissues are selectively destroyed by restricting light irradiation to a local area. Interestingly, TAT and arginine-rich peptides have been conjugated to PDT photosensitizers to improve the delivery of these compounds to mammalian or bacterial cells(219, 122, 220). A common assumption in these reports and in this field in general, is that a high singlet oxygen quantum yield is a required characteristic for an ideal PDT photosensitizer. This is based on the idea that the more singlet oxygen is generated, the more cellular damage is achieved. These results suggest, however, that addition of TAT to a chromophore can compensate for a low singlet oxygen quantum yield and convert

the innocuous TMR compound into a potent photosensitizer. Overall, this means that TAT can, in addition to improving the cellular distribution of known PDT photosensitizers, increase the photodynamic potential of compounds that would otherwise not be considered as photosensitizers. This principle might lead to significant opportunities for the development of novel peptide-based PDT agents.

2.4 Materials and methods

2.4.1 Peptide synthesis

To test the photo-endosomolytic activity of CPP-fluorophore conjugates, four peptides conjugated to the fluorophore 5(6)-carboxytetramethylrhodamine (TMR) were examined: the CPP TAT (GRKKRRQRRR), retro-inverso TAT (riTAT, rrrqrrkkrgy), the CPP R9 (RRRRRRRRR), and K9 (KKKKKKKKK). TMR was chosen as a model fluorophore because it is not toxic to cells in both the absence and presence of light. It is also commonly used for live cell imaging and it is synthetically readily accessible. Finally, the fluorescence of TMR is not as pH-dependent as that of fluorescein. Therefore, TMR is not affected by the acidic pH of endosomes to the extent that fluorescein is. Peptides were synthesized by solid-phase peptide synthesis using standard F-moc chemistry and purified by HPLC. In TMR-TAT and TMR-R9, the amino terminus of the peptide was directly coupled to TMR. riTAT, a peptide in which the TAT sequence is reversed and the constituent amino acids have a D rather than a L-configuration, was prepared to obtain an analogue of TAT that would be resistant to degradation by cellular proteases. TMR was conjugated at the N-terminus of the peptide. TMR-K9 is comprised of 9 positively charged lysine residues and serves as a control. This peptide is endocytosed by cells and therefore it is localized inside endosomes like TAT or R9. However, K9 does not have the cell penetration activity attributed to TAT and R9.

TMR-TAT (TMR-GRKKRRQRRRG-NH_2) expected mass: 1865.0 Da, observed mass: 1866.1 Da. TMR-R9 (TMR-RRRRRRRRRG-NH_2) expected mass: 1893.2 Da, observed mass: 1894.4 Da. TMR-riTAT (TMR-rrrqrrkkrgy-OH) expected mass: 1973.3

Da, observed mass: 1975.3 Da. TMR-K9 (TMR-KKKKKKKKK-NH_2) expected mass: 1583.0 Da, observed mass: 1583.3 Da.

2.4.2 Cell-based assays

HeLa (human cervical adenocarcinoma) and COS-7 (SV40 transformed African green monkey kidney fibroblast-like cell line) cells were obtained from ATCC. COLO 316 (human ovarian carcinoma) were obtained from Robert Burghardt (Department of Veterinary Integrative Biosciences, Texas A&M University)(221). Cells were cultured in DMEM supplemented with 10% fetal bovine serum (FBS) and maintained at 37°C in a humidified environment with 5% CO_2. Cells were plated in 8-well dishes so that the cells were 70% confluent after 24 h, washed 3 times with L-15 media, incubated with 3 to 10 μM peptides at 37°C for 1 h, washed 3 times with L-15, and imaged. Alternatively, cells were incubated in L-15 at 4 °C to inhibit the endocytic uptake of peptides. In this case, cells were imaged with the peptide still present in solution and the low temperature was maintained for the entire duration of imaging. For photosensitization, cells were exposed to light (λ_{ex}= 560±20 nm) for the indicated time points. Plasma membrane disruption was detected by addition of the cell-impermeable DNA stain SYTOX Blue (5 μM) during or after photosensitization. Whole blood was purchased from Gulf Coast Regional Blood Center (Houston, TX). Erythrocytes were centrifuged for 5 min at 1500g and the erythrocyte pellet was resuspended with PBS. This was repeated three times to remove plasma and buffy coat. The erythrocytes (50% volume in PBS) were diluted in PBS to a final concentration of 0.25%. Indicated concentration of peptide was added to the medium and the samples were added to the wells of an 8-well chamber glass slide (Nunc). Cells were typically allowed to settle to the bottom of the dish for 5 min prior to imaging so as to obtain a layer of cells in the focal plane.

2.4.3 Fluorescence imaging

Cells were placed on an inverted epifluorescence microscope (Model IX81, Olympus, Center Valley, PA) equipped with a heating stage maintained at 37 °C. The microscope is configured with a spinning disk unit to perform both confocal and wide-field fluorescence microscopy. Images were collected using a Rolera-MGI Plus back-

illuminated EMCCD camera (Qimaging, Surrey, BC, Canada). Images were acquired using bright field imaging and two standard fluorescence filter sets: Texas Red (Ex= 560±20 nm / Em= 630±35 nm), and CFP (Ex= 436±10 nm / Em= 480±20 nm). The excitation light was from a 100W halogen lamp (Olympus USH 1030C) passed through the filter cubes and 40 or 100X objective lenses. Neutral density filters (ND 1, 2, 3, or 4 on the instrument, corresponding to 100, 25, 12.5, or 5% transmittance) and different exposure times were used to modulate the amount of light samples were exposed to. The bright field and fluorescence intensities of cells and ghosts were measured using the SlideBook 4.2 software (Olympus, Center Valley, PA). To determine the percentage of cells stained by SYTOX® Blue, cells were imaged with a 20X objective by phase contrast. Ten to twenty images were acquired for each experiment. The total number of cells in a given image was determined from the phase contrast image while the number of dead cells was determined by identifying cells containing a blue fluorescent nucleus stained by SYTOX® Blue. Cell viability was determined by establishing a ratio of dead cells/total number of cells for each sample (at least 1000 cells were counted in each experiment and each experiment was repeated 3 times).

Irradiances at the specimen were 100 mW/cm^2 when no neutral density filter and no objective were present in the light path (and, for instance 5 mW/cm^2 when ND4 was inserted). Irradiances were measured using a monochromic photometer (model 840-c, Newport, Irvine, CA). Irradiation area has a diameter of 1.3 cm without objective but the light beam is focused into an area of $3x10^{-3}$ cm^2 by the 100X objective. Irradiances can therefore be approximated to be at 21 or 420 W/cm^2 with ND4 or ND1, respectively. Irradiances provided in the figure legends are based on these calculations. To confirm that the irradiances measured on the microscope were accurate, experiments were also reproduced, when possible, using light illumination with a collimated light source from Oriel (Stratford, CT) equipped with a 500 W Hg lamp. Selective irradiation at 560 nm was performed using an analytical line filter (Oriel, 9.4 nm bandwidth). In this case, irradiances of the light beam (diameter of 2.5 cm) could be measured more precisely using the monochromic photometer.

3. TAT MEDIATED PCI RESULTS IN CELL KILLING BY CAUSING RELEASE OF CALCIUM INTO CELL CYTOSOL*

3.1 Introduction

In Section 2, it was reported that TMR-TAT acts as a photosensitizer that can destroy membranes. TMR-TAT escapes from endosomes upon light exposure of moderate doses. The Fl-CPP conjugate TMR-TAT was also shown to trigger the photohemolysis of RBCs and that singlet oxygen production was involved in the process. The endosomal escape of TMR-TAT upon irradiation was however, accompanied by loss of plasma membrane integrity, membrane blebbing and cell death. The Fl-CPP conjugate also caused destruction of cells when applied extracellularly. The photolytic and photocytotoxic effects by TMR-TAT were reported to be inhibited by hydrophobic singlet oxygen quenchers but not by hydrophilic quenchers. It can be concluded hence from previous results obtained that the cell-penetrating peptide TAT can convert an innocuous fluorophore such as TMR into a potent photolytic agent. The TMR-TAT mediated photolytic effects involve the targeting of the fluorophore to cellular membranes and the production of singlet oxygen within the hydrophobic environment of the membranes. These findings can thus be relevant for the design of reagents with photo-induced endosomolytic activity. The photocytotoxic effects observed upon TMR-TAT endosomal release could limit the application of TMR-TAT as a delivery tools.

In this section, I investigate the mechanisms of cell death that accompanies endosomal release of the Fl-CPP conjugate TMR-TAT. The membrane blebbing and cell death effects are observed immediately following the release of TMR-TAT from the endocytic vesicles. The understanding of how lysis of endocytic organelles affects cellular physiology and causes cell death will be very crucial for the development of optimal delivery methodologies.

---

* Reprinted with permission from "Tat-mediated photochemical internalization results in cell killing by causing the release of calcium into the cytosol of cells" Muthukrishnan, N., Johnson, G. A., Lim, J., Simanek, E. E. and Pellois, J. P., 2012. *Biochim Biophys Acta* **1820**, 1734-43, Copyright 2014 by Elsevier B.V.

3.2 Results

3.2.1 Microinjection of TMR-TAT followed by light irradiation does not cause membrane blebbing or cell death

TMR-TAT is photolytic towards endosomes but also towards other biological membranes such as the plasma membrane of red blood cells(133). I was therefore interested in testing the hypothesis that TMR-TAT might kill cells after escaping from endosomes by causing photolytic damage to other intracellular organelles. In order to determine whether TMR-TAT induces a phototoxic response when present in the cytosolic space of cells, TMR-TAT was directly microinjected into the cytoplasm of HeLa cells (Fig. 3-1). Cells were then irradiated under conditions similar to that used for PCI. The cell impermeable DNA stain SYTOX® Blue was added to the media in order to assess the permeability of the plasma membrane. A PCI experiment for which TMR-TAT was incubated with cells to permit accumulation inside endocytic organelles was carried out in parallel. In both experiments, irradiation of the cells was performed directly on the microscope by using the RFP channel to excite TMR (Ex = 560 nm). In the PCI experiment, TMR-TAT escaped from endosomes and distributed in the cytosol and nucleus of cells upon brief irradiation (Fig. 3-1). As previously reported PCI was accompanied by rapid plasma membrane blebbing and staining with SYTOX® Blue, indicative of plasma membrane disruption and cell killing(133). In contrast, when similar irradiation conditions were used, cells containing microinjected TMR-TAT did not show loss of plasma membrane permeability or blebbing. In order to compare the amount of TMR-TAT microinjected inside cells to that of TMR-TAT released into the cell after PCI, the whole cell fluorescence intensities of cells post-PCI as well as the microinjected cells were measured. Based on this analysis, the amount of TMR-TAT present in the cytosol of microinjected cells was equal or greater than that obtained after PCI (please note the greater TMR fluorescence intensity for the cells microinjected in Fig. 3-1; the contrast is kept constant between the different images). Microinjected TMR-TAT therefore, appears to be overall less phototoxic than TMR-TAT released from endosomes.

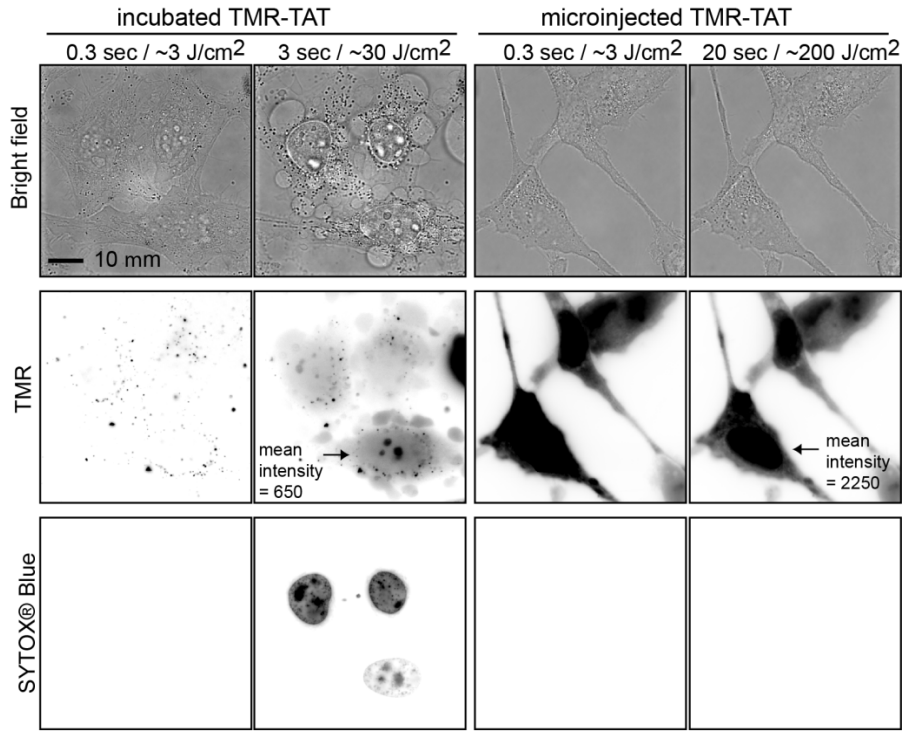

Figure 3-1. Irradiation of endocytosed TMR-TAT kills cell while irradiation of microinjected TMR-TAT does not.

A) HeLa cells were incubated with TMR-TAT (3 μM), washed, and irradiated at 560±20 nm through a 100 X objective on a wide-field microscope. The time displayed on the images represents the total light exposure time. The fluorescence signal of TMR-TAT (TMR channel) initially shows a punctate distribution consistent with the compound being present within endocytic organelles. Brief irradiation at 560 nm (TMR channel) causes TMR-TAT to redistribute throughout the cells. This is accompanied by blebbing of the plasma membrane (visible in the bright field image) and permeabilization of the plasma membrane, as seen by staining of the cells with SYTOX Blue. The TMR and SYTOX BLUE fluorescence signals are represented as inverted monochrome (black = fluorescent signal, white = no signal).

B) TMR-TAT was microinjected into the cell and irradiated at 560 nm immediately. Irradiation had no apparent effect on the cells under conditions where the peptide is more concentrated inside cells and the light dose is more intense than in the incubated sample. Identical data were obtained with the protease resistant TMR-riTAT (not shown).

3.2.2 TMR-S-S-TAT kills cells as efficiently as TMR-TAT

It has previously been shown that the attachment of TMR to TAT is necessary to mediate photo-induced lysis(133). I therefore reasoned that, if TMR-TAT exerts phototoxic effects after it escapes from endosomes, the phototoxicity of the compound could be abolished by introducing a linker between TMR and TAT that would cleave upon entry of the peptide into the cytosolic space of irradiated cells. With this principle in mind, TMR and TAT were attached to one another through a disulfide bridge to generate TMR-S-S-TAT. Disulfide bonds are cleaved within seconds in the reducing environment of the cytosol but not inside endosomes of HeLa cells(222). TMR-S-S-TAT was as efficient as TMR-TAT at inducing the lysis of red blood cells (Fig. 3-2A). Addition of the cytosolic reducing agent glutathione (GSH) however, abolished the photolytic effect of TMR-S-S-TAT but not that of TMR-TAT. These results are therefore consistent with the idea that TMR-S-S-TAT is inactivated by reduction. Like TMR-TAT, TMR-S-S-TAT was endocytosed by cells (Fig. 3-3) and released from endosomes upon irradiation with light (Fig. 3-4). Interestingly, TMR-S-S-TAT led to cell-death as readily as TMR-TAT. Cell-death was in particular not reduced when PCI irradiation was performed at a slow frequency (every 10 s) so as to allow sufficient time for TMR-S-S-TAT to be reduced in the cytosol in between small bursts of endosomal release (100 ms excitation, Fig. 3-5). Overall, these results suggest that TMR-TAT does not cause the cell-death observed during PCI by causing photolytic damage in the cytosolic space of cells.

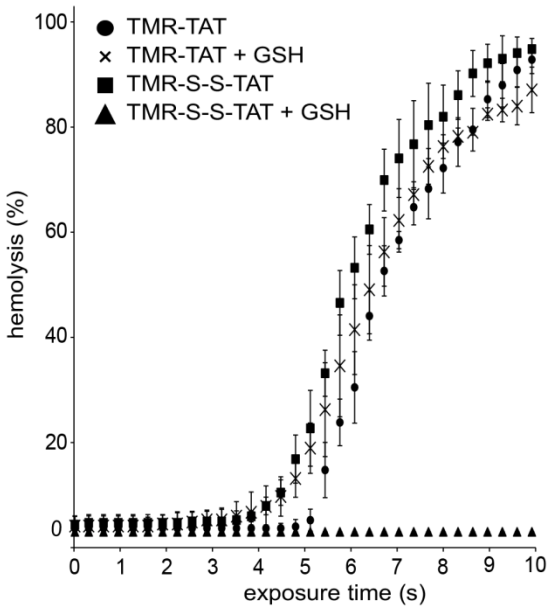

Figure 3-2. TMR-S-S-TAT loses its photohemolytic activity upon reduction but displays the same cell killing activity as TMR-TAT.

A) Peptide-mediated lysis of red blood cells as a function of exposure time (irradiation at 560 nm). TMR-TAT and TMR-S-S-TAT (3 μM each) display similar photohemolytic activity. The activity of TMR-TAT is unaffected by the reducing agent glutathione (GSH, 5 mM) but that of TMR-S-S-TAT is abolished.

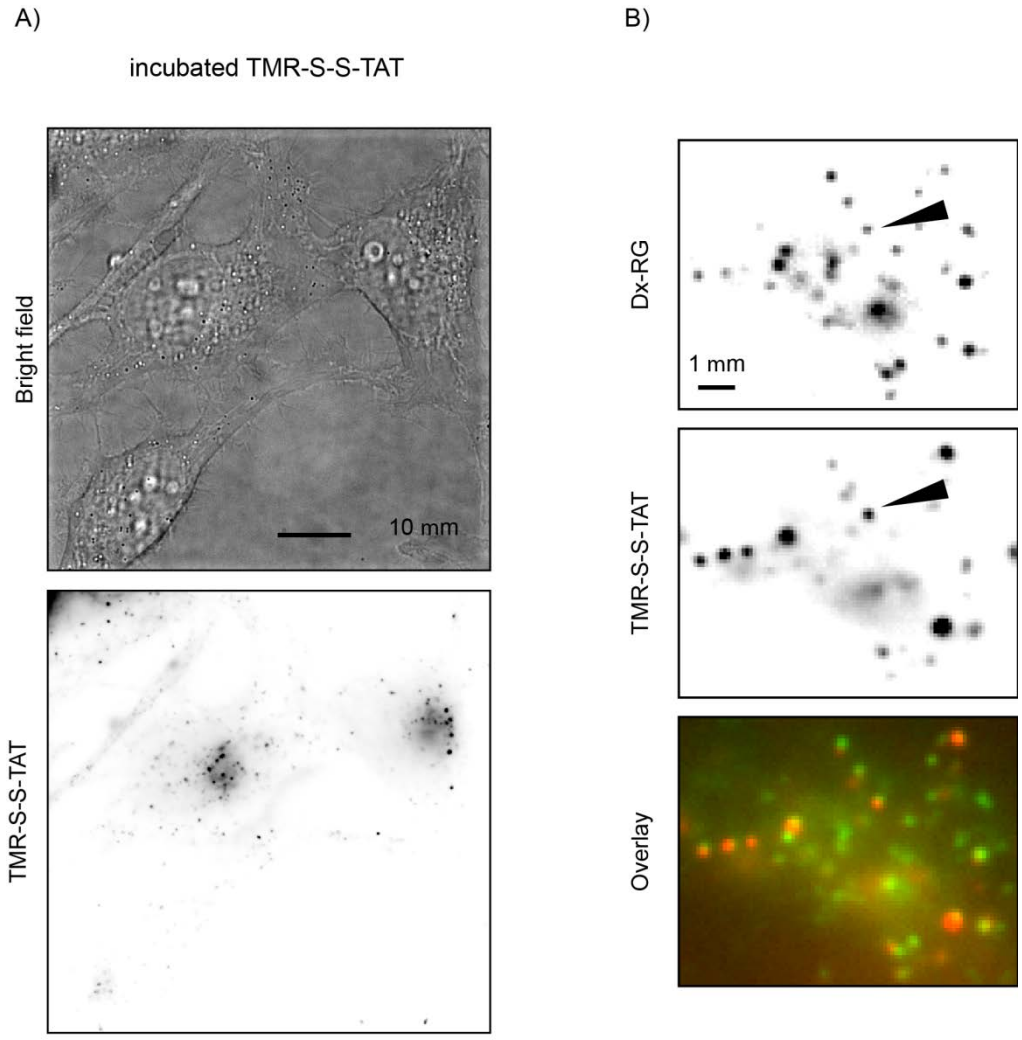

Figure 3-3. TMR-S-S-TAT is endocytosed by HeLa cells.

A) TMR-S-S-TAT has a punctate distribution inside cells. Bright field and fluorescence microscopy of HeLa cells incubated with TMR-S-S-TAT (3 μM) (the TMR image is represented as an inverted monochrome).

B) TMR-S-S-TAT co-localizes with the pinocytosis marker 3 kDa Dextran Rhodamine green (Dx-RG). A black arrow indicates an endocytic organelle that contains both TMR-S-S-TAT and Dx-RG.

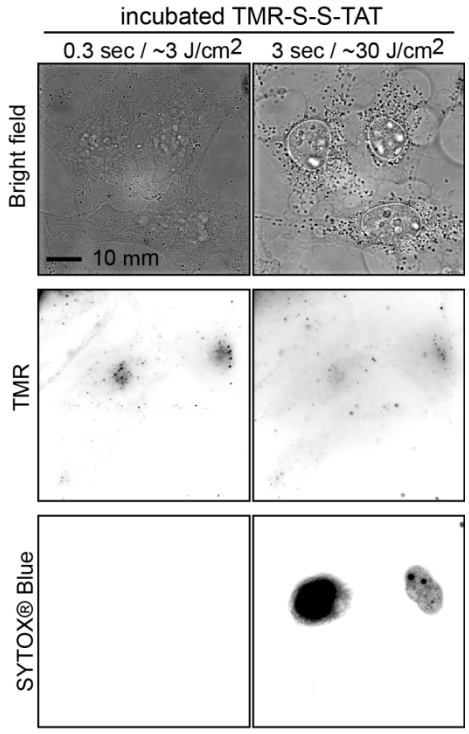

Figure 3-4. TMR-S-S-TAT endosomal release causes cell death in HeLa cells.

Irradiation of endocytosed TMR-S-S-TAT results in plasma membrane blebbing and permeabilization in a manner similar to TMR-TAT. Note that the TMR signal does not show the nucleoli staining typical of TAT after irradiation (see Fig. 3-1). The TMR signal is also weak, presumably because the reduced fluorophore is able to diffuse out of the permeabilized cell more readily than TMR-TAT.

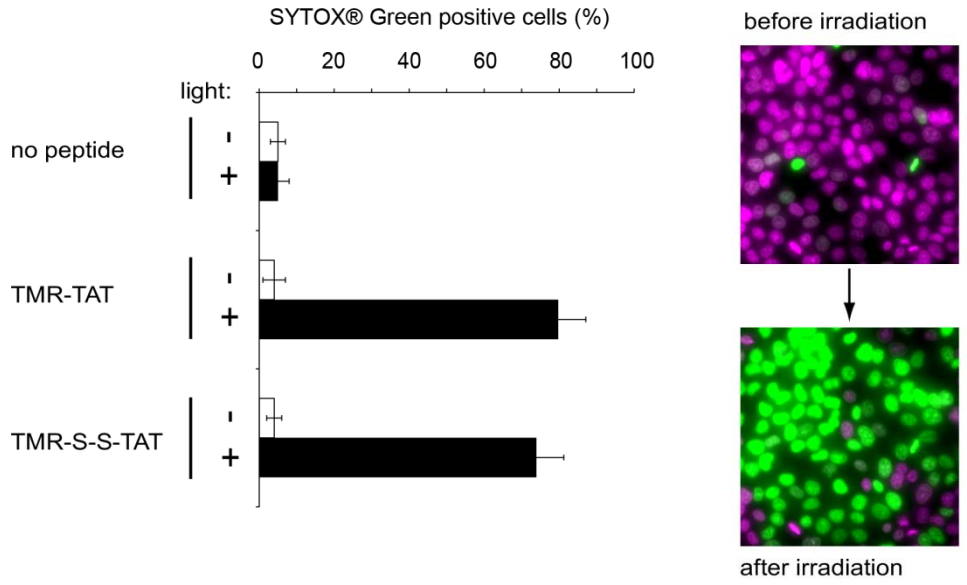

Figure 3-5. Cytotoxicity of TMR-S-S-TAT.

Cytotoxicity of TMR-S-S-TAT upon light irradiation (5 s light dose) as compared to TMR-TAT (left)

Representative fluorescence overlay images of HeLa cells stained with Hoechst (pseudo-colored purple) and SYTOX® Green (pseudo-colored green) before and after light exposure (right)

3.2.3 TMR-TAT endosomal release is accompanied by an increase in cytosolic calcium concentration

The previous results suggested that cell death observed during TMR-TAT mediated PCI (TM-PCI) might be a direct result of the photo-induced lysis of endocytic organelles. In particular, TM-PCI might induce the release of toxic molecules into cells other than the PCI agent itself. While the PCI-mediated release of lysosomal hydrolytic enzymes might impact cell viability, the rapidity with which cell death occurs prompted us to test other potential causes of cell death. In particular, it has been established that an increase in the concentration of calcium in the cytosol can cause cell death(141). Interestingly, early endosomes, late endosomes and lysosomes are thought to contain calcium at high concentrations(75, 223, 140, 224). I therefore hypothesized that TMR-TAT mediated PCI could trigger cell death by releasing pools of calcium from endosomes and lysosomes. To test this idea, the fluorescent calcium indicator, fluo-4 (Kd~345 nM) was used to detect the increase of cytosolic calcium during TM-PCI(225, 226). As shown in Fig. 3-6, TMR-TAT endosomal release was accompanied by a burst increase in the cytosolic calcium levels. This increase in fluorescence is consistent with the calcium indicator being saturated and indicates that the $[Ca^{2+}]_{cyt}$ increases from less than 100 nM to over 1 μM after PCI. The L-15 medium used for incubation in these assays initially contained calcium at a physiological concentration of 1.3 mM. Calcium might therefore enter the cell from the extracellular milieu during PCI. To test this hypothesis, the experiment was repeated with a medium formulated without calcium and supplemented with the calcium chelator EGTA. This medium was used to wash the cells after incubation with TMR-TAT and during light irradiation and microscopy. PCI was performed immediately after incubating the cells with the calcium-free medium so as to create a condition where calcium was removed from the extracellular milieu without causing the depletion of the intracellular pools of calcium. PCI performed under these conditions led to an increase in fluorescence of fluo-4 only slightly reduced in comparison to that observed when calcium is present in the medium (Fig. 3-6B). Moreover, plasma membrane blebbing and permeabilization also accompanied the PCI

procedure in calcium-free media. It should therefore be noted that permeabilization presumably accounts for the decrease in signal observed after 4 s of irradiation. Plasma membrane permeabilization might also contribute to the smaller signal observed for TM-PCI performed in the absence of extracellular calcium. Together, these results suggest that $[Ca^{2+}]_{cyt}$ increases greatly during PCI and that the calcium released into the cytosol comes from an intracellular pool rather than from the extracellular milieu.

3.2.4 Import of calcium into mitochondria induces TM-PCI mediated cell killing

Following the initial burst of fluorescence of fluo-4, it was observed that the signal of the calcium indicator localized at continuous tubular structures (Fig. 3-7) corresponding to mitochondria (Fig. 3-8). A link between mitochondrial calcium and cell death has been clearly established in the literature and therefore I decided to test whether calcium import into the mitochondria could account for the rapid cell death observed. To test this hypothesis, the inhibitor of mitochondrial calcium import ruthenium red (RuRed) was used(227, 173, 228). Mitochondrial calcium is also known to cause opening of the permeability transition pore (PTP), an event that can lead to apoptosis. PTP opening can be inhibited by cyclosporin A(229, 230, 172). TMR-TAT mediated PCI was therefore performed with cells incubated with RuRed or cyclosporin A to assess the relationship between Ca^{2+} mitochondrial import and cell death (Fig. 3-9). Cells treated with RuRed or cyclosporin A showed a burst of fluo-4 fluorescence similar to that observed in an untreated control sample, indicating that these inhibitors do not affect the cytosolic flux of Ca^{2+} (Fig. 3-9B). However, RuRed and cyclosporin A inhibited the rapid plasma membrane blebbing and permeabilization obtained during TM-PCI. These data suggest that calcium import into mitochondria and opening of the PTP are causative factors to the rapid cell death observed during the TM-PCI.

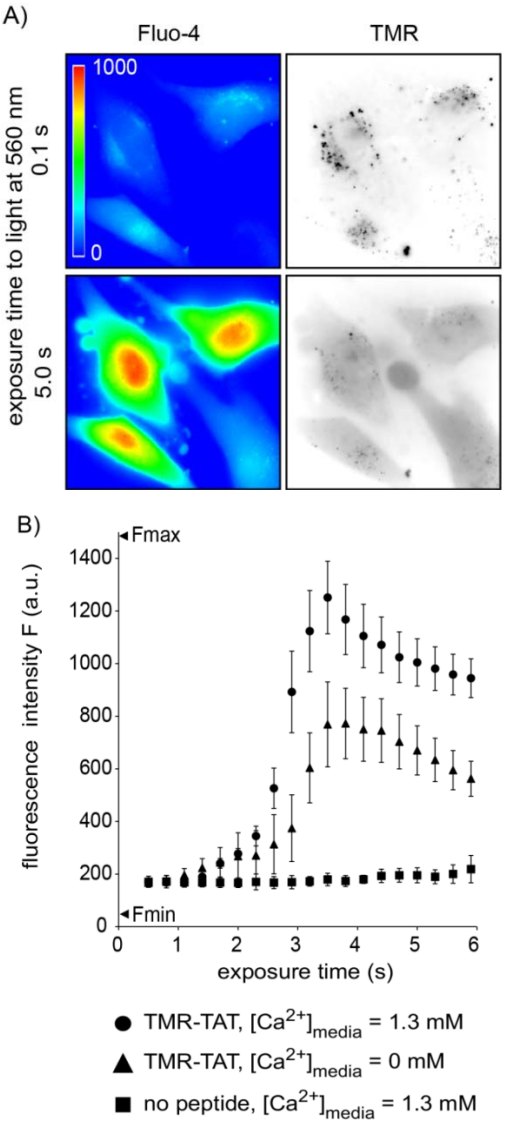

Figure 3-6. TM-PCI causes an increase in the cytosolic concentration of calcium.

A) Images of HeLa cells incubated with TMR-TAT and the calcium indicator fluo-4AM. The fluo-4 images are pseudo-colored based on the fluorescence intensity of the probe. Images representing the distribution of TMR-TAT before and after light irradiation are presented as inverted monochromes.

B) Intensity of the fluo-4 signal as a function of light exposure time (irradiation at 560 nm). Cells were incubated with fluo-4AM alone, or with TMR-TAT (3 μM) in L-15 containing 1.3 mM $CaCl_2$. Cells were then placed in fresh medium containing 0 or 1.3 mM $CaCl_2$. Cells were irradiated immediately so as to prevent depletion of calcium intracellular stores for the cells lacking calcium in the extracellular milieu.

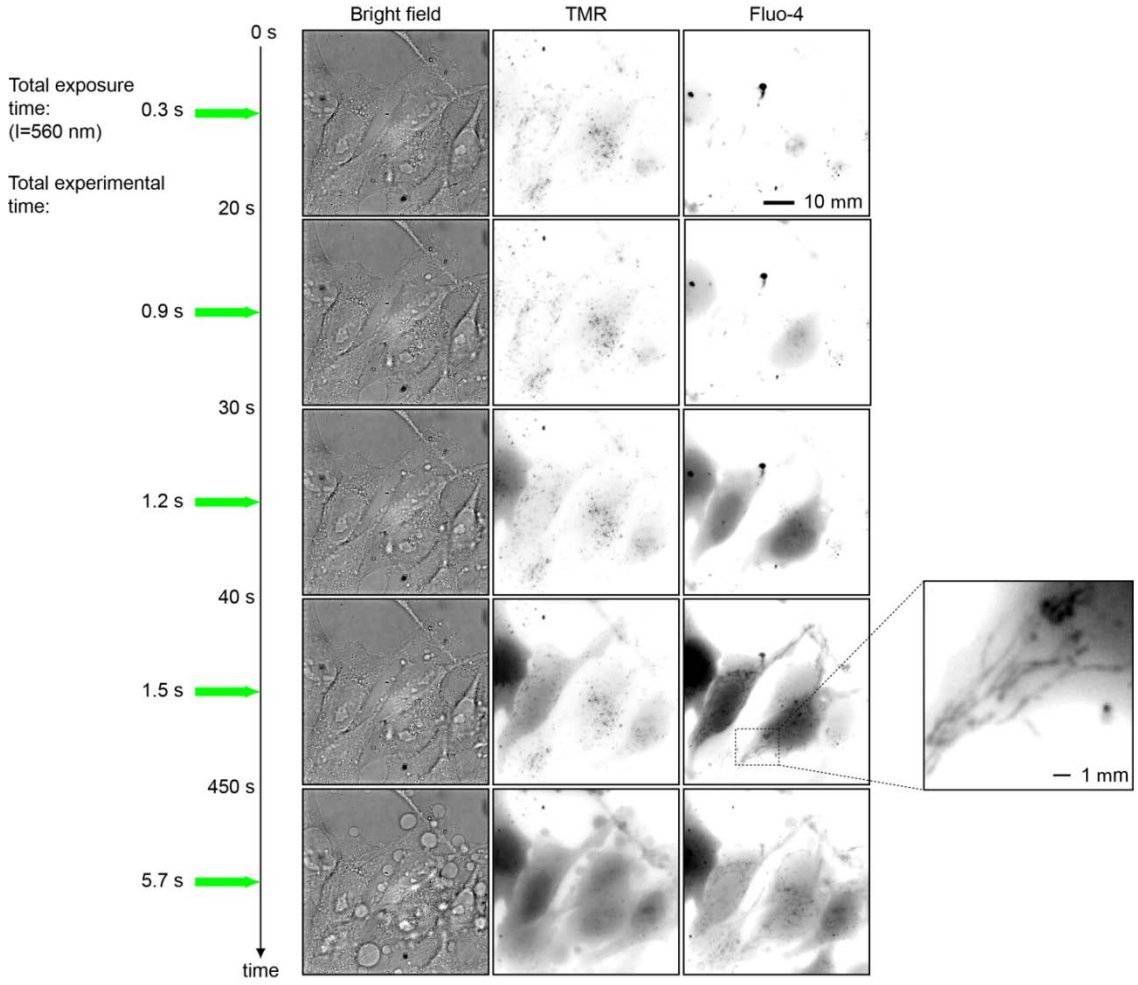

Figure 3-7. Time-lapse experiment of TM-PCI performed on HeLa cells incubated with TMR-TAT (3 μM) and fluo-4AM (5 μM).

Cells were irradiated at 560 nm for 300 ms every 10 sec. The total irradiation time is indicated with green arrows while the total experimental time is indicated on the axis. The fluorescence images of TMR-TAT and fluo-4 are represented as inverted monochromes.

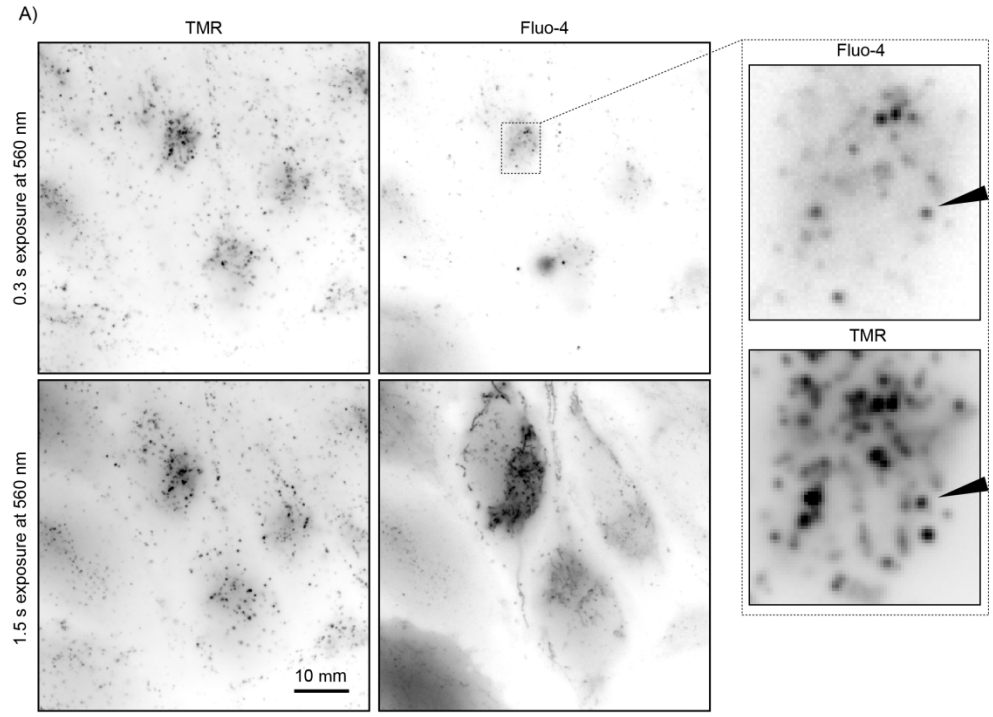

Figure 3-8. Fluo-4 localizes inside endocytic organelles before irradiation and in the mitochondria after light exposure.

A) Fluorescence imaging of HeLa cells incubated with TMR-TAT (3 μM) and fluo-4 AM (5 μM). Cells were irradiated at 560 nm for 0.3 and 1.5 sec. The black arrow indicates endocytic organelles that contain both TMR-TAT and a fluorescent signal for fluo-4. These results are consistent with those of Fig. 3-10 and indicate that calcium might be present inside endocytic organelles in which TMR-TAT is trapped prior to TM-PCI. Fluo-4 redistribute into tubular organelles after irradiation.

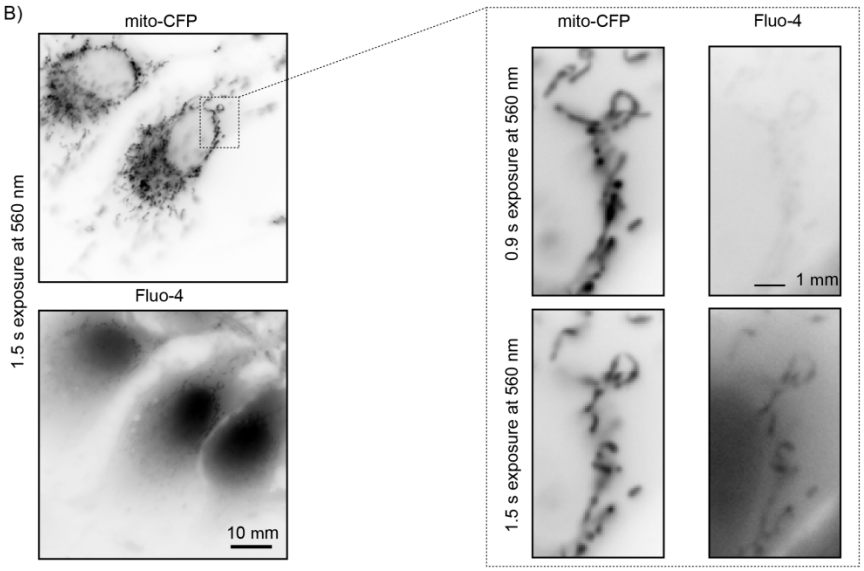

Figure 3-8. Continued.

B) Co-localization of fluo-4 with the mitochondrial marker pTagCFP-mito after TM-PCI. Experiments were performed as in A with cells transiently transfected with pTagCFP-mito. Images were acquired after 0.9 and 1.5 sec irradiation. These results indicate that fluo-4 can either detect an increase in calcium concentration in mitochondria or that fluo-4 can penetrate these organelles after TMR-PCI.

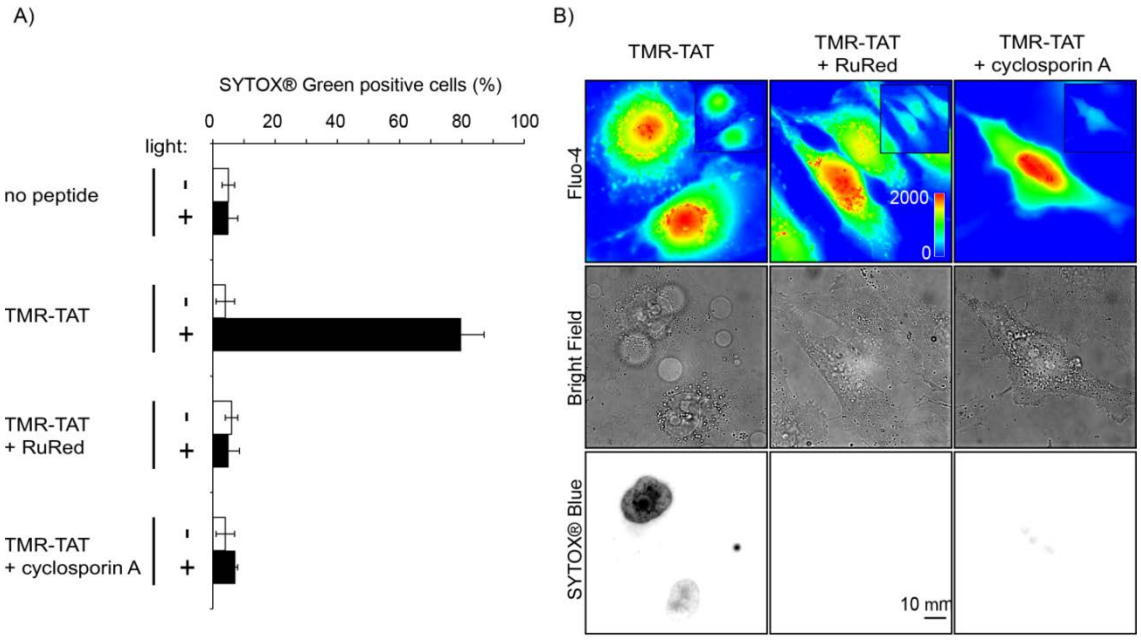

Figure 3-9. Ruthenium red (RuRed) and cyclosporin A inhibit cell death by TM-PCI.

A) HeLa cells were incubated with TMR-TAT (3 μM) in the absence or presence of RuRed (5 μM) or cyclosporin A (40 μM). Cells were irradiated at 560 nm for 3 sec and cell death was measured by counting the number of cells stained by SYTOX Blue 30 min after irradiation.

B) Images of a similar experiment performed with cells incubated with fluo-4AM (5 μM). Images of the fluo-4 signal before (insert) and after irradiation are pseudo-colored based on the intensity of the fluorescence signal. Presence of RuRed or cyclosporin A does not affect the increase of $[Ca^{2+}]_{cyt}$ observed upon irradiation. However, membrane blebbing and permeabilization are observed when cells are incubated with TMR-TAT alone but not when RuRed or cyclosporin A is added.

3.2.5 TMR-TAT co-localizes with calcium containing endocytic vesicles

The previous results establish that calcium is released into the cytosol of cells during TM-PCI. In order to test whether calcium is actually released from endocytic organelles during TM-PCI, calcium depletion experiments were performed. Cells were incubated with TMR-TAT in media in which calcium was chelated by EGTA (Fig. 3-10). Because EGTA is cell impermeable, it is expected that EGTA would be endocytosed along with TMR-TAT and chelate calcium in the lumen of endocytic organelles. After incubation, the medium was replaced with L-15 containing 1.3 mM calcium so as to not deplete other intracellular calcium stores. TM-PCI led to endosomal release of TMR-TAT without causing an increase in fluo-4 fluorescence in the cytosol of cells (TMR-TAT uptake and endosomal release was similar to the conditions lacking EGTA, Fig. 3-10B), These results are consistent with the notion that calcium present within endocytic organelles is involved in the increase in $[Ca^{2+}]_{cyt}$ observed during TM-PCI. In addition, a quantitative cell viability assay was performed to establish that cells incubated with EGTA did not die upon light irradiation (Fig.3-10C), further confirming that the release of calcium in the cytosol of cells is mediating cell death. Next, I tested whether TMR-TAT would localize inside late endosomes and lysosomes. This is because high concentrations of calcium have already been detected in these organelles(75, 140, 223, 224). For these experiments, cells were transfected with Cerulean-LAMP1, a marker of late endosomes and lysosomes(231). As shown in Fig. 3-11A, TMR-TAT co-localizes with these organelles prior to light irradiation. Upon irradiation, the TMR-TAT signal vanishes from Cerulean-LAMP1 positive organelles (as shown in Fig. 3-11A) and is distributed into the cytosol (as previously shown in Fig. 3-1). Importantly, the TMR signal is still present in some organelles, thereby indicating that the loss of signal observed is not due to photobleaching.

These data therefore suggest that TMR-TAT accumulates in organelles known to contain calcium and that TMR-TAT can escape from these organelles upon irradiation. To further confirm these results, it was tested whether endocytic organelles containing TMR-TAT also contain calcium. This was determined by incubating cells with TMR-

TAT and with the cell-impermeable calcium indicator fura-2. Fura-2 has an excitation maximum at 380 nm in its unbound form (emission is at 510 nm). This excitation maximum shifts to 340 nm when calcium is present inside endocytic organelles containing TMR-TAT.

3.2.6 TMR-TAT mediated PCI causes release of co-localized content from endocytic vesicles

Next, I tested whether TM-PCI causes the release of the luminal content of endosomes. TMR-TAT was co-incubated with the pinocytosis marker 3 kDa Dextran-Rhodamine Green (Dx-RG) (Fig. 3-11C). Prior to PCI, the fluorescence signals of TMR-TAT and Dx-RG co-localized in a punctate distribution consistent with the molecules being trapped inside endocytic organelles. Upon light irradiation, the signals of both TMR-TAT and Dx-RG redistributed homogeneously throughout the cell. These results therefore suggest that TMR-TAT is able to cause the release of molecules trapped in the lumen of endocytic organelles. Overall, these results indicate that TMR-TAT localizes within endocytic organelles that contain calcium in their lumen and that light irradiation can cause the release of the lumenal content of these organelles into the cytosol of cells.

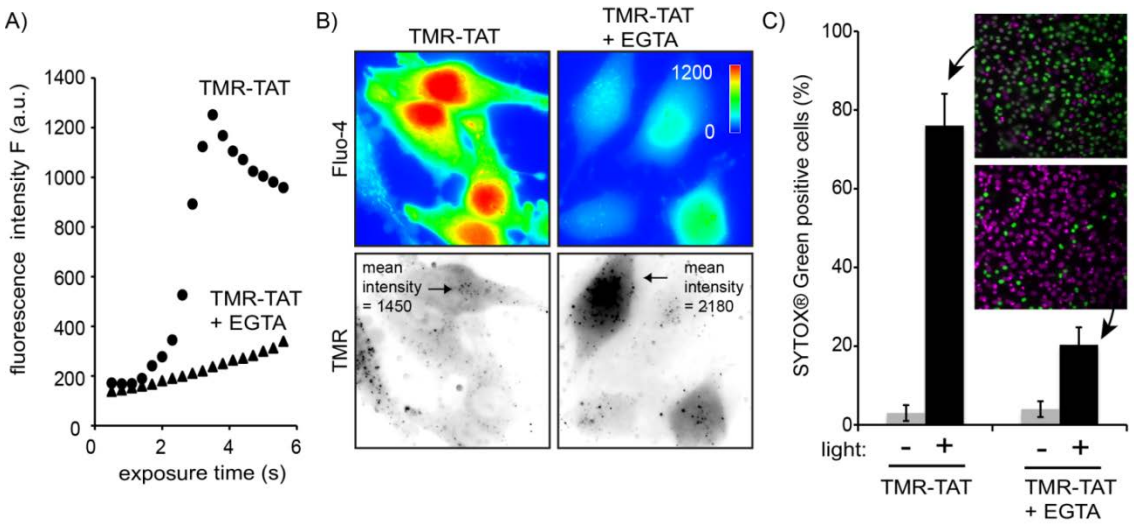

Figure 3-10. Co-incubation of TMR-TAT with the cell-impermeable calcium chelator EGTA inhibits cell death induced by TM-PCI.

A) HeLa cells were incubated with TMR-TAT (3 μM) in media containing calcium (1.3 mM) with or without EGTA (2 mM) for 30 min. Cells were then washed and imaged in media containing calcium (1.3 mM) to avoid calcium depletion of intracellular organelles. As EGTA is cell-impermeable, it is expected to accumulate inside endocytic organelles with TMR-TAT. Fluo-4 imaging indicates that TMR-PCI did not cause a significant increase in fluo-4 signal as compared to the control without EGTA present.

B) Fluorescence imaging of cells incubated with EGTA and TMR-TAT after exposure to light for 6 sec. The intensity of the fluorescence signals of TMR-TAT inside cells indicate that incubation with EGTA does not cause a significant reduction in the amount of TMR-TAT endocytosed and released into the cytosol after light irradiation.

C) Quantitative analysis of cell killing that accompanies TM-PCI in cells incubated without or with EGTA. A SYTOX® Green exclusion assay was used to distinguish live cells (stained by Hoechst, pseudo-colored purple) from dead cells (stained by SYTOX® Green, pseudo-colored green). The histogram represents the fraction of cells stained by SYTOX® Green before and after light irradiation. The average values of three experiments and the corresponding standard deviations are presented along with two representative SYTOX® Green and Hoechst overlay microscopy images.

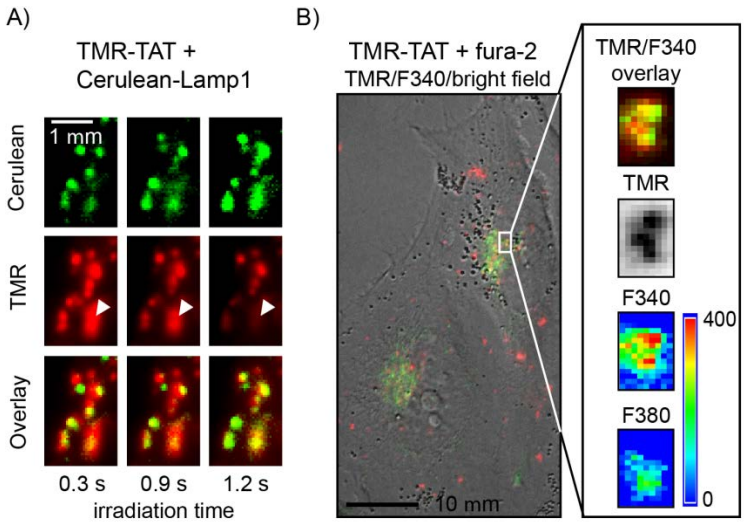

Figure 3-11. TMR-TAT co-localizes with endocytic organelles that contain calcium and TM-PCI causes the release of the content of endocytic organelles.

A) Microscopy images showing that TMR-TAT (pseudo-colored red) co-localizes with intracellular organelles expressing Cerulean-LAMP1 (pseudo-colored green). Upon irradiation, the TMR-TAT signal decreases from certain organelles as indicated by the white arrows.

B) TMR-TAT co-localizes with endocytic organelles that contain calcium. HeLa cells were incubated with TMR-TAT and the cell-impermeant calcium probe fura-2. Ratiometric imaging of fura-2 was performed by measuring the emission of the probe at 505 nm after excitation at 340 nm or 380 nm.

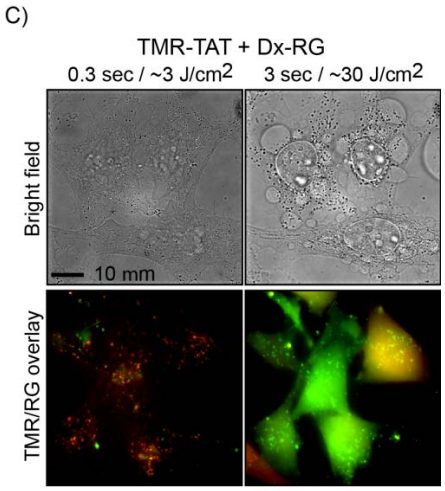

Figure 3-11. Continued.

C) TM-PCI causes the release of the pinocytosis marker 3 kDa Dextran Rhodamine green (Dx-RG). Representative images of HeLa cells incubated with TMR-TAT and RG-Dx before and after light irradiation at 560 nm. The overlay image of the TMR (pseudo-colored red) and RG (pseudo-colored green) shows a punctate distribution for both species prior to irradiation (a yellow color being indicative of co-localization). After irradiation, the fluorescent signals of TMR-TAT and Dx-RG are distributed throughout the cell. This does not happen if TMR-TAT is not present (not shown).

3.3 Discussion

PCI is an attractive approach to deliver molecules into cells. Light provides spatial and temporal control over the delivery process and endosomal lysis is efficient. It has been well appreciated, however, that this approach is potentially toxic to cells. The photosensitizers typically used for PCI are related to photodynamic therapy (PDT) agents, a treatment modality for which the goal is to actually kill cells with light(232). As in PDT, high doses of light during PCI induce cell apoptosis and necrosis(111, 137, 136). PCI experiments are therefore typically performed at low light doses that do not cause a significant reduction in cell viability. However, low doses of light might lead to a reduction in the efficiency with which endosomal release is achieved. In practice, optimal conditions therefore need to be found to achieve delivery while maintaining cell viability. In my experiments however, PCI mediated by TMR-TAT could not be achieved without cell killing being observed. The cell killing is rapid with plasma membrane blebbing and loss of permeability appearing within seconds. I was therefore interested in identifying the mechanisms associated with cell death in order to potentially circumvent this problem. My initial hypothesis was that the photolytic peptide might lyse intracellular organelles after escaping from endosomes. Light irradiation of TMR-TAT directly microinjected into the cytosol of cells however, did not reproduce the cell killing observed during PCI. TMR-S-S-TAT was also used to test this hypothesis. TMR-S-S-TAT is a compound that mimics the activity of TMR-TAT inside endosomes but that loses its photolytic activity upon reduction of the disulfide bond that links TMR to TAT. It has been shown that the reduction of such compounds takes place within seconds upon entry in the cytosol of cells(222). I therefore anticipated that, if TMR-TAT causes cell death because of a photo-induced activity in the cytosol, cell death would be abolished with TMR-S-S-TAT. However, TMR-S-S-TAT produces a similar killing as TMR-TAT. Together, these results suggest that TMR-TAT is not significantly phototoxic in the cytosol of cells and under the irradiation conditions used for PCI. Instead, the endosomal release process itself appears to be involved in the cell killing. TMR-TAT might lyse late endosomes or lysosomes during PCI. One can therefore

envision that PCI is accompanied by the release of hydrolytic enzymes from these organelles. This is a phenomenon that has been appreciated in the PDT field as being a potential causative factor for the phototoxic activity of various PDT photosensitizers(137, 139, 233, 234). Yet, there is usually a significant delay between lysosomal lysis and observable cell death. Because the cell death observed during TM-PCI is rapid, I wondered whether cell death could be caused by toxic molecules other than hydrolytic enzymes. Based on the well-documented link between calcium and cell death, the involvement of calcium during PCI was investigated. The concentration of calcium is typically low in the cytosol (100 nM) of cells. The flux of calcium into the cytosol and an increase in $[Ca^{2+}]_{cyt}$ has been linked to apoptosis and necrosis(141). It has also been well-established that an increase in $[Ca^{2+}]_{cyt}$ can cause the accumulation of calcium in mitochondria by transport through a low affinity uniporter(227, 235). The resulting increase of $[Ca^{2+}]$ in the mitochondrial matrix causes the opening of the permeability transition pore (PTP)(141, 159). Opening of the PTP can then result in the escape of mitochondrial matrix components, including the pro-apoptotic factor cytochrome c, into the cytosol. In my assays, TM-PCI caused a large increase in the fluorescence signal of the calcium indicator fluo-4. This fluorescence increase was observed when calcium was removed from the extracellular milieu immediately prior to irradiation of the cells. When cells where incubated in a media lacking calcium for more than 20 min to allow the calcium depletion of intracellular stores, the increase in fluorescence of fluo-4 was abolished. Taken together, these data indicate that calcium is released from intracellular stores during PCI. In addition, ruthenium red and cyclosporin A, inhibitors of the mitochondrial calcium uniporter and of PTP opening, respectively, led to an inhibition of the cell-killing observed during PCI even though the increase in $[Ca^{2+}]_{cyt}$ was still observable. These results therefore suggest that the plasma membrane blebbing and loss of permeability observed during PCI are caused by the release of calcium into the cytosol of cells followed by the transport of calcium into mitochondria and PTP opening (see Fig. 3-12 for a proposed model). Intracellular stores of calcium include the endoplasmic reticulum and mitochondria(141). Interestingly, endocytic

organelles also contain high concentrations of calcium(140, 223, 224, 75). Cells internalize calcium within endocytic vesicles by pinocytosis of calcium present in the extracellular milieu(140). The concentration of calcium drops to low micromolar concentration in early endosomes but several reports suggest that it rises to higher levels in late endosomes and lysosomes(223, 224). Christensen and coworkers have for instance measured that [Ca^{2+}] is 600 μM in the lysosomes of macrophages(223). To test whether calcium is released from endocytic organelles during TM-PCI, a calcium depletion experiment was first performed. The increase in fluo-4 fluorescence was abolished when calcium was chelated by EGTA in the incubation medium and in endocytic organelles. While these results are consistent with the model proposed in Fig. 3-12, these experiments have, however, a caveat.

Indeed, it is not possible to exclude the possibility that unbound EGTA might be released from endosomes during TM-PCI and that it might then chelate calcium ions released from other intracellular stores. Other experiments were therefore performed to test the hypothesis that calcium is released from endocytic organelles. I first tested whether TMR-TAT co-localizes with endocytic organelles that contain Ca^{2+}. Co-localization of TMR-TAT with late endosomes and lysosomes was demonstrated by expression of the fluorescent marker Cerulean-LAMP1. Irradiation of late endosomes or lysosomes labeled with both LAMP1 and TMR-TAT led to the local dissipation of the TMR-TAT signal, indicating that the peptide escapes from these organelles upon PCI. In addition, co-localization experiments between TMR-TAT and the endocytosed calcium indicator fura-2 were also performed. In principle, ratiometric imaging of fura-2 can be used to determine the concentration of calcium in a particular milieu. However, a complication arises when investigating calcium present in the endocytic pathway. This is because the pH of endocytic organelles is acidic and the Kd of fura-2 increases at acidic pH(236). In addition, the calcium-free form of fura-2 can potentially interact with proteins more preferentially at acidic pH(237). Together, these issues make the precise determination of calcium concentration within endosomes a technical challenge. However, I reasoned that, since both caveats lead to an underestimation of the actual

concentration of calcium in endosomes (both problems diminish the ability of fura-2 to bind to calcium ions), a lower limit for [Ca^{2+}]endo can nonetheless be determined. This lower limit was determined to be 470 nM, the concentration of calcium that would be present given a pH of 7.2. Considering that the pH of the endocytic organelles observed are likely to be acidic, the calcium concentration should be significantly higher (for instance, 3.9 μM at pH 5.5, a pH expected inside late endosomes).

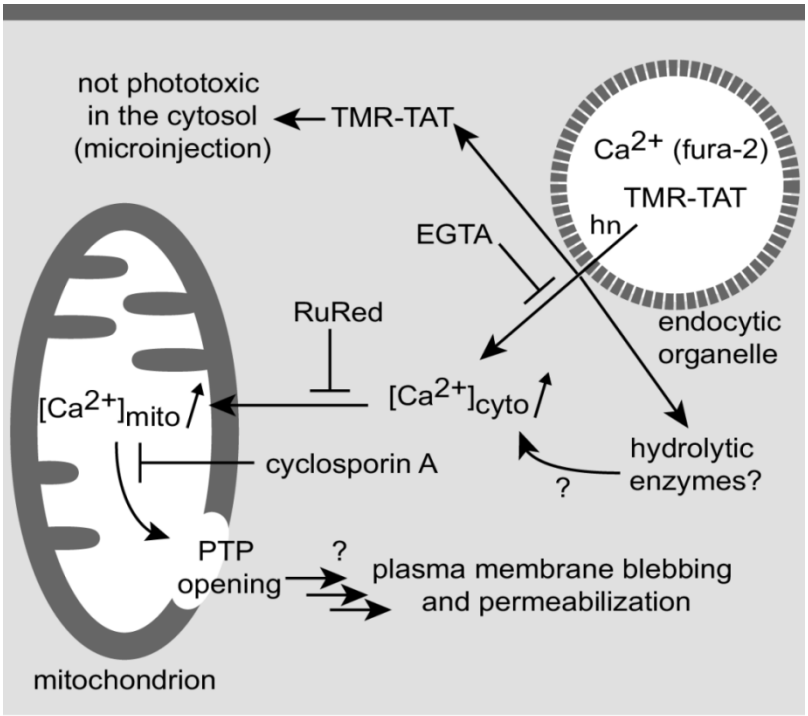

Figure 3-12. Proposed model for the increase of cytosolic calcium upon TM-PCI and for the induction of cell death.

Experimental evidence for some aspects of this model is provided in parentheses and the action of various inhibitors is indicated. Areas that remain to be tested are highlighted with question marks.

Overall, the results indicated that calcium is present in the lumen of endocytic organelles also containing TMR-TAT (Fig. 3-11). Finally, TM-PCI causes the release of the content of endocytic organelles, as demonstrated by the release of Dx-RG. Taken together, these results suggest that TM-PCI causes the release of Ca^{2+} from endocytic organelles. As indicated in Fig. 3-12, it is however interesting to note that the data does not reveal whether the increase in $[Ca^{2+}]_{cyt}$ detected originates solely from Ca2+ escaping from the endocytic pathway. As a matter of fact, it is possible that the release of endocytic calcium might trigger the release of more calcium from other organelles such as the endoplasmic reticulum(141, 238). Alternatively, other released molecules such as hydrolytic enzymes (but not TMR-TAT itself) might cause an increase in cytosolic calcium indirectly(141). Whether this is the case will be the object of future investigations.

Overall, these data support a model in which the flux of calcium in the cytosol during TM-PCI is a cause of cell photo-killing. These results also highlight how efficient and rapid disruption of the endocytic pathway might be problematic not only during PCI but also for other delivery methods relying on endosomal escape. Interestingly, crotamine, a cell-penetrating peptide derived from the venom of the rattlesnake Crotalus durissus terrificus, causes cell death in a manner dependent on the disruption of lysosomes and on rapid intracellular calcium release(239). While other endosomolytic agents have been used to deliver macromolecules into cells without affecting cell viability, the release of calcium from endosomal and lysosomal organelles could be a factor contributing to the toxicity associated with certain delivery procedures. Paradoxically, a goal in cellular delivery is often to make endosomal escape as efficient as possible(240). This is based on the principle that a greater biological effect can be achieved if more of a delivered macromolecule can escape from endosomes. Yet, my results suggest that the efficient lysis of endocytic organelles leads to calcium-induced cell death. This therefore highlights that a cell might remain viable during delivery only if endosomal lysis is relatively inefficient. Interestingly, it is also possible that TM-PCI causes cell death not because of the efficiency of endosomal escape per se, but because of the rapidity of this

process. In particular, a small increase in $[Ca^{2+}]_{cyt}$ can be tolerated by a cell(141). Calcium homeostasis can also be quickly reestablished by the various calcium pumps and channels present in the cell(141). It is therefore possible that slowing down the rate of endosomal release might allow the cell to cope with the calcium entering the cytosol. In the context of PCI, this might mean that low doses of light might be preferable to intense bursts of irradiation. This could for instance explain why extensive cell killing is not observed in reports of TM-PCI performed on laser-scanning confocal microscope (e.g. an intense laser is used but a particular endosome is irradiated only briefly with long time intervals between scans)(119, 118). Overall, it is clear that understanding the interplay between endosomal lysis and cell viability in greater details is required to permit the development of delivery procedures that have a minimum impact on cellular physiology.

3.4 Materials and methods

3.4.1 Peptide synthesis

TMR-TAT (TMR-GRKKRRQRRRG-NH2) and the protease-resistant TMR-riTAT were synthesized by solid phase peptide synthesis technique as previously described(133). Purified and lyophilized TMR-TAT was dissolved in water to obtain a 1 mM stock solution and diluted in PBS or cell culture media to desired concentrations for experiments.

TMR-S-S-TAT synthesis. The synthesis of 2-(2-pyridyldithio) ethylamine hydrochloride (PDA-HCl) was conducted as previously reported(241). EDCI (0.22 g, 1.2 mmol) was added to a solution of 5(6)-carboxytetramethylrhodamine (0.30 g, 0.70 mmol), PDA-HCl (0.12 g, 0.54 mmol), HOBt (0.18 g, 1.2 mmol), and TEA (0.20 mL, 1.4 mmol) in DMF (4 mL) at 0 °C. The reaction solution was stirred under N_2 at 0 °C for 30 min, and then warmed to room temperature.

After reacting overnight at room temperature, DMF was dried under vacuum. The resulting crude material was purified by silica gel chromatography (DCM:MeOH=6:1) to give the mixture of two TMR-PDA isomers (0.22 g, 68%). Mass spectrometry analysis (MALDI-TOF): calculated for $C_{32}H_{30}N_4O_4S_2$ 598.2, observed

599.4 (M+H)+. Cys-TAT (CGRKKRRQRRRG-NH2) was synthesized by adding Fmoc-Cys (StBu)-OH to the N-terminus of the TAT peptide assembled on the solid phase as Fmoc-Gly-Arg (Pbf)-Lys (Boc)-Lys (Boc)-Arg (Pbf)-Arg (Pbf)-Gln-Arg (Pbf)-Arg (Pbf)-Arg (Pbf)-Gly-Rink amide MBHA resin. The resin was deprotected with 20% piperidine to remove Fmoc and the Cys side chain was deprotected by treatment with tributylphosphine in dimethylformamide/dichloromethane (1:3:3 by volume). Cleavage of the peptide from the resin was then performed by treatment with trifluoroacetic acid/triisopropylsilane/ethanedithiol/water (92.5:2.5:2.5:2.5 by volume). The peptide was purified by semi-preparative HPLC and analyzed by mass spectrometry (calculated mass: 1555.9, observed: 1558.2 (M+H)+). The N-terminal cysteine of Cys-TAT was reacted with TMR-PDA in Tris buffer at pH 8.3 for 30 min. The product, TMR-S-S-TAT was purified by semi-preparative HPLC. Mass spectrometry analysis (MALDI-TOF): calculated mass: 2044.4, observed mass: 2045.7 (M+H)+.

3.4.2 Photohemolysis assay

Cells were centrifuged for 10 min at 1500 g to separate the erythrocytes from the plasma supernatant. Erythrocyte pellets were resuspended in PBS and the process was repeated four times to remove plasma and buffy coat. The erythrocytes (50% volume in PBS) were diluted in PBS to a final concentration of 0.1%. Peptides and erythrocytes were mixed in PBS and added to a 384 well plate. Cells were incubated with the peptide for 15 min and allowed to settle to the bottom of the dish prior to imaging to get a layer of cells at the focal plane. The photohemolytic activity of TMR-TAT or TMR-S-S-TAT was assessed by irradiation of the peptide and cell mixtures at 560 nm on the microscope (RFP channel). The number of lysed cells was counted after irradiation by using bright field images in which intact erythrocytes have a dark contrast while lysed ghosts do not. The data reported represents the averages and the corresponding standard deviations of five experiments for which a minimum of 500 cells were examined.

3.4.3 Fluorescence microscopy imaging

Multi-well dishes with 80% cell confluency in each well were placed on an inverted epifluorescence microscope (Model IX81, Olympus Center Valley, PA). The microscope is equipped with a heating stage which was maintained at 37 °C. The microscope is configured with a spinning disk unit to perform both confocal and wide-field fluorescence microscopy. Images were captured with a Rolera-MGI Plus back illuminated EMCCD camera (Qimaging, Surrey, BC, Canada). Imaging was performed using bright field imaging and the fluorescence filter sets: RFP (Ex=560±20 nm/Em=630±35 nm), FITC (Ex=488±10 nm/Em=520±20 nm) and CFP (Ex=436±10 nm/Em=480±20 nm). The excitation light was from a 100 W mercury lamp (Leeds Precision Instruments # L202 Osram) passed through the filter cubes and 20, 40, or 100X objectives. Neutral density filters (ND 1, 2, 3 and 4 on the instrument corresponds to 100, 25, 12.5 and 5% transmittance) and different exposure times were used to adjust the dose of light given to the cells. The bright field and fluorescence intensities of HeLa cells were measured with the SlideBook 4.2 software (Olympus, Center Valley, PA). Irradiances at the specimen were 100 mW/cm2 when no neutral density filter and no objective were present in the light path (and, for instance, 5 mW/cm2 when ND4 was inserted). Irradiances were measured using a monochromic photometer (model 840-c, Newport, Irvine, CA). Irradiation area has a diameter of 1.3 cm without objective but the light beam is focused into an area of 3x10-3 cm2 by the 100X objective. Irradiances can therefore be approximated to be at 21 or 420 W/cm2 with ND4 or ND1, respectively. To determine the percentage of cells with a compromised plasma membrane after light irradiation, cells were incubated with SYTOX® Green and Hoechst. SYTOX® Green is cell-impermeable and only stains cells with a compromised plasma membrane while Hoechst stains all cells. Cells were imaged with a 40X objective. Ten to twenty images were acquired in the green and blue channels for each experiment. The total number of cells in a given image was determined from the blue channel image (Hoechst) by counting the number of blue nuclei present. The number of dead cells was determined by identifying cells containing a green fluorescent nucleus stained by SYTOX® green. Cell

viability was determined by establishing a ratio of dead cells/total number of cells for each sample (at least 1000 cells were counted in each experiment and each experiment was repeated 3 times).

3.4.4 Calcium imaging and calibration

The calcium indicators fluo-4AM and fura-2 were used from 1 mM DMSO stock solutions and diluted to 5 μM in media for experiments. Fluo-4AM was incubated with cells for 1 h. After incubation, cells were washed with fresh medium and imaged 20 min later to allow intracellular cleavage of the acetoxymethyl esters. The maximum fluorescence intensity of fluo-4 (Fmax) was determined *in cellulo* by addition of the calcium ionophore ionomycin (1 μM) in L-15 supplemented with 2 mM calcium chloride. The fluorescence intensity of fluo-4 in the absence of calcium (Fmin) was determined by addition of EGTA (10 mM) to cells incubated in L-15. Quantification of emitted fluorescence was calculated by taking the mean fluorescence intensity of the nucleus of a cell using the Slidebook software. The approximate calcium concentrations reported in the text were calculated from the formula [Ca2+]=Kd*(F−Fmin)/(Fmax−F)(225). Ratiometric imaging of fura-2 was performed on a Stallion digital imaging workstation with a c-apochromat 63X/1.2 W objective. Excitation was performed at 340 nm and 380 nm with rapid switching (< 2 ms) between excitation wavelengths. Emission was collected at 505 nm. Calibration experiments were performed in vitro on the microscope using fura-2 solutions buffered at pH 7.2 and pH 5.5 in 20 μm flat capillary tubes (vitrotubes 5002–050, Vitrocom). The fluorescence signals from the 380 and 340 nm excitation images, F380 and F340, were measured in each case in the absence or presence of 2 mM calcium chloride. Alternatively, in *cellulo* calibration experiments were performed as described for fluo-4 by using the cell permeable fura-2 analog fura-2AM. Quantification of F380 and F340 was calculated by taking the mean fluorescence intensity of a region of interest (ROI) using the Slidebook software after subtraction of the fluorescence background obtained from a ROI outside the cell. The ratio of F340/F380 signals, R, were calculated for each set of images (Rmin

and Rmax corresponding to the ratios in the absence or presence of saturating amount of calcium, respectively) and the calcium concentrations reported in the text were calculated from the formula [Ca2+]=Kd*[(R−Rmin)/(Rmax−R)]*(F380max/F380min) as previously described(225). The apparent Kd of fura-2 used in my calculations were 130 nM at pH 7.2 and 1188 nM at pH 5.5, as previously established(236).

3.4.5 Microinjection of TMR-TAT

HeLa cells were cultured on 35 mm plates (P35G-1.5-7-C-grid, MatTek Corp., Ashland, MA). Cells were washed and incubated with Leibovitz's L-15 Medium and placed on the microscope. Femtoliter aliquots of TMR-TAT (10 μM) were directly injected into the cytoplasm of live HeLa cells using an InjectMan NI2 micromanipulator equipped with a FemtoJet microinjector (Eppendorf, Westbury, NY). The microinjected cells were imaged immediately after microinjection. Irradiation was performed in the microscope as described for TM-PCI.

4. SYNERGY BETWEEN ROS GENERATOR AND CPP LEADS TO EFFICIENT MEMBRANE PHOTOLYSIS[†]

4.1 Introduction

In section 2, it was shown that the Fl-CPP TMR-TAT could internalize into endocytic vesicles within cells and upon irradiation escape into the cell's cytosol. However, the overall mechanism of how the Fl-CPPs lyse the membrane of endosomes remains unclear. Fluorophores used for CPP-mediated photo-endosomolysis are often used for live-cell fluorescence microscopy assays without any observable membrane damage effects. Thus, it seems to appear that the CPPs such as TAT confer a photolytic activity to otherwise innocuous fluorophores. It has been shown that the mechanism of Fl-CPP mediated endosomolysis involves production of singlet oxygen within endosomes that might cause lysis. However, the TMR-K9 conjugate does not cause endosomal release as TMR-TAT does when endocytosed to the same extent. This suggests that the peptide moiety of the Fl-CPP might directly participate in the endosomolytic activity observed.

In this section, I test the hypothesis that CPPs enhance the photolytic activity of fluorophores by destabilizing membranes photo-oxidized by singlet oxygen. Because RBCs represent a simpler system than endosomes, TMR-TAT photohemolysis is investigated as a means to gain possible mechanistic insights into the photo-endosomolytic activity of Fl-CPPs.

4.2 Results

4.2.1 Fl-CPPs cause photohemolysis by $^1O_2$ generation

The TMR-TAT and RBCs were irradiated with light using the microscope and photohemolysis was monitored as a function of irradiation time. As shown in Fig. 4-1A,

[†] Reprinted with permission from "Synergy between cell-penetrating peptides and singlet oxygen generators leads to efficient photolysis of membranes" by Muthukrishnan, N., Johnson, G., Erazo-Oliveras, A. and Pellois, J. P., 2012. *Photochem Photobiol* **89**, 625-30, Copyright 2014 by John Wiley and Sons

TMR-TAT photolysis RBCs after a short lag time. Irradiation of TMR or TAT alone did not reproduce this activity, indicating that conjugation of TMR to TAT is required for photohemolysis. TAT is mainly composed of arginine and lysines residues. To assess the effect of peptide composition, the control peptides TMR-R9 and TMR-K9 were tested. TMR-K9 showed a significantly reduced photohemolytic activity as compared to TMR-TAT. In contrast, TMR-R9 displayed a photohemolysis activity similar to that of TMR-TAT (Fig. 4-1A). Together, these results indicate that the arginine residues in TAT account for the photohemolytic activity of this Fl-CPP. To examine the mechanism(s) by which TMR-TAT promotes membrane lysis upon irradiation, the involvement of singlet oxygen was tested. The lipophilic singlet oxygen quencher tocopherol and the singlet oxygen inhibitor crocetin both led to a significant decrease in photohemolytic activity (Fig. 4-1B). To confirm that singlet oxygen is produced upon irradiation of TMR-TAT, a RNO spectroscopic assay was performed. In this assay, a peroxide intermediate is formed upon reaction of $^1O_2$ with imidazole. Reaction of the chromophore RNO with the intermediate results in bleaching(242). As a result, there is a loss of absorbance of RNO at 450 nm wavelength which is used to determine the rate of production of $^1O_2$. Rose Bengal and eosin Y, compounds with reported singlet oxygen quantum yields of 0.76 and 0.57 in water were used as standards(243, 244). As shown in Fig. 4-1C, production of singlet oxygen upon irradiation of RB or eosin Y could be detected at low light doses. In contrast, TMR-TAT caused a decrease in RNO absorbance only after extended irradiation. Together, these results indicate that TMR-TAT produces very low levels of singlet oxygen upon irradiation, but that the singlet oxygen produced is definitely required for photohemolysis.

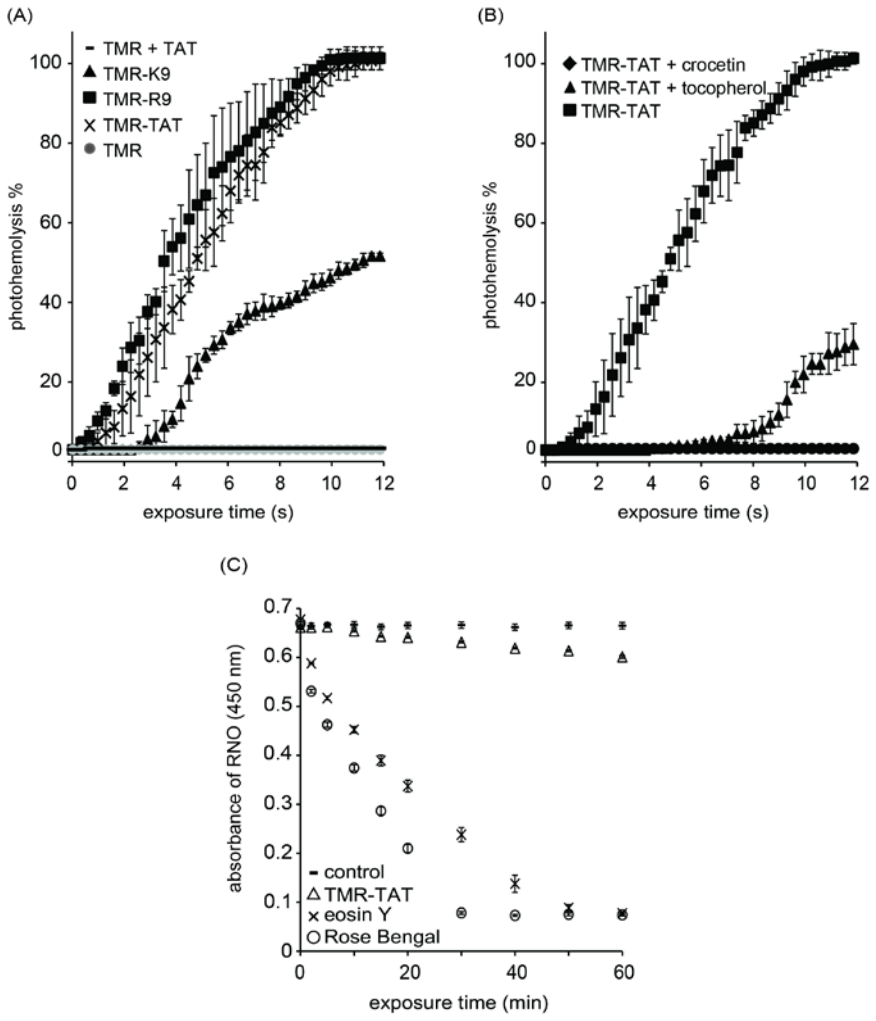

Figure 4-1. **Fl-CPPs lyse RBCs upon irradiation and the production of singlet oxygen is involved in this process.**

A) Photohemolysis curves for TMR-TAT, TMR-R9 and TMR-K9. B) Effect of tocopherol and crocetin on TMR-TAT mediated photohemolysis. C) Quenching of RNO absorbance by TMR-TAT as a function of irradiation time. Rose Bengal and eosin Y are used a singlet oxygen generators of known singlet oxygen quantum yields (0.76 and 0.57, respectively). All experiments were performed in triplicates to obtain standard deviation and the data represents the average of 3 sets of readings.

4.2.2 TAT causes shrinkage of photosensitized red blood cell membranes

To investigate how the peptide moiety of a Fl-CPP might contribute to photohemolysis, TMR-TAT was compared with known photolytic photosensitizers such as RB and hematoporphyrin (HP). In these experiments, RBCs were incubated with TMR-TAT, RB or HP and the photohemolysis of cells was monitoring by fluorescence and bright-field microscopy. Based on the fluorescence distribution of TMR-TAT, the peptide showed little association with RBCs prior to irradiation (Fig. 4-2). In contrast, strong fluorescence signals were present on the surface of the cells when RBCs were incubated with the fluorescent RB and HP. In addition, whereas the morphology of RBCs incubated with TMR-TAT was that of cells incubated in buffer alone, RBCs incubated with RB or HP formed echinocytes. This morphology is indicative of the insertion of the photosensitizers in the outer leaflet of the lipid bilayer of RBCs(193). Upon irradiation, cells lysed rapidly and lost their dark contrast in bright-field imaging because of the release of hemoglobin into the medium(93). The lysed membrane of ghost cells remained, however, visible in both bright-field and fluorescence imaging. Interestingly, the fluorescence signals of TMR-TAT bound to RBCs significantly increase after lysis (ghosts appear as fluorescent rings in Fig. 4-2A). It has previously been shown that TAT displays a stronger affinity for lysed RBCs than for intact cells and that exposure of the negatively charged phosphatidylserine lipids on the surface of lysed cells might be involved in this effect (phosphatidylserine is present in the inner leaflet of the lipid bilayer and not accessible to the peptide prior to lysis)(93). To test whether phosphatidylserine is also exposed on the membrane of RBCs upon TMR-TAT mediated photohemolysis, FITC-annexin V was added to RBCs before and after irradiation with light. (Fig. 4-2C). Based on fluorescence imaging, annexin V did not bind to intact RBCs. However, upon irradiation, both TMR-TAT and annexin V stained the membrane of lysed RBCs. These results therefore suggest that phosphatidylserine becomes accessible for binding upon photohemolysis and that TMR-TAT might interact with this negatively charged lipid. For all the photosensitizers tested, photohemolysis led to the formation of ghosts with an initial morphology similar to that observed for the intact

RBCs prior to light exposure (i.e. crenated for RB and HP and round for TMR-TAT, Fig. 4-2). The morphology of ghosts obtained with RB or HP did not change when irradiation was extended beyond what is required for lysis (Fig. 4-2B). In contrast, TMR-TAT caused a significant shrinking of the membrane of ghosts (Fig. 4-2B). Shrinkage was not observed when ghosts were not irradiated after photolysis. This indicates that TMR-TAT mediated shrinkage requires continued photolytic degradation of the membrane.

4.2.3 TAT and R9 enhance photolytic activity of membrane-associated photosensitizer Rose Bengal

The shrinkage of ghosts by TMR-TAT but not by RB suggested that the Fl-CPP might damage photo-oxidized membranes in a way that cannot be simply accounted for by the generation of singlet oxygen. While shrinkage was only observable after photohemolysis was finished, this phenomenon nonetheless raised the possibility that TAT might destabilize the membrane of intact RBCs before or during the photolytic event. To test this idea, the effect of TAT on the membrane of RBCs photodamaged with RB was investigated. In this assay, RBCs were incubated with RB, exposed to light and the extent of photohemolysis after each irradiation dose was determined to obtain a photohemolysis curve. In parallel experiments, the unlabeled CPPs TAT and R9 were co-incubated with RB and RBCs and the samples were then irradiated. The non-CPP control K9 was also tested under the same conditions. As shown in Fig. 4-3, photohemolysis was accelerated by addition of TAT in a concentration- dependent manner. This effect was also reproduced with R9 but not with K9. This indicates that

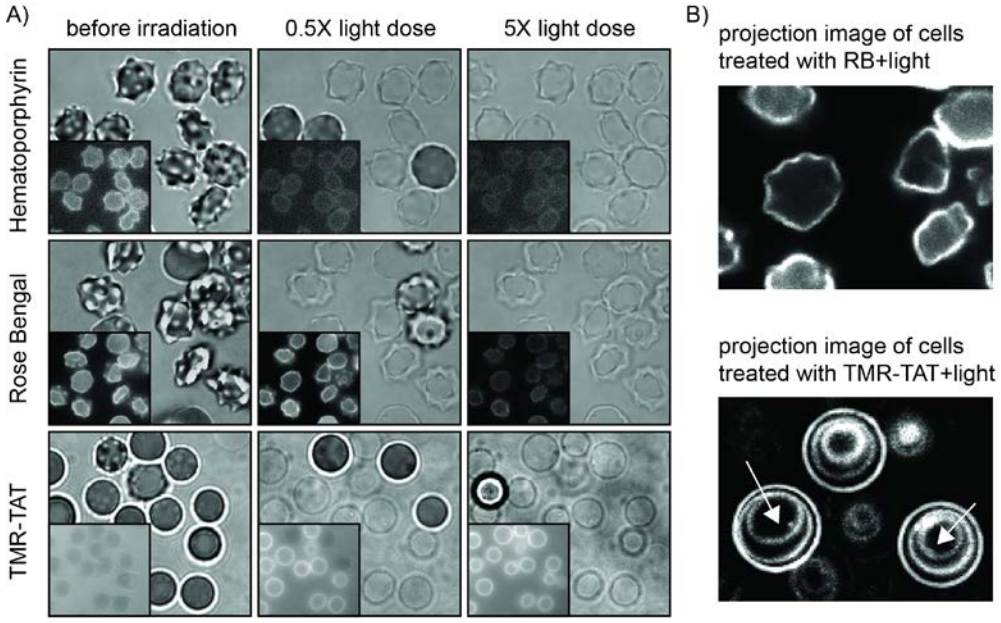

Figure 4-2. TMR-TAT mediated photohemolysis is accompanied by cell shrinkage but photolysis mediated by RB or hematoporphyrin (HP) is not.

A) Bright field and fluorescence imaging of RBCs treated with HP, RB, or TMR-TAT. Images were acquired at 0.5x light dose (light dose that yields 50% photohemolysis) and 5x light dose (a light dose 10 times that required for 50% photohemolysis). Insert: fluorescence images.

B) Projection images of cells treated with RB or TMR-TAT and light. The fluorescence images of the cells exposed at 0.5x, 2x and 5x light dose were super-imposed in a single overlay image. The fluorescence signal corresponds to either RB or TMR-TAT binding to the surface of lysed cells. In the case of cells treated with RB, the projection image is identical to the 0.5x image, indicating that the morphology of the cells is unchanged during light exposure. In contrast, the projection image of the cells treated with TMR-TAT shows concentric circles that correspond to the cell membrane shrinking with increasing light exposure (white arrows indicate the direction of membrane shrinking with increasing irradiation).

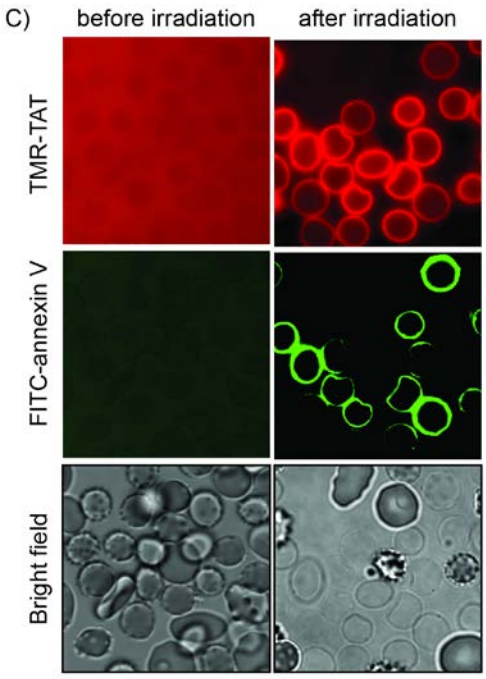

Figure 4-2. Continued.

C) AnnexinV staining of membrane of RBCs lysed with TMR-TAT upon irradition. FITC-annexinV was added before or after lysis of RBCs with TMR-TAT and light irradiation.

arginine residues mediate the enhancement in lysis observed, but that positive charges are not sufficient to account for this effect. To examine whether TAT or R9 might cause an increase in lysis by simply causing an increase in binding of the photosensitizer to the membrane of RBCs, the fluorescence signal of RB associated with the cells was quantified (Fig. 4-3C). The amount of RB bound to the RBCs decreases by three-fold in the presence of TAT (10 μM) (similar results were obtained with R9, data not shown). These results were further confirmed by measuring the concentration of RB present in solution after incubation with RBCs and with or without TAT. Samples were centrifuged to separate RB associated with RBCs (pellet) from soluble (RB). In this assay, addition of TAT caused an increase in the amount of RB present in solution, indicating again that the association of RB with RBCs decreases in the presence of TAT (results not shown). Although the reasons for this decrease remain unclear, these results indicate that the propensity of TAT or R9 to promote photolysis is not caused by an increase in RB binding that would lead to an increase in the singlet oxygen produced in the membrane environment. Instead, the data obtained support the notion that TAT and R9 might act directly on photo-oxidized membranes. To further characterize how TAT or R9 might accelerate photolysis, RBCs were treated with RB and the peptide was added post-irradiation as opposed to during illumination. RBCs were treated with RB and irradiated with a single dose of light. After completing the irradiation, the peptides TAT, R9 or K9 were added (10 μM) to the cells. A control experiment where PBS was added instead of TAT or R9 was also performed. Hemolysis was measured before and after addition of peptides to the samples. As shown in Fig. 4-4, addition of TAT and R9 post-irradiation caused an increase in hemolysis. In particular, although the photohemolysis obtained for RB alone was only 24±6 % under the conditions tested, addition of R9 led to 69±7 % (for comparison, the experiment performed with RB and R9 co-incubated leads to 93±3 % lysis, data not shown). In contrast, the addition of K9 did not have a significant effect on lysis. The peptides alone had no effect in the dark or when cells were irradiated without RB present. These data therefore suggest that TAT or R9 promotes the lysis of membranes that have been photo-oxidized by a photosensitizer.

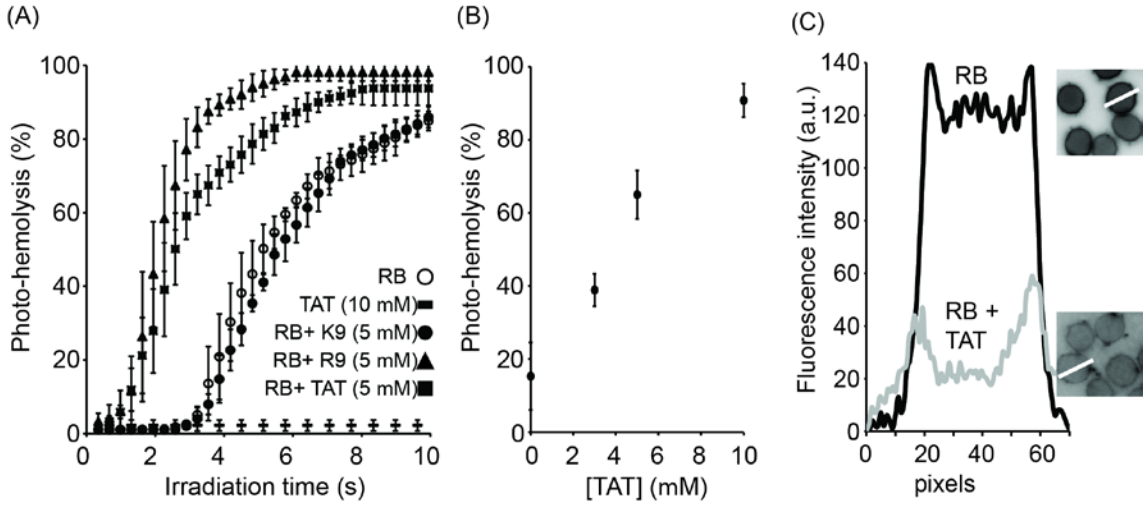

Figure 4-3. TAT and R9 enhance the photolytic activity of Rose Bengal.

A) Photohemolysis monitored as a function of irradiation time. RB (200 nM) was incubated with RBCs and photohemolysis was assessed by bright field microscopy.

B) Photohemolysis mediated by RB as a function of the concentration of TAT present. Photohemolysis was measured after exposing the cells with 560 nm light for 4 s.

C) Fluorescence intensity profiles of RBCs incubated with RB alone or with RB and TAT (10 μM). Fluorescence images of the cells are represented as inverted monochrome. White lines highlight the regions of interest from which the intensities were measured. Membrane intensities were calculated for 10 different RBCs and the data was consistent for each cell.

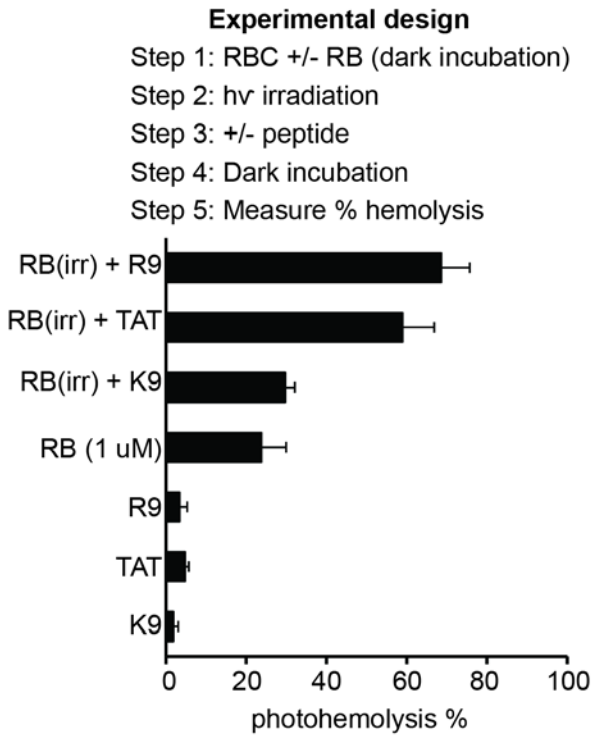

Figure 4-4. **TAT and R9 lyse the membrane of RBCs photoxidized by Rose Bengal.**

Irradiation of RBCs incubated with RB followed by addition of K9, TAT and R9. Addition of TAT and R9 (10 μM) post-irradiation increases hemolysis but addition of K9 does not have a significant effect. Conditions of 100% hemolysis were determined by addition of Triton X to RBCs. The control sample consists of untreated RBCs. The data represent the average of triplicate experiments and error bars represent the corresponding standard deviations

4.3 Discussion

The results indicate that Fl-CPPs such as TMR-TAT are photolytic by promoting the formation of singlet oxygen within biological membranes upon irradiation. Singlet oxygen is a reactive oxygen species that is generated when a molecule absorbing light forms an excited triplet state and transfers its energy to molecular oxygen. Singlet oxygen can in turn oxidize both lipids and membrane proteins(132). The singlet oxygen quencher tocopherol and the inhibitor crocetin abolished the photolytic activity of TMR-TAT(133). Moreover, the production of singlet oxygen upon irradiation of TMR-TAT could be detected using an RNO spectrometric assay. However, under conditions of irradiation comparable to those used for photohemolysis, the production of singlet oxygen detected from TMR-TAT was very poor. On one hand, this result is consistent with the low triplet state quantum yield (0.001–0.003) reported for TMR(132, 199). On the other hand, it is surprising that an inefficient singlet oxygen generator such as TMR might cause lysis of membranes. Looking for clues on how TMR-TAT might lyse RBCs, the activity of the fluorescent peptide was compared with that of the singlet oxygen generator RB. A striking difference between cells photolysed by RB and those photolysed by TMR-TAT was the significant shrinking that accompanied the photolysis mediated by TMR-TAT. The shrinkage observed suggests that TMR-TAT might dissolve certain membrane components, thereby leading to a reduction in the membrane surface area. Similar phenomena have been observed with antimicrobial peptides(245). In this case, however, the results indicate that the "detergent-like" effect of the peptide is only expressed upon photo-oxidation of the membrane. On the basis of these results, I hypothesized that TAT might contribute to photolysis by destabilizing photo-oxidized membrane components. To test this hypothesis, RBCs were photo-oxidized with the photosensitizer RB, a photosensitizer that produces singlet oxygen within the membrane environment upon irradiation. Unlabeled TAT and R9 were added in trans to assess whether the peptides might promote the lysis of the photodamaged membranes. When present during irradiation, both TAT and R9 significantly enhanced the photolytic activity of RB. This effect was observed at a concentration range at which TMR-TAT or

TMR-R9 can cause photolysis of RBC (e.g. 2 μM), suggesting that what is observed when RB and CPPs are co-incubated might also take place in the context of Fl-CPPs. Moreover, TAT or R9 did not increase the binding of RB to RBCs. This therefore excludes the possibility that photohemolysis was enhanced because more singlet oxygen generating RB was bound to the membrane of RBCs in the presence of the peptides. These results instead suggested that TAT or R9 might participate directly in the lytic event. In particular, although TAT and R9 are not lytic by themselves, these peptides could aggravate the oxidative damage initiated by the photosensitizers or fluorophores. In this model, TAT and R9 would therefore have a latent membrane-disrupting activity that is only expressed on partially oxidized membranes. To test this possibility, TAT was added to RBCs treated with RB after rather than during irradiation. In these experiments, both TAT and R9 caused an increase in hemolysis while the control peptide K9 did not. These results therefore support the notion that arginine-rich CPPs such as TAT and R9 can interact with oxidized membranes and promote their lysis. Interestingly, it has been shown that TAT and R9 have membrane translocation properties(246, 247). Whether photolysis and translocation share some mechanistic features remains, however, to be investigated.

Overall, these data establish how the fluorophore and CPP moieties of a Fl-CPP might both contribute to photolysis. Upon irradiation, the fluorophore generates singlet oxygen and this singlet oxygen damages membrane components. The peptide is then able to aggravate this damage and lysis takes place more readily. Fluorophore and peptide might therefore act in synergy and this in turn might explain how a poor singlet oxygen generator such as TMR-TAT might be able to achieve lysis relatively efficiently. The molecular basis for the lytic activity of the peptide remains to be explored. Understanding what membrane components interact with CPPs after initial photodamage should be especially interesting. CPPs are well known to interact with lipid bilayers(100). One can therefore speculate that CPPs might interact with oxidized lipids and that these interactions are involved in destabilizing membranes.

RBCs provide a membrane environment different than that found inside endosomes. It is therefore unclear whether photohemolysis closely resembles the photolysis activity of Fl-CPPs observed inside endocytic organelles. Both protein composition and membrane curvature are for instance very different between RBCs and endosomes(248). However, RBCs and endosomes have similar lipid composition and the lipid asymmetry between outer and inner leaflets is conserved in these membrane systems(207). It should also be noted that the difference in photo-endosomolytic activity observed between TMR-K9 and TMR-TAT can be reproduced with photohemolysis(133). The photolytic effects of TMR-TAT on RBCs presented in this report might therefore be relevant to those observed with endocytic organelles. I therefore propose that, just as with RBCs, Fl-CPPs cause the photolysis of endosomes by the combined action of singlet oxygen and of a peptide moiety that destabilizes oxidized membranes. Understanding how the oxidized membranes are destabilized could lead to the development of efficient light-inducible drug delivery tools. Moreover, it is interesting to note that the enhancement that TAT or R9 provides toward the photolytic activity of photosensitizers such as RB could potentially be exploited in other applications. In particular, photosensitizers are commonly used in photodynamic therapy, a treatment modality that exploits light to kill cells locally. As photolysis is one of the modes of action by which photosensitizers kill cells, it is therefore possible that CPPs might sensitize cells to the photokilling of photodynamic therapy drugs and thereby enhance their potency.

4.4 Materials and methods

Reagents for solid phase peptide synthesis (SPPS) were purchased from Novabiochem. The fluorophore 5,6-carboxytetramethylrhodamine was purchased from Novabiochem. Eosin Y, Rose Bengal, α-tocopheryl acetate and imidazole were obtained from Sigma. Crocetin was purchased from MP Biomedicals. Whole blood was purchased from Gulf Coast Regional Blood Center (Houston, TX).

4.4.1 Peptide synthesis

TAT (GRKKRRQRRRG-NH2), R9 (GRRRRRRRRR-NH2) and K9 (KKKKKKKKK-NH2) were synthesized by Fmoc solid-phase peptide synthesis using rink amide MBHA resin according to previously reported protocols (Novabiochem). Coupling of carboxytetramethylrhodamine to the N-terminus of the peptides was performed after Fmoc deprotection of the N-terminal amino group. Peptides and Fl-CPPs were purified using HPLC and their identity was confirmed by mass spectrometry (MALDI-TOF). TAT expected mass: 1451.92 Da, observed mass: 1452.41 Da; R9 expected mass: 1478.96 Da, observed mass: 1479.52 Da; K9 expected mass: 1169.88 Da, observed mass: 1170.96 Da; TMR-TAT expected mass: 1865.07 Da, observed mass: 1866.1 Da; TMR-K9 expected mass: 1583.0 Da, observed mass: 1583.30 Da; TMR-R9 expected mass: 1893.20 Da, observed mass: 1894.4 Da. The pure lyophilized peptides were dissolved in water to make 1 mM stock solutions that were then diluted to desired working concentrations in PBS for photohemolysis experiments.

4.4.2 Photohemolysis assay

Photohemolysis methods have been published previously(133). Briefly, a concentration of 0.1% by volume of RBCs was used for photohemolysis experiments. Peptides and RBCs were mixed in PBS in a 384-well plate. RBCs were incubated with a given peptide for 15 min during which time RBCs could settle to the bottom of the dish prior to imaging. The photohemolytic activity of the photosensitizing compounds was assessed by irradiation of the sample at 560 nm (RFP channel) on the microscope. The number of lysed cells was counted after each irradiation by using bright-field images in which intact erythrocytes have a dark contrast while lysed ghosts do not. The data reported represent the averages and the corresponding standard deviations of five experiments in which a minimum of 500 cells were examined. In parallel experiments, irradiation was performed using light from a 600 W halogen lamp (Utilitech) which was filtered with a 1.5-inch water filter, homogenizing glass and a green optical plastic filter NT46-624 (Edmund optics). The maximum transmission was in the range 450– 580 nm

with a final photon flux output of 3.3 * 10^{17} photons s^{-1} cm^{-2}. The RBCs incubated with peptides were irradiated for a given amount of time and spun down. The absorbance of the supernatant was measured at 450 nm using a plate reader to establish a percentage photohemolysis (100% hemolysis was set using RBCs lysed with 0.1% Triton X). Each condition was done in triplicaltes to obtain a standard deviation. For experiments involving annexin V staining of RBCs, 0.1% RBCs were incubated with 2 μM TMR-TAT and 0.25 μg/mL of FITC-annexin V in PBS containing 1.5 mM $CaCl_2$. Photohemolysis was performed as described before with the exception that FITC-annexin V was added to lysed RBCs after irradiation. Images were recorded before irradiation and after irradiation using the RFP, FITC and phase channels. The signal seen in the FITC channel due to RFP cross-talk was subtracted from all the FITC images shown (cross-talk was determined using the RFP and FITC images obtained with RBCs and TMR-TAT incubated alone).

4.4.3 RNO assay for detection of singlet oxygen formation

The RNO spectrophotometric assay was used to detect singlet oxygen formation upon irradiation of TMR-TAT(249). Briefly, the assay uses p-nitrosodimethylaniline (RNO) and imidazole. Singlet oxygen reacts with imidazole, to form a peroxide intermediate. This intermediate then reacts with RNO to cause bleaching of the chromophore. The rate of loss of RNO absorbance is measured to determine the rate of singlet oxygen production(249). RNO (50 μM) and imidazole (10 μM) were mixed with the peptide solutions in PBS. Rose Bengal and eosin Y were used as standards for calculation of the quantum yield as the fluorescence spectra is similar to that of the TMR fluorophore. The singlet oxygen quantum yield of RB and eosin Y in aqueous solution is 0.76 and 0.57 respectively(249). The absorbance of the samples used in this assay was set to 0.63 at 556 nm in all cases, as described in reported protocols(131). The decrease in the absorbance of RNO was monitored using the plate reader (450 nm) at periodic intervals. Irradiation was performed using the halogen lamp described in the previous section.

4.4.4 Microscopy imaging

Imaging was performed on an inverted epifluorescence microscope (Model IX81; Olympus, Center Valley, PA). Images were captured with a Rolera-MGI Plus back-illuminated EMCCD camera (Qimaging, Surrey, BC, Canada). Imaging was performed using bright field and fluorescence imaging with the RFP filter set (Ex= 560±20 nm/Em= 630±35 nm). The excitation light was from a 100 W mercury lamp (Leeds Precision Instruments # L202 Osram) passed through the filter cubes and a 1009 objective. The bright-field and fluorescence images were captured with the SlideBook 4.2 software (Olympus).

5. PHOTODAMAGE OF LIPID BILAYERS BY IRRADIATION OF A FLUORESCENTLY LABELED CELL-PENETRATING PEPTIDE[‡]

5.1 Introduction

In section 2 and 4, I have shown using red blood cells as a model system that the singlet oxygen produced by Fl-CPPs in the membrane environment is involved in the mechanism behind Fl-CPP mediated photolytic activity. In addition, my results also suggest that the CPP moiety acts in synergy with the singlet oxygen-generating fluorophore to disrupt membranes efficiently(134). The molecular details of Fl-CPP mediated photolytic activity still remains unclear. Moreover, the membrane components involved in the photolysis induced by Fl-CPPs have not been identified.

The data reported in this section is a result of collaborative effort between Dr. Igor Meerovich and myself. We use large unilamellar vesicles (LUVs) as simplified membrane models to evaluate the implication of lipids in TMR-TAT mediated photolysis. In particular, we tested the hypothesis that TMR-TAT promotes lipid oxidation by local generation of ROS. We also tested whether membrane destabilization by the peptide contributes to photolysis. We show that TMR-TAT destroys liposomes upon light irradiation. First, TAT brings TMR in close proximity to lipid bilayers by binding to negatively charged lipids. Excitation of TMR then causes singlet oxygen and superoxide formation followed by lipid oxidation. Importantly, lipid oxidation is not sufficient to account for liposome destruction. Instead, the arginine-rich CPP promotes the aggregation of photo-oxidized LUVs and accelerates their lysis. These results therefore reveal a unique synergy between oxidized lipids and CPPs that leads to enhanced photolysis.

[‡] Reprinted with permission from "Photodamage of lipid bilayers by irradiation of a fluorescently labeled cell-penetrating peptide" by Meerovich, I., Muthukrishnan, N., Johnson, G. A., Erazo-Oliveras, A. and Pellois, J. P., 2013. *Biochim Biophys Acta* **1840**, 507-15, Copyright 2014 by Elsevier B.V.

Results

5.2.1 TMR-TAT binds to negatively charged LUVs but not to neutral LUVs

While trafficking within the endocytic pathway of cells, one can expect that Fl-CPPs might encounter zwitterionic (e.g. Phosphatidylcholine or PC) as well as anionic phospholipids (e.g. Phosphatidylserine or PS). To begin this study, we characterized the binding of TMR-TAT to LUVs composed of PC and PC/PS (all LUVs also contain 30 mol% of cholesterol as this reflects the lipid composition of mammalian membranes(250, 251)). The association of TMR-TAT with lipid bilayers was investigated by steady-state fluorescence anisotropy. The anisotropy of TMR-TAT increased significantly upon addition of negatively charged PS-containing LUVs but remained unchanged upon addition of PC liposomes. The data obtained were fitted to a one site-specific binding model and the dissociation constant of TMR-TAT for PC/PS liposomes was determined to be 164.6±14.7 μM (Fig. 5-1A). In addition, the fluorescence anisotropy of TMR alone (with or without 5(6)-carboxy moieties) was unaffected by addition of liposomes. This in turn suggests that TMR does not bind to LUVs and that the binding of TMR-TAT to negatively charged liposomes is primarily mediated by the CPP.

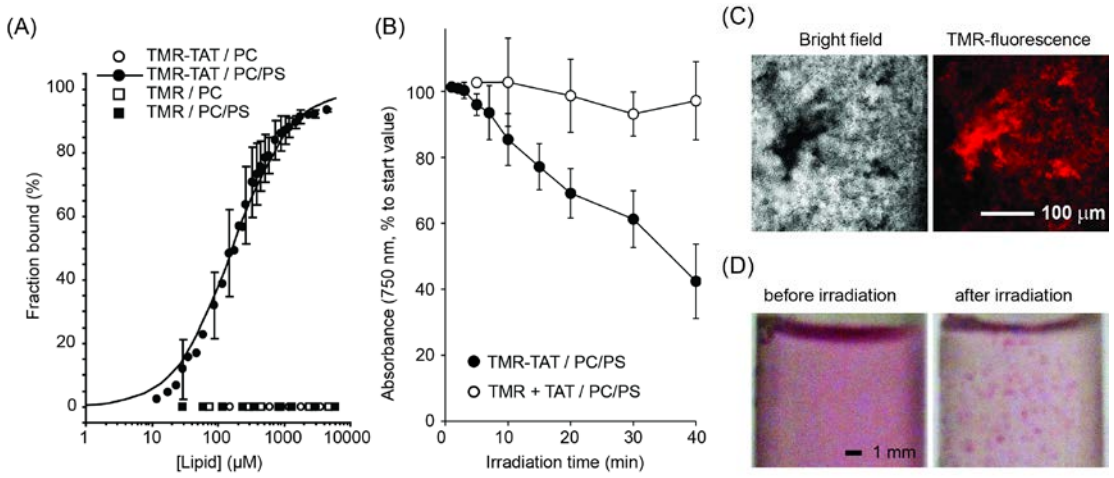

Figure 5-1. TMR-TAT binds to negatively charged LUVs and induces photodamage to these LUVs selectively.

A) Fraction of TMR and TMR-TAT bound to PC or PC/PS LUVs as a function of total lipid concentration. Fluorescence anisotropy was used to estimate the fraction bound, taking into account change of fluorescence quantum yield of bound fluorophores. The binding of TMR-TAT with PC/PS LUVs was fit with one site-specific binding model (R-value= 0.95). B) Irradiation of PC/PS LUVs with TMR-TAT (2 μM; peptide to total lipids ratio P:L is 1:400) causes loss of turbidity of liposomal dispersion. This is not observed when PC/PS LUVs, TMR (2 μM) and unlabeled TAT (2 μM) are irradiated, or with other control conditions (including incubation in dark or after illumination of neutral PC LUVs with TMR-TAT, data not shown). All experiments were performed in triplicates (averages and corresponding standard deviations are represented). C) Irradiation of PC/PS LUVs with TMR-TAT is accompanied by formation of fluorescent liposomal aggregates, observed by bright field and fluorescence microscopy. D) At high doses of irradiation, large aggregates are directly visible to human eye (photographs of liposome suspensions in test tubes are shown, the pink color being is due to TMR-TAT).

5.2.2 TMR-TAT destroys negatively charged LUVs in a light-dependent manner

In order to establish whether irradiation of TMR-TAT leads to the disruption of lipid bilayers, a leakage assay that monitors the release of calcein from the lumen of liposomes was initially performed (Fig. 5-2). An increase in calcein fluorescence was detected when PC/PS LUVs were irradiated in the presence of TMR-TAT. On the other hand, this was not observed with PC LUVs, when TMR-TAT is absent, or when the sample is kept in the dark. These data therefore suggest that TMR-TAT mediates calcein escape from negatively charged LUVs upon irradiation. However, irradiation was also accompanied by the apparent precipitation of components from the solution, thereby preventing the quantitative analysis of these results. To test whether TMR-TAT might be involved in this phenomenon, free liposomes (i.e. not loaded with calcein) were incubated with TMR-TAT and irradiated. After short-spin centrifugation to remove potential precipitates, the optical density of the liposomal suspension was monitored at 750 nm as a function of irradiation time. The rationale was that this turbidometry assay could be used to monitor whether liposomes aggregated during irradiation as precipitation would be accompanied by a loss of light scattering(127, 252).

As shown in Fig. 5-1B, irradiation of PC/PS LUVs in the presence of TMR-TAT caused a significant reduction in turbidity of the sample. In contrast, the turbidity of a suspension of PC LUVs was not significantly affected under similar conditions. In addition, irradiation of PC/PS LUVs irradiated with TMR alone, TAT alone or TAT mixed with TMR (1:1 stoichiometry) did not lead to a loss of turbidity (Fig. 5-1B). Finally, the turbidity of all samples remained unchanged after incubation in the dark (Fig. 5-3). Together, these data therefore suggest that loss of turbidity requires conjugation of TMR to TAT, binding of TMR-TAT to liposomes, and light excitation of TMR-TAT.

To further investigate the origin of the loss of turbidity observed, liposomal suspensions were examined by bright field and fluorescence microscopy. As shown in Fig. 5-1C, aggregates could be observed in irradiated solutions containing TMR-TAT and PC/PS LUVs. These aggregates were brightly fluorescent, indicating that the labeled-

peptide is one of the components present (Fig. 5-1C and 5-3). At high doses of light, the formation of large colored aggregates was visible to the eye (Fig. 5-1D). To confirm that the loss of turbidity observed is due to a loss of lipid content, the relative change of lipid concentration of LUV suspensions irradiated in the presence of TMR-TAT was evaluated. As with the turbidity assay, samples were centrifuged briefly at low speed after irradiation to remove possible aggregates formed and the supernatants were analyzed for phospholipid content with an ammonium ferrothiocyanate assay. As shown in Fig. 5-4, the phospholipid content of the supernatants decreases with irradiation time at a rate proportional to the loss of turbidity previously observed. Overall, these data therefore indicate that TMR-TAT and liposomes form large aggregates after light irradiation and that the loss of turbidity measured is a result of this aggregation process.

5.2.3 Photodestruction of liposomes is mediated by the formation of reactive oxygen species in close proximity to lipid bilayers and by oxidation of lipids

To gain some mechanistic insights on how TMR-TAT mediates the liposome photodestruction observed, the dependence of this activity on oxygen was assessed. A turbidometry assay was performed on suspensions of PC/PS LUVs irradiated with TMR-TAT in buffer saturated with argon or oxygen. As shown in Fig. 5-5A, irradiation of samples saturated with argon did not cause a loss of turbidity. In contrast, samples saturated in oxygen led to a decrease in turbidity similar to that observed in Fig. 5-1 where air-equilibrated buffer is used. The requirement for both light and oxygen suggested that TMR-TAT photosensitize LUVs with the formation of singlet oxygen (Type II) or superoxide (Type I mechanism) as primarily generated ROS, with molecular oxygen being respectively an acceptor of either electron or energy transfer from the excited fluorophore/photosensitizer molecule(253).

In order to detect whether TMR-TAT might produce singlet oxygen upon irradiation, a RNO assay was performed(242). In this assay, a peroxide intermediate is formed upon reaction of $^1O_2$ with imidazole. Reaction of the chromophore RNO with the intermediate results in bleaching(242). As a result, there is a loss of absorbance of RNO at 450 nm wavelength which is used to determine the rate of production of $^1O_2$. The

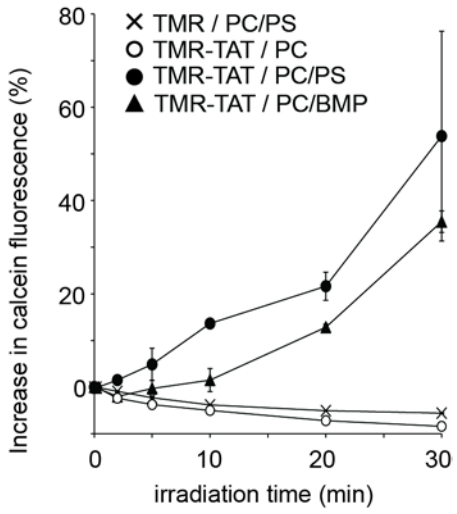

Figure 5-2. Irradiation of FL-CPPs causes leakage of liposomal load from negatively-charged LUVs but not from neutral LUVs.

Leakage of calcein from LUVs irradiated with eosin-TAT and TMR-TAT (5 μM; peptide to total lipids ratio P:L is 1:40) was measured by detecting the increase in fluorescence that occurs upon calcein dilution and unquenching. The average values and corresponding standard deviations of triplicate experiments are represented.

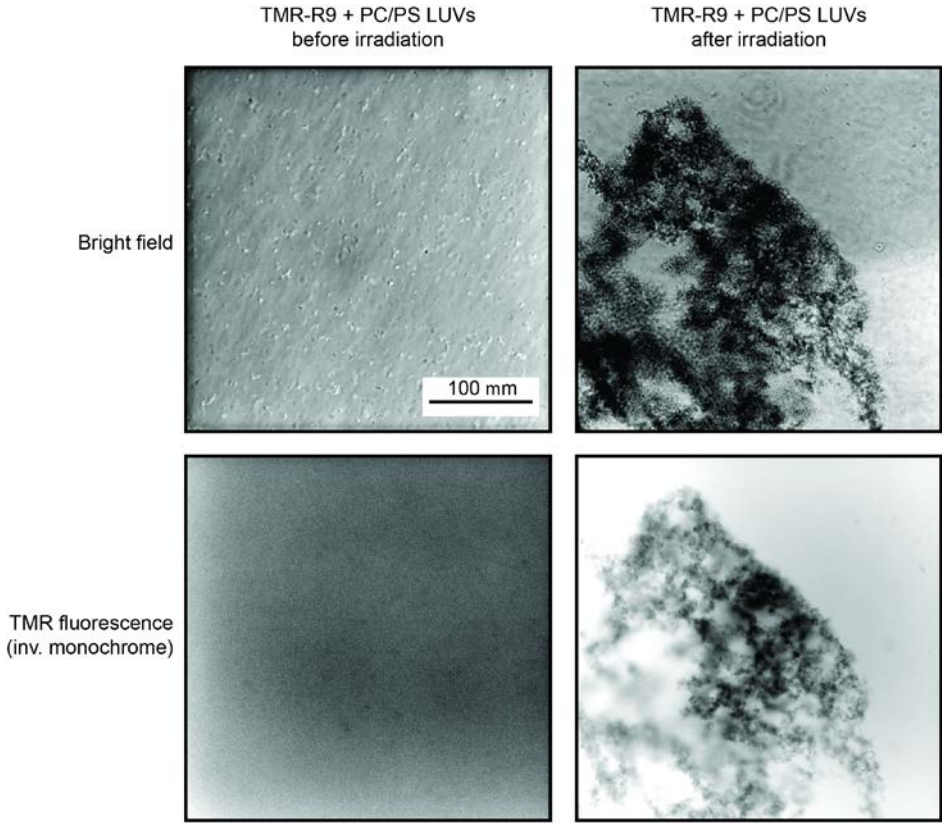

Figure 5-3. Formation of TMR-R9/lipids aggregates upon irradiation of PC/PS LUVs.

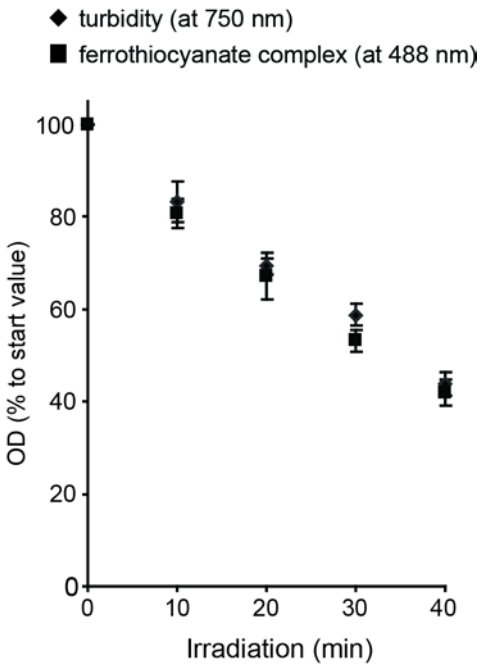

Figure 5-4. Comparison of relative decrease of turbidity and relative phospholipids content.

Samples contain PC/PS LUVs irradiated with TMR-TAT (2 μM; P:L=1:400).

photosensitizer Rose Bengal (RB) was used as a positive control. In addition, 5(6)-carboxyeosin Y, another halogenated xanthene derivative known to produce singlet oxygen upon irradiation, was conjugated to TAT to improve the solubility of the photosensitizer in water. Eosin-TAT was then used as an additional control. Upon irradiation, production of singlet oxygen from TMR-TAT could be detected (Fig. 5-5B). Consistent with the small triplet state quantum yields of TMR reported in the literature, singlet oxygen production was however very inefficient in comparison to Eosin-TAT (singlet oxygen quantum yield of 0.57 for Eosin Y) or RB (singlet oxygen quantum yield 0.72-0.79(254-256)).

In order to determine whether TMR-TAT also produces superoxide upon irradiation, a NBT assay was utilized. In this assay, NBT gets reduced upon reaction with superoxide radicals and forms an insoluble purple compound formazan(257). Eosin Y has been previously shown to produce superoxide in addition to singlet oxygen upon excitation(258). Eosin-TAT was therefore used a positive control in this assay as well (singlet oxygen does not interfere with the NBT assay(257)). As shown in Fig. 5-5C, irradiation of TMR-TAT caused a chemical reduction of NBT, as observed by an increase in absorbance. NBT reduction was inhibited by addition of the superoxide quencher tiron, suggesting that superoxide is indeed detected in this assay (Fig. 5-5D). However, a concern is that the hydroxyl radical, a ROS that can potentially be produced from superoxide, might interfere with the NBT assay (tiron can also potentially quench the

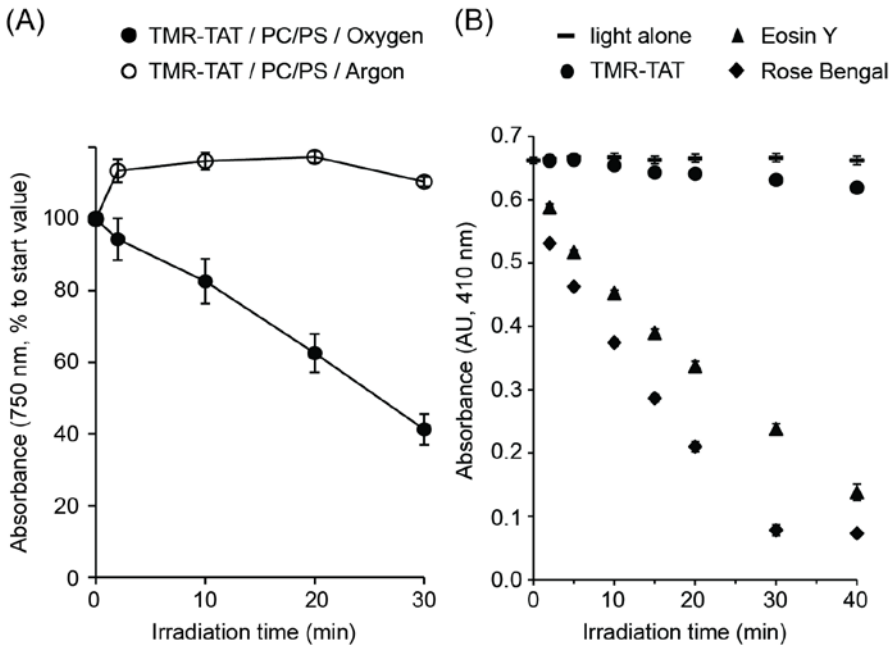

Figure 5-5. TMR-TAT-induced photodamage is oxygen dependent and TMR-TAT produces singlet oxygen and superoxide.

A) Dependence of photolytic efficiency of TMR-TAT (as evaluated by turbidometry) on oxygen. The graph shows difference in relative turbidity change for PC/PS LUVs irradiated with TMR-TAT (2 μM, P:L=1:400) in samples saturated with argon or oxygen gas prior to experiment. B) Detection of singlet oxygen photogeneration by the RNO assay, performed with TMR-TAT and eosin-TAT and Rose Bengal as positive controls (all at 7 μM).

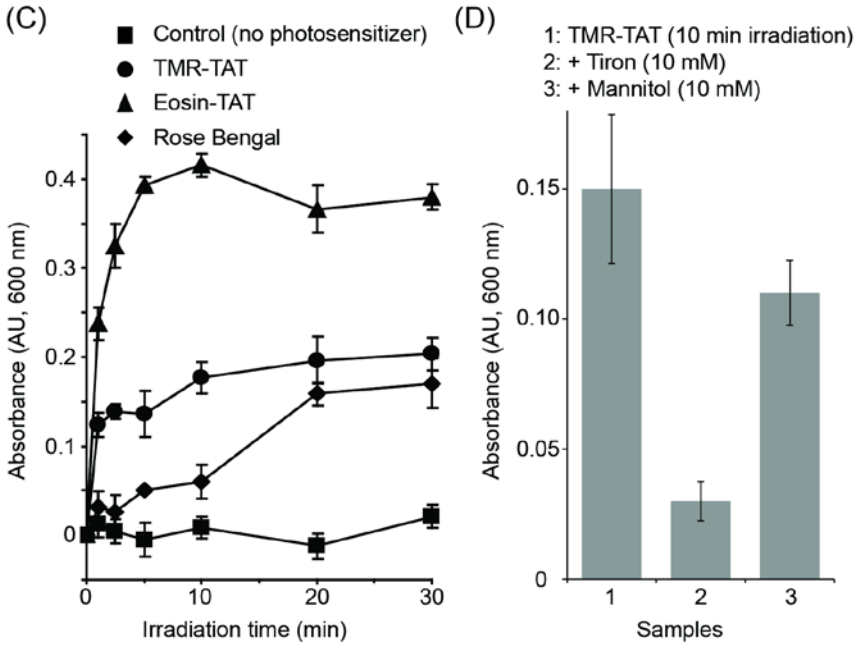

Figure 5-5. contd.

C) Detection of superoxide photogeneration by the NBT assay, performed with TMR-TAT, eosin-TAT and Rose Bengal (all at 10 μM). D) Effect of the quenchers tiron and mannitol on the chemical reduction of NBT mediated by irradiation of TMR-TAT. Samples were treated with TMR-TAT as described in C) with the exception that tiron (10 mM) or mannitol (10 mM) were added prior to irradiation. All experiments were performed in triplicates (averages and corresponding standard deviations are represented).

hydroxyl radical(259)). To address this issue, mannitol, a quencher with specificity for the hydroxyl radical over other ROS, was added to the NBT assay(260, 261). As shown in Fig. 5-5D, addition of mannitol had a relatively small effect on the chemical reduction of NBT mediated by TMR-irradiation. These results therefore indicate that the NBT reduction observed is mainly reporting formation of superoxide. Together, these data suggest that TMR-TAT produces both singlet oxygen and superoxide upon light irradiation.

Next, we tested whether TMR-TAT might photosensitize LUVs by causing oxidative damage in the lipid bilayer. Singlet oxygen and superoxide are known to oxidize unsaturated lipids to form lipid hydroperoxides(262). In order to detect whether irradiation of TMR-TAT resulted in the formation of lipid hydroperoxides, a colorimetric assay was performed with the peroxide indicator TMPD. TMPD is oxidized by lipid hydroperoxides and this can be detected by so called "Wurster's blue" coloration and an increase in the absorbance of the compound at 610 nm(263-265). For these experiments, LUVs were incubated and irradiated with TMR-TAT, TMPD was added to the sample after 40 min of irradiation, and the absorbance of TMPD was measured. As shown in Fig. 5-6A, PC LUVs irradiated with TMR-TAT in PBS did not give rise to a TMPD signal markedly higher than PBS alone. In contrast, PC/PS LUVs subjected to a similar treatment led to a five-fold increase in TMPD absorbance at 610 nm. This was not observed when the sample was kept in the dark. Together, these results are consistent with the notion that TMR-TAT oxidizes lipids upon irradiation and that binding to the lipid bilayer is required for this effect.

While the TMPD assay confirmed the presence of lipid peroxides, this assay is not very sensitive and oxidized TMD was detected only after irradiation times of 30-40 min. At this light dose, the turbidity of negatively charged LUVs is significantly reduced. This therefore raised the concern that lipid hydroperoxides formation might be a consequence of TMR-TAT/lipid aggregation as opposed to a cause. To address this issue, the effect of α-tocopherol, a lipophilic antioxidant, on LUV photodestruction was determined. When

added to PC/PS LUVs, α-tocopherol inhibited the loss of turbidity mediated by TMR-TAT irradiation (Fig. 5-6B).

In a complementary assay, the lipid peroxidation reporter cis-parinaric acid (PnA) was incorporated into LUVs (1%). PnA is a conjugated polyunsaturated fatty acid that emits a fluorescence signal at 410 nm upon excitation at 320 nm. PnA is sensitive to oxidative damage and oxidation results in loss of fluorescence. PnA-LUVs and TMR-TAT samples were irradiated and the fluorescence of PnA was monitored over time. Experiments were performed with P:L ratio of 1:400. The total duration of irradiation was limited to 4 min of light exposure, so as to assess the activity of TMR-TAT under conditions where the loss of turbidity was minimal (the light of irradiation set-up used here is also less intense than that used for the turbidometry assay, see material and methods for details). As shown in Fig. 5-6B, irradiation of PnA-liposomes with TMR-TAT caused a rapid loss of PnA fluorescence when incubated with PC/PS LUVs. PC LUVs were not significantly oxidized by irradiation with TMR-TAT, suggesting that TMR-TAT present in solution and not bound to lipids does not contribute to oxidative damage in the lipid bilayer. These data also establish that oxidation can be detected before lipid aggregation is observed and that inhibiting oxidation inhibits LUV photodestruction.

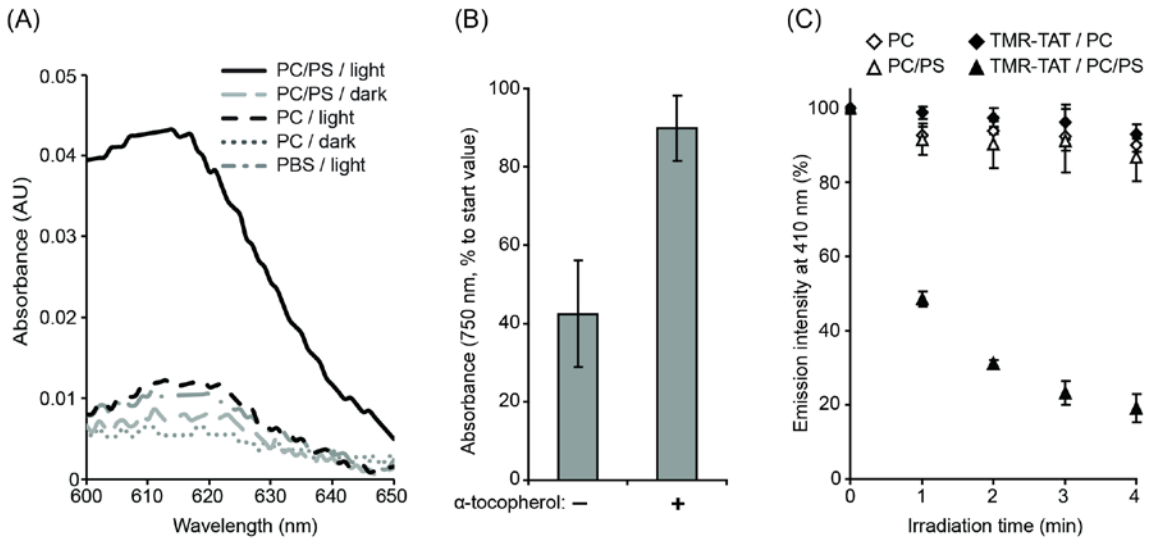

Figure 5-6. Irradiation of TMR-TAT mediates the oxidative damage of lipids in PC/PS LUVs.

A) Irradiation of PC/PS LUVs with TMR-TAT results in the formation of lipid peroxides visualized by reaction with TMPD and the production of "Wurster's Blue" coloration of oxidized cation-radical with a characteristic absorption near 610 nm. B) The lipophilic anti-oxidant α-tocopherol inhibits the photodestruction of PC/PS LUVs after 40 min of irradiation with TMR-TAT (2 μM, P:L=1:400). C) Evaluation of relative oxidation conditions created in lipid membrane by using the oxidation reporter PnA. PnA (1% total lipids) was added to PC and PC/PS LUVs and its oxidation is monitored by measuring the loss of fluorescence that accompanies the irradiation of LUVs without and with TMR-TAT (2 μM, P:L=1:400). All experiments were performed in triplicates (averages and corresponding standard deviations are represented).

5.2.4 Photodestruction of liposomes with TMR-TAT is mediated by the action of the cell-penetrating peptide

Previous data suggests that photo-oxidation of the lipid bilayer is required for LUV photodestruction. Next, we tested whether photo-oxidation is sufficient for this phenomenon. RB possesses a spectral maximum of excitation similar to that of TMR-TAT (see Fig. 5-7) and also produces singlet oxygen and superoxide. In addition, RB is lipophilic and readily associates with lipid bilayers (see Table 5-1, K_d determined with PC/PS LUVs is 213.8±26.6 μM). we therefore reasoned that, if lipid bilayer photo-oxidation is sufficient for the formation of lipid aggregates, irradiation of RB should lead to a loss of turbidity similar to that seen with TMR-TAT. To test this idea, the activity of RB was first quantified with the PnA assay previously described. As shown in Fig. 5-8A, irradiation of RB (2 μM) incubated with PC/PS LUVs containing 1% PnA (P:L=1:400) also led to a rapid loss of PnA fluorescence, with higher rate than that of TMR-TAT, consistent with the notion that RB is a photosensitizer more effective at generating singlet oxygen than TMR. Yet, irradiation of LUVs incubated with RB did not lead to significant loss of turbidity (Fig. 5-8B). Overall, these data therefore suggest that, despite being more photo-oxidative than TMR-TAT, RB is unable to cause lipid aggregation.

These results therefore raised the possibility that the peptide moiety of TMR-TAT, in addition to bringing TMR in close proximity to the lipid bilayer, might contribute to lipid aggregation. To test this hypothesis, the peptides TMR-K9 and TMR-R9 were synthesized. Like TMR-TAT, TMR-K9 and TMR-R9 are positively charged (both possess overall charge of +9) and both species bind to PC/PS LUVs but not to PC LUVs (Table 5-1, K_d of binding with PC/PS LUVs were 153.0 ± 10.1, and 202.8 ± 19.3 mM for TMR-R9 and TMR-K9, respectively). In order to compare the activity of the peptides quantitatively, TMR-TAT, TMR-R9 and TMR-K9 were incubated with PC/PS LUVs at a P:L ratio of 1:1400 providing conditions where all three species are 92-93% bound to lipids. Under these conditions, irradiation of TMR-R9 led to a loss of turbidity similar to that observed with TMR-TAT. In contrast, TMR-K9 was unable to reproduce this effect. In addition, a PnA assay performed under similar conditions showed that

TMR-K9, while slightly less active than TMR-R9 and TMR-TAT, could nonetheless promote the rapid oxidation of the PnA probe. The activities of TMR-R9 and TMR-K9 were also compared at a P:L ratio of 1:400 (Fig. 5-9). Under these conditions, the fraction of TMR-R9 bound to liposomes is greater than that of TMR-K9. However, in both cases, the density of peptide on the surface of liposomes should be increased and the contribution of the peptide to membrane destabilization should be increased as well. Consistent with this idea, the loss of turbidity mediated by TMR-R9 was significantly faster at a 1:400 than at a 1:1400 P:L ratio. However, TMR-K9 remained inactive under these more stringent conditions (Fig. 5-9). Together, these results therefore indicate that, like RB, TMR-K9 does not cause lipid aggregation after oxidation of the lipid bilayer. Instead, because TAT and R9 are both arginine-rich peptides, these data suggest that arginine residues are important for this photodestructive activity.

Combinations	Dissociation constant K_d(μM)	R^2 value
TMR-TAT / PC/PS	164.6±14.7	0.954
Rose Bengal / PC/PS	213.8±26.5	0.974
TMR-K9 / PC/PS	202.8±19.3	0.956
TMR-R9 / PC/PS	153.0±10.1	0.974
TMR-R9 / PC/BMP	114.9±13.5	0.916

Table 5-1. Parameters of binding of fluorophores to PC/PS and PC/BMP LUVs determined by fluorescence anisotropy titrations for 2 μM samples and fit by "one site-specific binding" model.

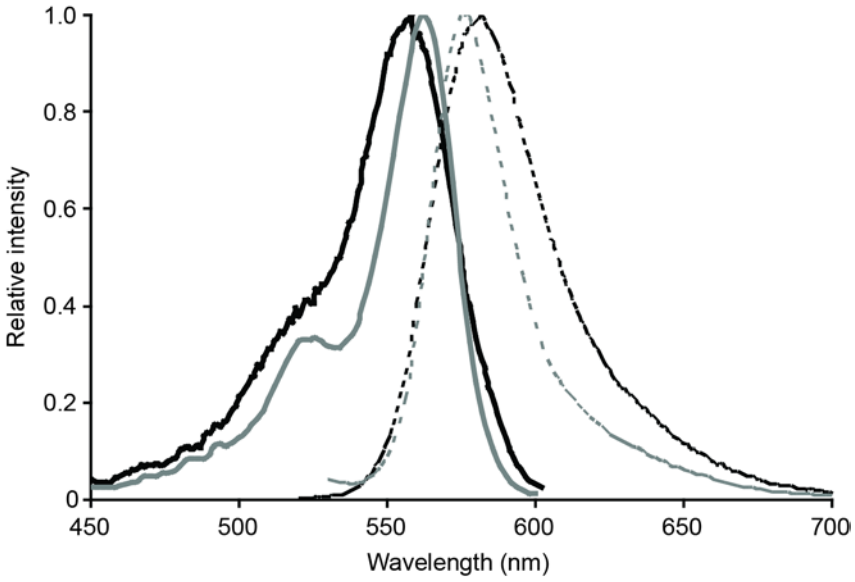

Figure 5-7. Comparison of optical properties of TMR-TAT and Rose Bengal.

Excitation and emission fluorescence spectra of TMR-TAT and Rose Bengal in presence of PC/PS liposomes (fluorophore to total lipid ratio 1:400) collected using SLM-8000C fluorometer (SLM Instruments, Bath, UK) with Vinci v.1.6 PC software (ISS, Champaign, IL) and (ISS). Excitation spectra are collected with registration of emission at 620 nm; spectra of emission - with excitation at 510 nm.

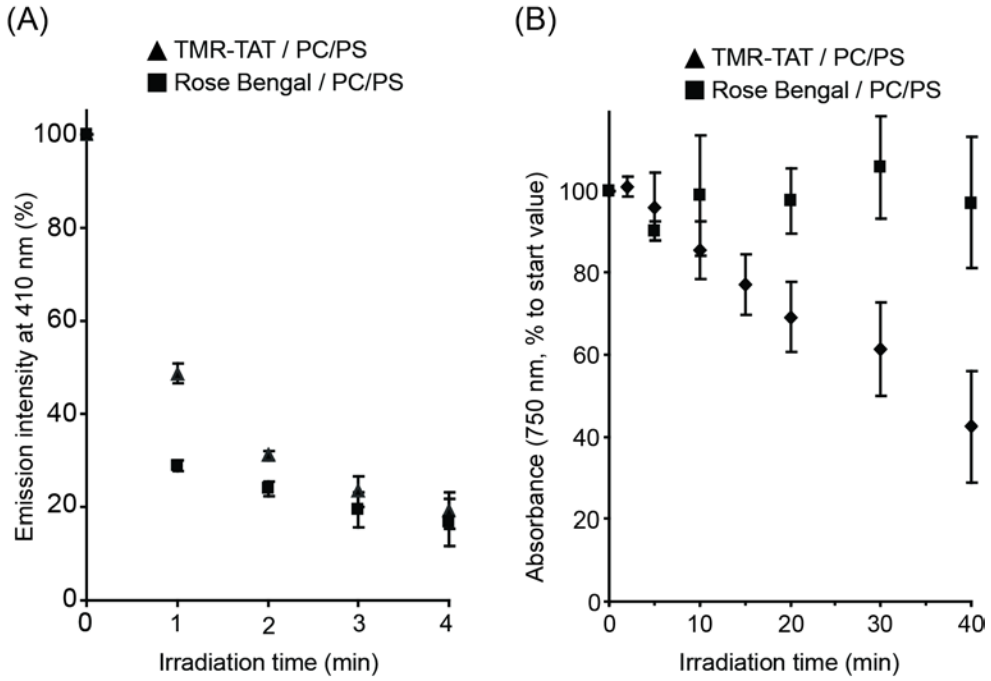

Figure 5-8. TMR-TAT causes the photo-oxidation and photodestruction of PC/PS LUVs while the photosensitizer RB only mediates photo-oxidation.

A) RB (2 μM) and TMR-TAT (2 μM, P:L=1:400) cause a similar decrease in PnA fluorescence upon irradiation of PC/PS LUVs. (B) Irradiation of RB and PC/PS LUVs is not accompanied by a loss of turbidity as seen with TMR-TAT. All experiments were performed in triplicates (averages and corresponding standard deviations are represented).

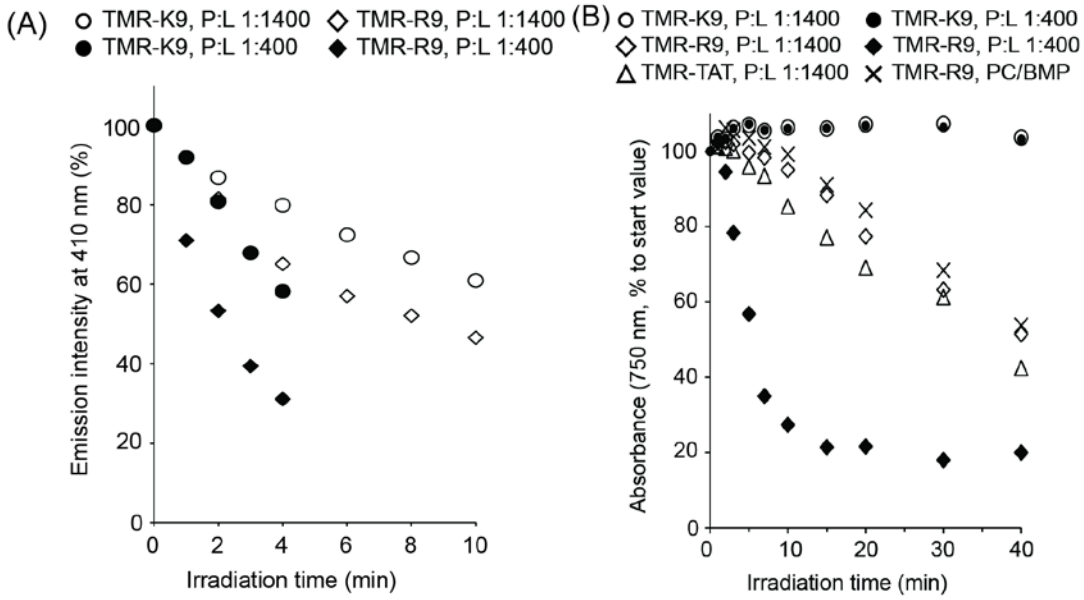

Figure 5-9. TMR-R9 and TMR-K9 both promote the oxidation of PC/PS LUVs but only irradiation of TMR-R9 leads to liposomal photodestruction.

A) Oxidation of PnA in PC/PS LUVs irradiated with TMR-R9 and TMR-K9 at P:L ratios of 1:1400 and 1:400. B) Loss of turbidity and photodestruction of PC/PS LUVs illuminated with TMR-K9, TMR-TAT and TMR-R9 at P:L ratios of 1:1400 and 1:400 (effect of TMR-TAT on PC/PS LUVs at P:L=1:400 is similar to that of TMR-R9, data not shown). The photodestruction of PC/BMP liposomes by TMR-R9 at a P:L of 1:400 is also presented. All experiments were performed in triplicates. The data presented corresponds to the average values calculated. The standard deviations are 10% or less of the value of each data point (not represented for clarity).

Because the binding of TMR-R9 to PC/PS LUVs is presumably mediated by interactions between arginine side chains and the negatively charged polar head of PS, we tested whether the photo-induced CPP/lipid aggregation observed was specific to LUVs containing PS. Because a fluorescent CPP might encounter the phospholipid bis(monoacyl-glycero)-phosphate (BMP) inside late endosomes, the photo-induced activity of TMR-R9 towards PC/BMP LUVs was measured. Like PS, BMP is negatively charged but the structures and properties of these two lipids are otherwise quite different (e.g. propensity to induce membrane curvature). The binding affinity of TMR-R9 towards PC/BMP LUVs was determined by fluorescence anisotropy and was found to closely match that obtained with PC/PS LUVs (Fig. 5-10, Table 5-1). In addition, irradiation caused a reduction of PnA fluorescence identical to that measured with PC/PS LUVs (add figure). Interestingly, loss of turbidity, while reduced in comparison to that obtained with PC/PS LUVs, was also observed when TMR-R9 was irradiated with PC/BMP LUVs. These data therefore suggest that the photodestructive capacity of Fl-CPPs such as TMR-R9 can affect LUVs composed of different negatively charged phospholipids.

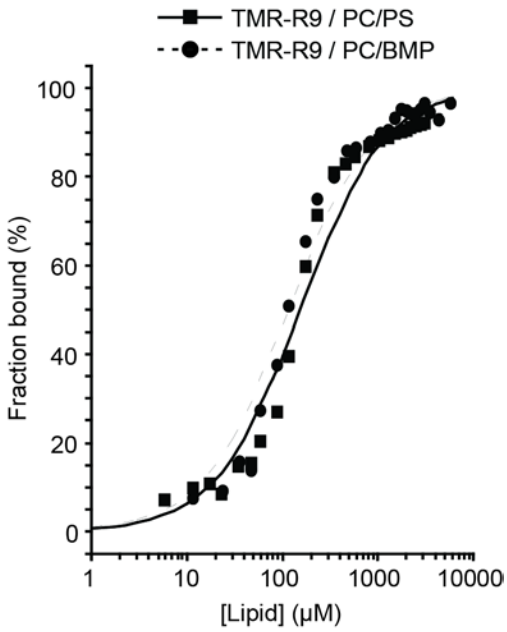

Figure 5-10. Fractions of fluorophores and Fl-CPPs bound to LUVs containing 30 %mol. of PS or BMP as a function of total lipids concentration.

Binding was evaluated by titrations of fluorescence anisotropy of samples and their conversion to fraction curves taking in account change of fluorescence quantum yield of bound fluorophores. Each curve is derived from 3 independent experiments, using 2 µM samples; error bars are not shown for clarity.

5.3 Discussion

The data establish that lipids are potential targets for the photolytic activity that Fl-CPPs exert on biological membranes. The CPPs TAT and R9, labeled with TMR could in particular cause liposomal leakage and destruction upon irradiation. The results obtained suggest that TMR produces singlet oxygen and superoxide upon irradiation and that the CPPs in the photolytic activity of Fl-CPPs by binding to negatively charged phospholipids. By bringing a fluorophore in close proximity to the lipid bilayer, the ROS produced locally oxidizes lipids. In contrast, the fraction of Fl-CPP in solution, while still producing ROS upon irradiation, contributes little to lipid damage. For instance, no peroxidation and no PnA oxidation are detected when TMR-TAT does not bind to LUVs. These results are consistent with the notion that ROS such as singlet oxygen are both very reactive and short-lived and that, as a consequence, the oxidative damage they promote is more pronounced at the sites at which they are produced (i.e. where the fluorophore is in the case of a Fl-CPP)(262, 266).

While membrane binding and proximity to the bilayer are necessary for photodestruction, experiments with RB and TMR-K9 indicates that binding might not be sufficient to account for the photodestruction of liposomes observed with TMR-TAT and TMR-R9. On one hand, TMR-K9, like TMR-R9, binds to negatively charged LUVs and photo-oxidizes PnA in the bilayer. On the other hand, irradiation of TMR-K9 did not lead to the destruction of PS-containing liposomes observed with TMR-R9 and TMR-TAT. These data therefore indicate that the photo-destruction of liposomes observed with labeled TAT and R9 might be mediated by the peptide themselves. In particular, the arginine-rich peptides might aggregate with oxidized lipids in a way that a lysine-rich analog cannot mimic. These results therefore support the notion that, while generation of ROS is necessary to initiate membrane photodamage, it is the CPP moiety that contributes to the photodestruction of LUVs observed. These results are therefore in good agreement with the photohemolysis study that has shown that RB can photolysis red blood cells without affecting membrane morphology while TMR-TAT causes photolysis as well as membrane shrinkage. It is now plausible that the membrane

shrinkage observed in this context is caused by the aggregation of TMR-TAT with oxidized lipids.

Overall, these results provide some mechanistic insights on how Fl-CPPs might lyse endosomes upon light irradiation. The fact that binding to negatively charged lipids is required for the lysis of liposomes suggests that Fl-CPPs might preferentially lyse endocytic organelles that contain negatively charged membranes. This could be the case for late endosomes as these organelles are uniquely enriched in BMP(267). PS is typically thought to be present in the cytoplasmic leaflet of endocytic organelles but not in the luminal leaflet(268). This is based on the idea that the PS asymmetry observed at the plasma membrane is maintained upon endocytosis. Whether an endocytosed Fl-CPP might encounter PS in the endocytic pathway remains therefore unclear. However, it has been shown that PS flip-flop is enhanced in liposomes containing oxidized PC(269). It is therefore possible that, upon irradiation, Fl-CPPs initially cause minimal damage to the membrane of endosomes. If this initial damage however results in PS exposure on the luminal leaflet, the binding of a Fl-CPP to the membrane would dramatically increase. This, in turn, would further favor photo-induced membrane destruction. We thus propose that this model might serve as a starting point for the design of optimally photo-endosomolytic compounds. Finally, it should be noted that cells experience oxidative stress and that cellular membranes can contain oxidized lipids(262, 266). Given the unique interactions detected in this report between CPPs and oxidized lipids, it is tempting to speculate that oxidized lipids might play an important role in the cell-penetration activity of CPPs (i.e. in the dark).

5.4 Material and methods

All peptide synthesis reagents were obtained from Novabiochem (EMD/Merck, Darmstadt, Germany). The fluorophores 5(6)-carboxytetramethylrhodamine and 5(6)-carboxyeosin Y were purchased from Novabiochem and Marker Gene Technologies (Eugene, OR) respectively. Eosin Y, tetramethylrhodamine, Rose Bengal, *p*-nitrosodimethylaniline (RNO), sodium azide, α-tocopheryl acetate, imidazole, salts for buffer preparation were received from Sigma-Aldrich (St. Louis, MO). For liposome

preparation, 1-stearoyl-2-oleoyl-sn-glycero-3-phospho-choline (PC), 1,2-dioleoyl-sn-glycero-3-phosphocholine (PC'), 1,2-dioleoyl-sn-glycero-3-phospho-L-serine (PS), bis-(mono-oleoylglycero)-phosphate (BMP) and cholesterol were bought from Avanti Polar Lipids (Alabaster, AL).

5.4.1 Peptide synthesis

The peptides TAT (GRKKRRQRRRG-NH_2), R9 (GRRRRRRRRR-NH_2) and K9 (KKKKKKKKK-NH_2) were prepared using Fmoc solid-phase chemistry on a 0.72 mmol scale using rink amide MBHA resin to obtain C- terminal amides. The amino acids Fmoc-Gly-OH, Fmoc-Arg(Pbf)-OH, Fmoc-Lys(Boc)-OH, Fmoc-Gln-OH, 5(6)-carboxytetramethylrhodamine and 5(6)-carboxyeosin Y were used to synthesize the required peptides. All reactions were performed at room temperature and with constant agitation using dry N2 gas. The Fmoc on the peptide resin was first deprotected by addition of a 20% piperidine solution in DMF. The deprotection was performed twice for 5 min and 15 min respectively followed by DMF washes each time. Then, the amino acids were added on the resin using a coupling reaction. The coupling reactions were carried out using a mixture of the Fmoc amino acid (2.88 mmol), HBTU (1.06 g, 2.80 mmol) and DIEA (1.25 mL, 7.2 mmol) in DMF for 3 hr. The resin was washed with DMF after each coupling step and the Fmoc-deprotected before each coupling reaction. After synthesis of the peptide on the resin corresponding to TAT, R9 or K9 sequence, 20% piperidine in DMF was added for 1×5 and 1×15 min to deprotect the Fmoc on the N terminal residue of the peptide while keeping the side-chain protecting groups on the amino acids intact. The fluorophores were then coupled onto the peptide by reacting the peptide with a mixture of 5(6)-carboxytetramethylrhodamine or 5(6)-carboxyeosin Y (2.88 mmol), HBTU (1.06 g, 2.80 mmol) and DIEA (1.25 mL, 7.2 mmol) in DMF overnight.

After assembly of the Fl-CPP on the solid support, the resin was treated with a solution of TFA containing 2.5% H_2O and 1% triisopropylsilane for 2 hr in order to deprotect all the side chains on the peptide and cleave the Fl-CPP off the resin. The crude Fl-CPPs present in the TFA solution were then washed with cold anhydrous Et2O to

achieve peptide precipitates. The crude peptides were then dissolved in aqueous acetonitrile and lyophilized. Fl-CPPs were purified using semi-preparative HPLC and their purity was confirmed by mass spectrometry (MALDI-TOF) analysis.
TAT expected mass: 1451.92 Da, observed mass: 1452.41 Da; R9 expected mass: 1478.96 Da, observed mass: 1479.52 Da; K9 expected mass: 1169.88 Da, observed mass: 1170.96 Da; TMR-TAT expected mass: 1865.07 Da, observed mass: 1866.1 Da; TMR-K9 expected mass: 1583.0 Da, observed mass: 1583.30 Da; TMR-R9 expected mass: 1893.20 Da, observed mass: 1894.4 Da, . The pure lyophilized peptides were dissolved in water to make 1 mM stock solutions that were diluted to desired working concentrations in PBS (NaCl 137 mM, KCl 2.7 mM, Na_2HPO_4 10 mM, KH_2PO_4 1.8 mM; adjusted to pH 7.4) for experiments.

5.4.2 Preparation of liposomes

Lipids in chloroform were mixed in a glass vial at molar ratios of 7:3 PC:cholesterol for neutral liposomes and 4:3:3 PC:PS:cholesterol or 4:3:3 PC:BMP:cholesterol for negatively charged liposomes. Alternatively, neutral liposomes were prepared with a composition of 4:3:3 PC:PC':cholesterol, in order to generate neutral LUVs that contain the same amount of unsaturated lipids as their negatively charged counterparts. Lipid films were prepared by evaporating the solvent from the mixture using a flow of nitrogen gas, then removing trace solvent by freeze-drying. The films were hydrated with only PBS buffer or buffer solution of calcein (60 mM) by vigorous vortexing and then allowed to swell for 2 h at 10°C under nitrogen to obtain multilamellar lipid vesicles. Liposomes were extruded through Nuclepore polycarbonate membranes (Whatman, Clifton, NJ) with pore sizes of 100 nm (21 passes; for fluorometric studies) or 200 nm (11 passes; for turbidometry studies) using a Mini-Extruder device (Avanti Polar Lipids, Alabaster, AL). The respective size distribution of liposomes was on average 140 and 236 nm, as determined by dynamic light scattering using a Zeta Sizer device (Malvern instruments, Worcestershire, UK). The extruded large unilamellar vesicles (LUVs) were stored at 4°C and used within two weeks of preparation.

When required for calcein-leakage experiments, calcein-loaded LUVs were separated from non-entrapped fluorophore by gel filtration on Sephadex G-50 (GE Healthcare, Pittsburgh, PA) column (2.5×14 cm). Additionally, for experiments performed with cis-parinaric acid (PnA), the latter was added in ethanol solution to the lipid mixtures listed above at 1% mol. to the total lipids. PnA-containing lipid mixtures were dried with a flow of nitrogen and freeze-dried. Lipids were then re-dissolved in a minimum amount of chloroform and dried again, in order to provide a homogeneous distribution of constituents. PnA-containing LUVs were hydrated as described above and extruded through 100 nm pore size Nuclepore membranes (21 passes). Because of their sensitivity to oxidative damage, the PnA-containing LUVs were used within 40 h of preparation.

5.4.3 Fl-CPP binding to liposomes and fluorescence anisotropy

The binding of peptides to lipid bilayers can be described by an apparent molar partition coefficient K(270, 271). The measurements used molar concentrations of lipid [L] much greater than that of the peptide bound to the liposomes $[P]_b$. Under these conditions:

$$[P]_b = K[P][L] \qquad (1)$$

Because the peptides might permeate membranes, [L] is the total molar concentration of lipid in the solution. In addition, the free peptide molar concentration [P] can be substituted for $[P]_{tot}$-$[P]_b$ in Eq.1 to obtain:

$$[P]_b/[P]_{tot} = K[L]/(1+K[L]) \qquad (2)$$

where $[P]_{tot}$ is the total molar concentration of peptide in solution. To obtain K, the binding of Fl-CPPs to lipid bilayers was determined by titrating the samples with neutral or anionic LUVs and determining the change of the fluorescence anisotropy for different total lipid concentrations. Fluorescence anisotropy was determined using a SLM-8000C fluorometer (SLM Instruments, Bath, UK) upgraded with the Phoenix package (ISS,

Champaign, IL) and Vinci v.1.6 PC software (ISS). The contributions of light scattering and inner filter effect were minimized by filtering out the excitation wavelength from the emission beam and by using a low concentration of Fl-CPPs (0.25 to 2 μM). Titration with liposomes and acquisition of fluorescence anisotropy were performed in 3 mm optical path micro-cuvettes with 100 nm liposomes. Fluorescence anisotropy (*r)* was calculated automatically by Vinci v.1.6 PC software from four intensities of fluorescence measured under different positions of excitation and emission polarizers according to reported protocols (272). Titration of each Fl-CPP was repeated at least three times and average r values were determined for each data point. Since binding of conjugates to liposomes caused change of their fluorescence quantum yield due to change of environment, fraction bound was calculated from anisotropy-concentration dependencies using the following equation:

$$f_B = \frac{r - r_F}{(r - r_F) + R \cdot (r_B - r)} \qquad (3)$$

where f_B is the bound fraction of fluorophore; r, r_F and r_B – respectively values of fluorescence anisotropy at some current point, for fully free and fully bound fluorophore (on start and saturation of titration), and R is ratio of intensities of fluorescence of fully bound and fully free fluorophore forms, evaluated after correcting for dilution measured total fluorescence intensity values (determined by Vinci software in process of anisotropy calculation; derived from emission intensities for parallel and perpendicular polarizers orientations I_{VV} and I_{VH} as $I_{VV} + 2 \cdot G \cdot I_{VH}$, where G is the device-specific parameter) (273). The resulting binding curves were plotted and fitted to a one site-specific binding model using the GraphPad Prism v.5 software. The reciprocal of K, the dissociation constant K_d, was derived from these plots and used to compare the relative binding efficiency of the conjugates to lipids. K_d corresponds to the total molar concentration of lipid in solution that causes binding of half of the Fl-CPP present.

5.4.4 Photodamage of liposomes

Samples were irradiated for a given amount of time using a 600 W Utilitech halogen lamp, filtered via 1.5-inch water filter, diffusing glass and green optical cast plastic filter NT46-624 (Edmund Optics, Barrington, NJ) with a maximum transmission in the range of 450 to 580 nm. The final photon flux output is 3.3×10^{17} photons$\times s^{-1}\times cm^{-2}$. This photon flux is approximately 3200 fold less than what has been reported for the irradiation of Fl-CPP trapped inside endosomes of live cells on an epifluorescence microscope (irradiance is high because of the focusing of light beam after 100× objective). For comparison purposes, 40 min irradiation with the described set-up is equivalent to 0.75 sec irradiation on a microscope, a time scale at which most endosomes are photolysed (274).

Disruption and permeabilization of lipid bilayers upon photolytic treatment were evaluated using a calcein leakage assay (see section 5.4.8). The destruction of LUVs mediated by the Fl-CPPs (2 μM) was evaluated by turbidometry(127, 252). LUVs were diluted to the final concentration of 800 μM of total lipids in PBS. These liposome solutions are turbid and consequently have an optical density at 750 nm. Fluorophores or Fl-CPPs were added to these samples at different final concentrations and the samples were optionally supplied the lipophilic antioxidant α-tocopherol (60 μM). After irradiation, samples were subjected to low speed centrifugation to remove aggregates from soluble LUVs. Photodestruction was monitored by measuring the optical density of the solutions at 750 nm using UV-1700 PharmaSpec (Shimadzu, Kyoto, Japan) spectrophotometer with 1 cm quartz cuvettes.

5.4.5 Evaluation of production of singlet oxygen

A spectrometric RNO assay was performed to evaluate the formation of singlet oxygen upon light irradiation of TMR-TAT, Eosin Y and Rose Bengal (RB) in aqueous solution(242). Solutions of RNO (50 μM) and imidazole (10 μM) were prepared in PBS and mixed with Fl-CPPs or RB, a photosensitizer with a reported quantum yield of singlet oxygen of 0.76 in water, was used as a positive control(242). The concentration used in this assay were 7 μM for TMR-TAT, Eosin Y, and RB(131). The decrease in the

absorbance of RNO was monitored using a plate reader (450 nm) at periodic intervals. The conditions of irradiation for this experiment were the same as described for the turbidometry assay.

5.4.6 Evaluation of production of superoxide

The formation of superoxide was monitored by the nitro blue tetrazolium (NBT) method(257, 275-277). Reduction of NBT by superoxide (O_2^-) results in formation of an insoluble formazan, which can be detected by absorbance at 560-600 nm. Each sample was prepared in phosphate buffer containing NBT (80 μM), NADH (10 mM), and EDTA (1 mM). Samples were also supplemented with the desired concentration of photosensitizing agent, and without or with 10 mM of the quenchers tiron (4,5-Dihydroxy-1,3-benzenedisulfonic acid disodium salt) or mannitol. Samples were irradiated as described for the turbidometry assay. After irradiation, each sample was diluted in DMSO 5-fold. The absorbance of the resulting solution was measured at 600 nm (at this wavelength, the contribution of TMR and eosin Y is negligible). The absorbance reported represents the absorbance of each sample after subtraction of the absorbance measured before irradiation.

5.4.7 Detection of photo-oxidation in the lipid bilayer

Formation of oxidative conditions during photolysis with various Fl-CPPs under different conditions was studied using liposomes with lipid composition additionally supplied with 1 %mol. of 9Z,11E,13E,15Z-octadecatetraenoic acid (cis-Parinaric acid, PnA). Experiments were performed with freshly prepared liposomes at a final concentration of 800 μM by total lipids, with and without addition of Fl-CPPs to the final desired peptide to total lipid ratio (e.g. 2 μM for P:L of 1:400), irradiated with the Oriel model 67705 Hg-Xe arc light source (Oriel Instruments, Stratford, CT) equipped with HQ 560/55 filter (Chroma Technology Corp., Bellows Falls, VT) providing an irradiance with the final photon flux output of 1.9×10^{17} photons$\times s^{-1}\times cm^{-2}$. Oxidation of PnA was evaluated by measuring the decrease of its fluorescence emission at 410 nm (Ex= 320 nm), from spectra collected using a SLM-8000C fluorometer (SLM

Instruments) operated with Vinci v.1.6 PC software (ISS). To account for the fact that LUVs might aggregate upon irradiation (as shown in Fig. 5-1) and that this might cause a reduction in PnA signal, the fluorescence of PnA was recorded before or after addition of the detergent Triton X (0.2%). The results obtained before or after addition of detergents were similar in all cases, indicating that the loss of fluorescence of PnA presented in Fig. 5-6, 5-8 and 5-9 is not due to an overall loss of the amount of LUVs present in solution. The data represented in the figures are those obtained prior to addition of Triton X. Oxidation of phospholipids during photolysis was additionally confirmed by reaction with redox-indicator N,N,N',N'-tetramethyl-1,4-phenylene-diamine.

5.4.8 Study of permeabilization of liposomal membranes by calcein leakage assay

Disruption and permeabilization of lipid bilayers upon photolytic treatment were evaluated using a calcein leakage assay(278, 279). This assay is based on the quenching of calcein fluorescence at high concentrations within the lumen of LUVs. Upon release and dilution outside LUVs, calcein is unquenched and its fluorescence increases. LUVs were loaded with calcein at a fluorescence-quenching concentration of 60 mM. Loaded liposomes were separated from non-entrapped calcein by gel filtration. Diluted liposomal suspensions were irradiated without or with TMR-TAT or TMR (5 μM). The fluorescence of calcein was then measured using the blue channel (Ex= 490 nm, Em= 520-560 nm) of a Promega GloMax-Multi plate reader (Promega, Madison, WI) and monitored as a function of irradiation time. In this assay, calcein is susceptible to bleaching by light or by the effect of the TMR-TAT. The relative extent of liposomal load release was therefore calculated in relation to the total amount of non-photobleached calcein. This was in turn evaluated by solubilizing LUVs with 0.2% Triton X detergent after respective irradiation times, as follows:

$$\text{Release } (\%) = 100\% \times \left(FI_t - FI_0\right) / \left(FI_{max,t} - FI_0\right)$$

where FI_t is fluorescence intensity of a liposomal sample at current time point of irradiation, FI_0 is the intensity of the sample prior to treatment, and $FI_{max,t}$ is the fluorescence of the sample after treatment with detergent.

5.4.9 Detection of oxidation of phospholipids

Oxidation of phospholipids during photolysis was confirmed by reaction with redox-indicator N,N,N',N'-tetramethyl-1,4-phenylenediamine (TMPD)(263-265). Irradiated and non-irradiated samples containing TMR-TAT conjugate (2 μM) and liposomes (800 μM) were mixed with equal volume of saturated solution of TMPD in degased methanol. Absorption spectra were measured for formation of "Wurster's Blue" coloration of the oxidized cation-radical with characteristic band at 610 nm against control mixture of equal volumes of methanol TMPD solution and PBS immediately after mixing (TMPD cation-radical has pair characteristic absorption peaks at 560 and 610 nm, however the former wasn't used due to overlap with TMR).

5.4.10 Microscopy of liposomes

The photolytic damage to liposomes was monitored by bright field and fluorescence microscopy. Imaging was performed on an inverted epifluorescence microscope (Model IX81, Olympus, Center Valley, PA). Images were captured with a Rolera-MGI Plus back-illuminated EMCCD camera (Qimaging, Surrey, BC, Canada). Imaging was performed using bright field and fluorescence imaging with the RFP filter set (Ex= 560±20 nm / Em= 630±35 nm). The excitation light was from a 100 W mercury lamp (Leeds Precision Instruments # L202 Osram) passed through the filter cube and a 20× objective. The bright field and fluorescence images were captured with the Slidebook 4.2 software (Olympus, Center Valley, PA).

5.4.11 Evaluation of relative phospholipid content by ammonium ferrothiocyanate assay

Relative evaluation of the change in total phospholipids content in irradiated samples was done by procedure modified from an ammonium ferrothiocyanate assay(280). This assay is based on the fact that, while ammonium ferrothiocyanate does not dissolve in chloroform, its complexes with phospholipids do. Standard 0.1 N solution of ammonium ferrothiocyanate was prepared by dissolving 27.03 g of ferric chloride hexahydrate ($FeCl_3 \cdot 6H_2O$) and 30.4 g of ammonium thiocyanate (NH_4SCN) in 1 liter of milliQ water. LUV/TMR-TAT samples (non-irradiated or after chosen durations of irradiation) were centrifuged at low speed, and 200 μl of supernatant of each sample was extracted by vigorous shaking with 625 μl of chloroform. The chloroform phase was mixed and vigorously shaken with equal amount of standard ammonium ferrothiocyanate solution. The amount of colored phospholipid complexes present in the chloroform phase was determined by measuring the absorbance at each sample at 488 nm.

6. THE PHOTOLYTIC ACTIVITY OF FLUOROPHORE-CPP CONJUGATES IS MODULATED BY ARGININE RESIDUE CONTENT AND FLUOROPHORE CONJUGATION SITE

6.1 Introduction

In section 4 and 5, it was revealed that the presence of arginine in the peptide sequence appears to be of importance to accelerate the lysis of photo-oxidized membranes. The structural features of the peptide that are required to maximize photolysis remain unclear. This is important as optimizing the structures of photosensitizer-CPP or Fl-CPP constructs could facilitate PCI-based delivery approaches. For instance, optimally engineered constructs could be active at lower concentrations or might require less light than current compounds. These compounds could in turn be more appropriate for *in vivo* applications. In this section, I aim to identify how the number of arginine residues of a TMR-peptide conjugate affects photolysis. In addition, because proximity of the TMR moiety to the membrane is important, I also test the hypothesis that the positioning of TMR in the peptide sequence impacts photolysis. Red blood cells are used as a model system to establish structure-activity relationships that should assist the future optimization of CPP-based PCI.

6.2 Results

6.2.1. Length of the CPP affects the lytic ability of Fl-CPPs of RBC membranes

To determine whether the length of the CPPs and its arginine content affects TMR-CPP mediated membrane photolysis, the lytic activity of TMR-Rn conjugates, with n = 3,5,7,9,11,13 was tested with red blood cells (RBCs) using a photohemolysis assay. For this assay, 0.1% RBCs was incubated with 2 μM TMR-Rn conjugates. The mixture was irradiated with green light at 560±20 nm. The light induced lysis of RBCs was monitored using time-lapse bright-field imaging using a microscope with a 100X

objective. Photohemolysis curves were generated for each conjugate by counting the number of lysed ghosts in images obtained at each time point.

As shown in Fig. 6-1A, TMR-R1 and TMR-R3 (2 μM) were not significantly photohemolytic. In comparison, increasing the length of the peptide to R5, R7, and R9 caused an increase in the photohemolytic response. In particular, the total percentage of lysed cells at each time point increased with peptide length (Fig. 6-1A). The irradiation time required to initiate lysis also reduced as arginine content was increased. Interestingly, photohemolysis did not further increase when the conjugates TMR-R11 and TMR-R13 were tested (Fig. 6-1A). Because the saturation in the lytic activity of TMR-R11 and TMR-R13 might be a result of a saturating concentration of the Fl-CPP, a concentration dependent study of the photolysis activity with all TMR-Rn conjugates was performed. Photohemolysis was measured as a function of the number of arginine residues at 0.5 μM, 1 μM, 1.5 μM and 2 μM TMR-Rn concentration (Fig. 6-1B). At a concentration of 0.5 μM, the photohemolytic activity of TMR-Rn increased linearly with 'n'. However, at concentrations 1.5 μM and above, TMR-Rn lytic activity reached saturation for n>9 (Fig. 6-1C). Interestingly, 100% photohemolysis was not achieved under these conditions, indicating that saturation does not happen simply because all RBCs in the sample are lysed. Overall, these results suggest that lytic activity of a TMR-Rn conjugates can be varied by altering the concentration of conjugate in solution as well as the number of arginine residues in the CPP.

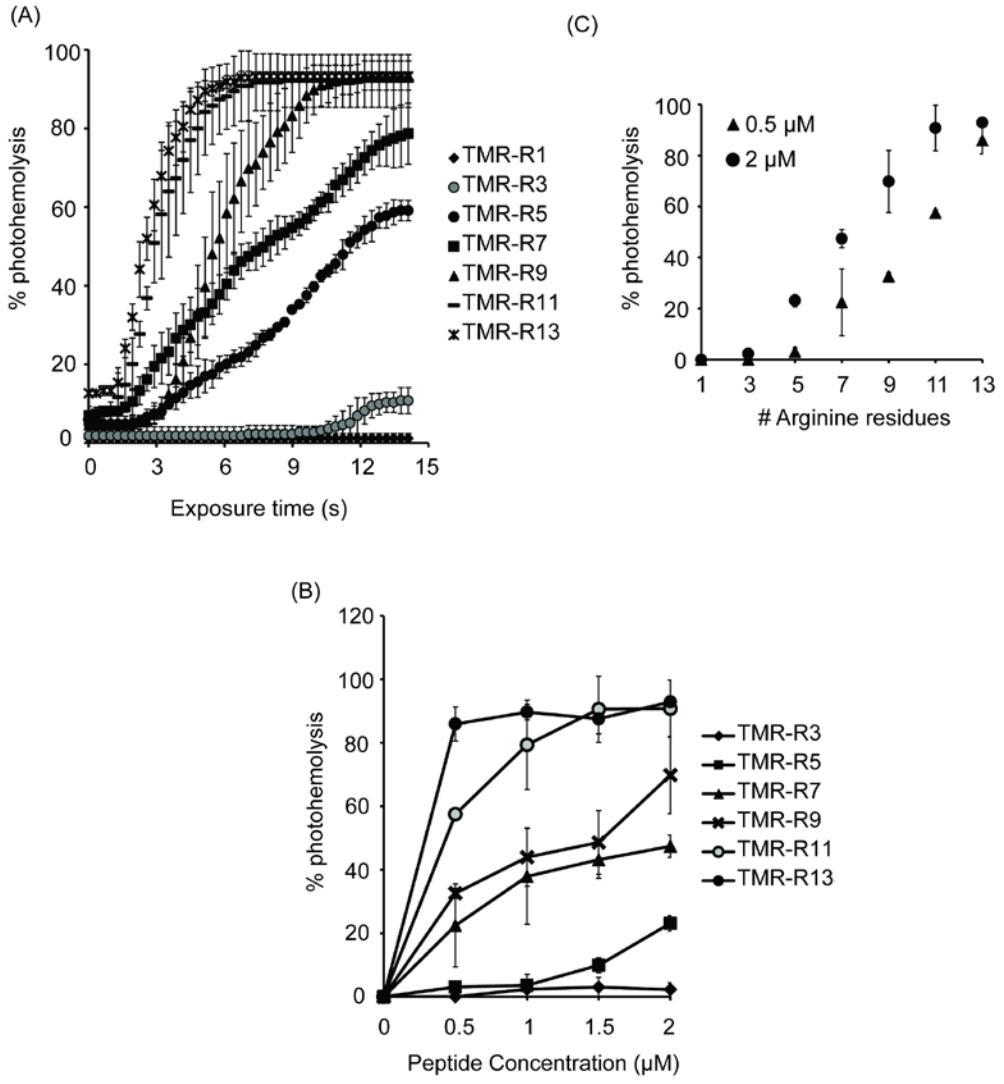

Figure 6-1. The photohemolytic activity of TMR-Rn increases with arginine content.

A) Photohemolysis curves of TMR-Rn conjugates (n=1,3,5,7,9,11,13) at 2 μM concentration. B) Comparison of photohemolytic activity of TMR-Rn conjugates at 0.5 μM and 2 μM respectively after 7 s of light irradiation. C) Concentration dependence on the photohemolytic activity of TMR-Rn conjugates. Each data point represents the average from 3 experiments. The corresponding standard deviations are included.

6.2.2 The position of fluorophore with respect to CPP affects the lytic ability of Fl-CPPs

TMR-R9 was chosen as a template to investigate how positioning of the fluorophore with respect to the peptide might affect lytic activity. In order to obtain compounds that would differ in this specific structural parameter, the peptides K(TMR)-R9, R4-K(TMR)-R5, and R9-K(TMR) were synthesized using SPPS. For each peptide, TMR was conjugated to the side chain amino group of the lysine residue. The labeled lysine was placed at the N-terminus of the peptide, at the central position in the peptide sequence as well as at the C-terminus. The photohemolytic activity of each peptide (2 μM) was then measured and compared to that of the control TMR-R9 (where TMR is conjugated to the N-terminal amino group of the peptide). As shown in Fig. 6-2A, both TMR-R9 and K(TMR)-R9 showed similar photolytic activity. However, shifting the TMR fluorophore from N to C terminus had a dramatic effect as R9-K(TMR) displayed a light-induced activity significantly lower than TMR-R9 and K(TMR)-R9. In contrast, shifting TMR to the center of the peptide improved lytic activity as R4-K(TMR)-R5 was the most photolytic conjugate tested. In particular, 50% photohemolysis is achieved with R4-K(TMR)-R5 with only half the light dose required to obtain similar results with TMR-R9. Interestingly, it is worth noting that both K(TMR)-R9 and R9-K(TMR) were more hemolytic than TMR-R9 in the dark (Fig. 6-2A, time t=0). To compare the relative activities of these TMR-peptides further, photohemolysis was monitored at different concentrations of these conjugates. As shown in Fig. 6-2B, K(TMR)-R9, R4-K(TMR)-R5, and TMR-R9 followed a similar dose response. In contrast, the lytic activity of R9-K(TMR) was not significantly affected by concentration. While surprising, these data nonetheless indicate that placing TMR at the C-terminus of the peptide greatly diminishes the photolytic activity of the conjugate. Overall, these results highlight how the position of the fluorophore in respect to the peptide sequence is an important structural factor in the conjugate's lytic activity and how alterations in structure can both lead to increase or loss in activity.

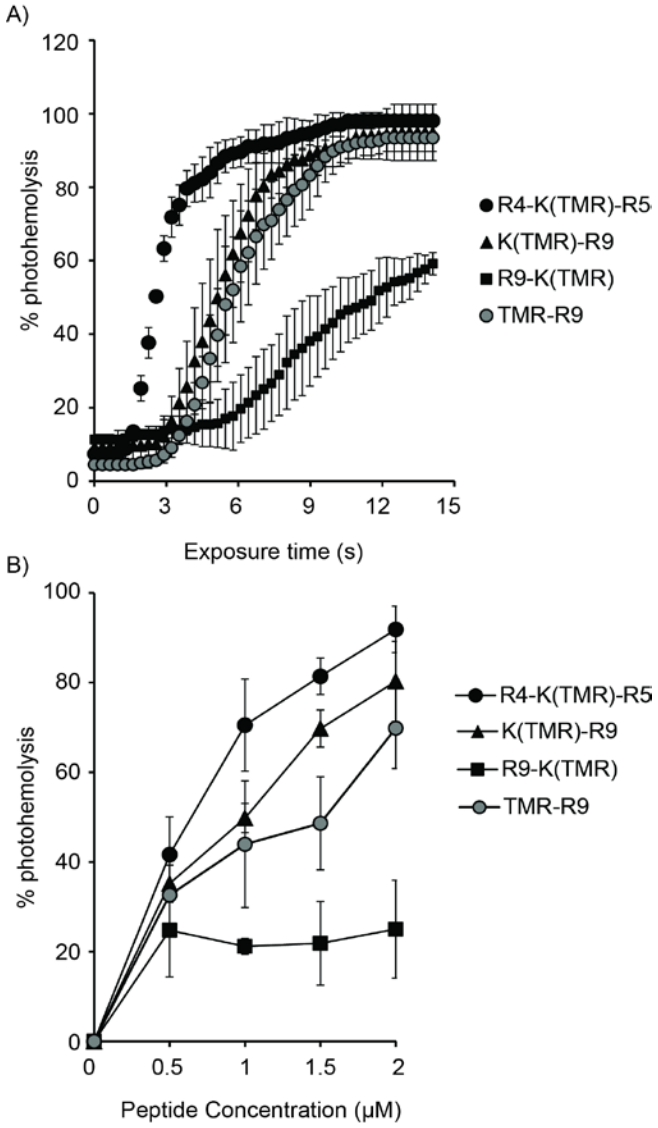

Figure 6-2. Photohemolysis is affected by the position of the fluorophore in the peptide sequence.

Photohemolysis curves were generated TMR-R9, K(TMR)-R9, R9-K(TMR) and R4-K(TMR)-R5 at 2 μM. B) Concentration dependence on the photolytic activity. The reported percent hemolysis is obtained after 7 s of light irradiation. Each data point represents the average from 3 experiments. The corresponding standard deviations are included.

6.2.3 Effect of conjugation on singlet oxygen and superoxide generation

In principle, ROS generation of TMR might be affected by the peptide to which the fluorophore is attached. This would then potentially explain the different behaviors observed for the Fl-CPP conjugates tested. It was previously determined that the photolytic activity of TMR-R9 is oxygen dependent and mediated by formation of both singlet oxygen and superoxide (135). The generation of these ROS by all TMR conjugates was therefore measured. A RNO assay was used to establish the rate of formation of singlet oxygen. In this assay, a peroxide intermediate is formed upon reaction of $^1O_2$ with imidazole. Reaction of the chromophore RNO with the intermediate results in bleaching(242). As a result, there is a loss of absorbance of RNO at 450 nm wavelength which is used to determine the rate of production of $^1O_2$. Rose Bengal was used as a positive control in this assay (the reported $^1O_2$ quantum yield for RB is 0.76) (131). As shown in Fig. 6-3A, $^1O_2$ formation by the TMR-CPPs upon light irradiation was detectable, although very inefficient in comparison to Rose Bengal. Importantly, the production of singlet oxygen was similar among all TMR conjugates, indicating that conjugation to different CPPs does not affect this activity significantly. Next, a NBT assay was used to detect superoxide formation. In this assay, eosin-TAT, a known superoxide producer, was used as a positive control. The samples were irradiated at 560 nm and the reduction of NBT was monitored spectroscopically. Here again, the rates of superoxide formation for all TMR-CPPs were found to be identical (Fig. 6-3B-C). This in turn indicates that superoxide radical production is not affected by conjugation to CPPs. Overall, these results suggest that the observed differences in photolytic activities are not caused by differences in ROS production.

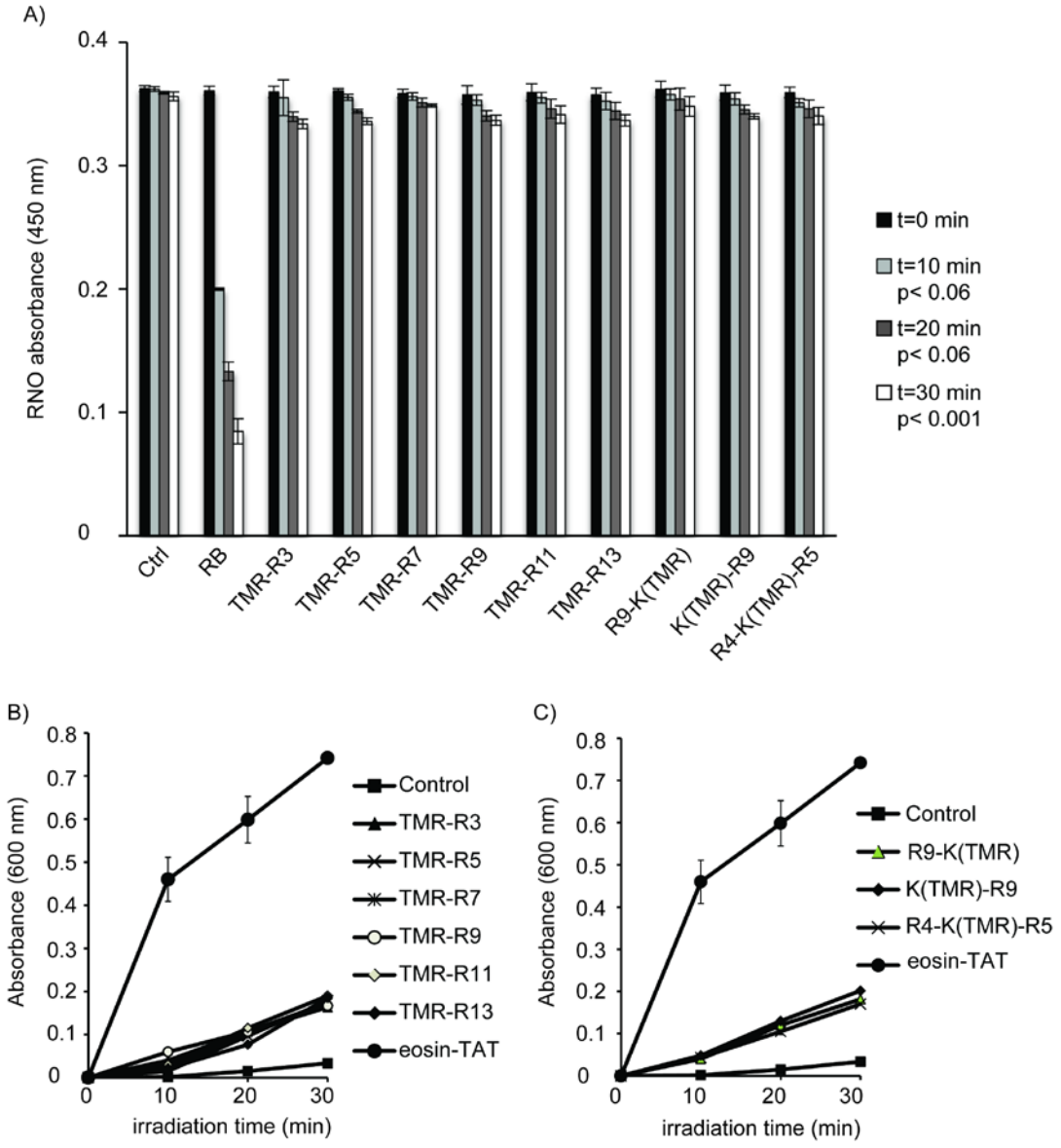

Figure 6-3. Effect of conjugation of TMR to different peptides on singlet oxygen and superoxide production.

A) Detection of singlet oxygen formation by TMR-CPPs. The formation of singlet oxygen upon irradiation of TMR-CPPs was monitored using the RNO assay with Rose Bengal as a positive control (all at 10 μM). B,C) Detection of photo-generation of superoxide radicals by TMR-CPPs. using the NBT assay with eosin-TAT as the positive control (all at 10 μM). The control sample contained all reagents necessary for NBT assay but no peptide.

6.2.4 Increasing the length and arginine content of CPPs improves its lytic activity on oxidized membranes

While R9 and TAT are not significantly hemolytic in the dark, these arginine-rich CPPs destabilize the membrane of RBCs upon photo-oxidation of membrane components(134). We therefore reasoned that the photohemolytic efficiencies observed with the various conjugates tested might in part be due to differences in this particular activity. To test this hypothesis, the effect of K(TMR)R9, R9-K(TMR), R4-K(TMR)-R5 and the TMR-Rn peptides on photo-oxidized membranes was investigated. In this assay, 1.25% RBCs were first incubated with 1 μM of the lipophilic photosensitizer Rose Bengal (RB) and exposed to a single dose of light irradiation. RB, like TMR, produces singlet oxygen and superoxide(135). It also binds to the plasma membrane of RBCs and lyses these cells upon irradiation(134). RB-mediated membrane oxidation might therefore be similar to what is obtained upon TMR-CPP irradiation. In this experiment, RB irradiation was limited to a few seconds so as to avoid premature lysis (irradiation of RB alone lyses RBCs if irradiation is extended, data not shown). After irradiation, the TMR-CPP conjugates were added to the RB and RBC mix, and incubated for 15 min in the dark at 37 ºC (Fig. 6-4A). The mixture was then spun down and the absorbance of the supernatant was measured at 450 nm to calculate the extent of hemolysis. As shown in Figure 4, addition of the CPPs to RBCs partially photo-oxidized by RB enhanced the lysis of the RBCs. This enhancement in lysis after Fl-CPP addition in the dark increased with the length of the peptide and the arginine content (Fig. 6-4B). Hemolysis also increased with Fl-CPP concentration (Fig. 6-4C). Interestingly, the TMR-R11 and TMR-R13 peptides showed significant lysis in the dark (hemolysis obtained after RBCs are treated with RB and TMR-Rn in the dark) (Fig. 6-4C). This suggests that damage of membranes by a mixture of RB and TMR-R11 or TMR-R13 can occur without a light trigger.

A plot comparing the ability of TMR-Rn peptides to lyse photo-oxidized RBCs (lysis obtained in the dark was subtracted from the lysis obtained after partial photosensitization) (Fig. 6-4D). At 1 μM, the Rn CPPs enhanced the lysis of partially

photodamaged RBCs proportionally to the number of arginine residue n. At higher concentrations, the disruption of photo-oxidized membrane was instead optimal at n=9 arginines residues. In particular, while R11 and R13 are more hemolytic in the dark than R9, R11 and R13 led to a relatively smaller improvement in lysis after light exposure. Overall, these data suggest that increasing arginine content in a CPP (n>9) does not necessarily increase the disruption of oxidized membranes.

Unlike the TMR-Rn series, the conjugates R9-K(TMR), K(TMR)-R9, R4-K(TMR)-R5 did not cause an increase in hemolysis of RBC incubated with RB in the dark. However, upon membrane photo-oxidation by RB, the conjugate R9-K(TMR), K(TMR)-R9 increased hemolysis in a manner similar to that obtained with TMR-R9 (Fig. 6-5). Interestingly, R4-K(TMR)-R5, the most efficient photolytic compound in the experiment presented in Fig. 6-3, displayed a slightly lower capacity to damage partially oxidized RBCs. Overall, these results suggests that these conjugates are all capable of disrupting partially-oxidized membranes. However, this activity does not account for the differences observed in Fig. 6-2.

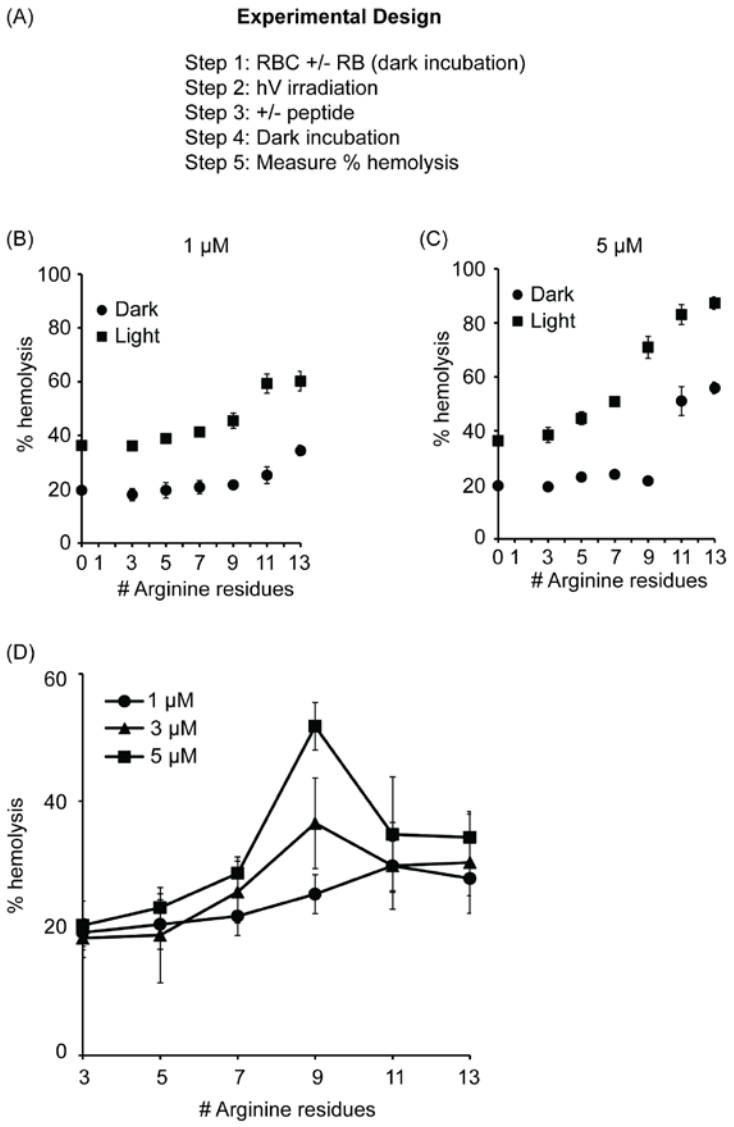

Figure 6-4. The propensity of TMR-Rn to disrupt photo-oxidized RBCs is optimal for n=9.

A, B) In the dark, TMR-Rn peptides lyse membrane of RBCs photo-oxidized by Rose Bengal. RBCs incubated with 1 µM RB were irradiated followed by addition of 1 µM and 5 µM TMR-Rn peptide in the dark. This is represented as light conditions. Alternately, the ability if Rn CPPs to disrupt un-oxidized (no irradiation but RB added) at 1 µM and 5 µM is also represented and referred to as dark conditions. High arginine content in CPPs resulted in dark lysis of un-oxidized RBC membranes but also enhanced disruption of photo-oxidized RBCs membranes. Hemolysis was measured at 450 nm and plotted against number of arginine residues on the CPP. The data shown represents the average of 3 experiments and the corresponding standard deviations. C) Net lysis of RBCs caused by Rn CPPs at 1 µM, 3 µM and 5 µM is shown here. The lysis caused by CPPs under dark conditions was subtracted from lysis caused by CPPs of photo-oxidized RBCs. 100% hemolysis was determined by addition of Triton X-100 to RBCs.

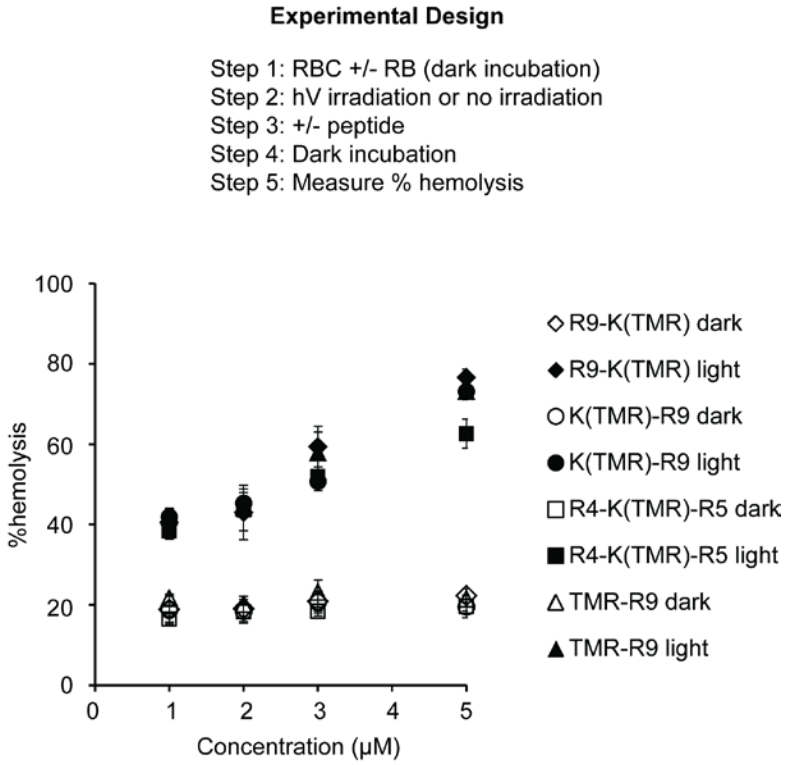

Figure 6-5. Fl-CPPs with TMR at different positions enhance disruption of RBC membranes partially photo-oxidized by Rose Bengal with comparable efficiencies.

For each Fl-CPP conjugate, the disruption of un-oxidized (no irradiation step but RB added) and photo-oxidized (irradiation in the presence of RB) RBC membranes is compared at different concentrations. The protocol used is the same as for the experiment in Figure 6-4.

6.3 Discussion

While CPP-mediated PCI is potentially useful in a number of cellular delivery applications, structure-activity relationships (SARs) for Fl-CPPs have not been established. In this study, our goal was to establish how the structure of CPPs might impact the lytic activity of Fl-CPPs. Measuring and comparing the photo-endosomolytic activity of Fl-CPPs, however, is complex. For instance, multiple parameters such as the amount of ROS generated, membrane binding and peptide-induced membrane disruption contribute to the photo-endosomolytic activity of Fl-CPPs. Direct assessment of the lytic activity of Fl-CPPs in live cells is also challenging because the concentration of Fl-CPPs inside endosomes will be influenced by the endocytic uptake of the peptide. In addition, the lumen of an endosome contains proteases that can degrade Fl-CPPs. Overall, quantitatively comparing the photo-endosomolytic activity of Fl-CPPs that have different propensities to be endocytosed and degraded is therefore difficult. To circumvent these complications and measure the intrinsic photolytic activity of Fl-CPPs more simply, the photohemolysis rather than photo-endosomolytic activity of Fl-CPPs was determined. Admittedly, many differences exist between the membranes of endosomes and that of RBCs. Topology and surface curvature are, for instance, quite different between these two systems. Yet, the plasma membrane of RBC and the membrane of endosomes have several features in common. In particular, both membrane systems display an asymmetry in the distribution of phosphatidylserine between cytoplasmic and external/luminal leaflets(281, 268). This asymmetry has been proposed to be important for the membrane translocation activity of CPPs(282). In addition, parallels between the lysis of endosomal and that of RBCs have previously been observed(133). For instance, TMR-R9, is both photo-endosomolytic and photohemolytic. In contrast, TMR-K9 is much less efficient then TMR-R9 at causing endosomal leakage upon irradiation, even when a greater amount of TMR-K9 than TMR-R9 accumulates inside endosomes(133). Similarly, TMR-K9 is poorly photohemolytic. These results therefore support the notion that the photohemolytic activity of Fl-CPP conjugates mirror their photo-endosomolytic activity.

Two aspects of the structure of Fl-CPPs were tested herein: the arginine residue content and the respective positioning between Fl and CPP moieties. Based on previous reports, both arginine residues and proximity between Fl and CPPs were suggested to be of importance for the photolytic activity of Fl-CPPs (134, 135). To establish SARs, a series of polyarginine Rn (n=1,3,5,7,9,11,13) peptides were labeled with the fluorophore TMR at the N-terminus to obtain TMR-Rn conjugates. In addition, TMR was conjugated to the side chain of a lysine residue positioned in the center or N and C-termini of the peptide R9. Overall, several clear trends could be identified from these SAR studies: 1) increasing the number of arginine residues accelerates photolysis, 2) R9 shows the highest propensity to disrupt photo-oxidized membranes, 3) positioning TMR in the center of the R9 peptide sequence increases the photolytic activity of the conjugate when compared to peptides conjugated at the termini, 4) N and C-terminus labeling are not equivalent. These simple rules should provide a guiding framework for the development future peptide-based photo-endosomolytic agents. Yet, our studies also highlight complex behaviors that are currently still poorly understood. For instance, the saturation behavior of TMR-R11 and TMR-R13, their hemolytic activity in the dark or reduced propensity to disrupt oxidized membranes are non-trivial. Along the same line, the reason why R9-K(TMR) is so poorly active when all R9 conjugates are photolytic is surprising. Because all conjugates were found to generate ROS in similar yield, a possible explanation for some of these observations is that membrane binding is very different among these species. For example, the sites of TMR-R13 binding on the surface of RBCs could be saturated even at all the concentrations tested. This could then explain why the activity TMR-R13 is relatively concentration independent in our assays. However, the binding of these TMR-CPPs to RBCs is relatively weak and we could not experimentally quantify how binding contributes to photohemolysis(133). While this represents a limitation of our study, this is in itself very interesting. In particular, previous studies have revealed that binding of Fl-CPPs to membranes is required for photolysis(135). For instance, liposomes containing negatively charged phospholipids that bind to CPPs are photo-destroyed by TMR-CPPs while liposomes containing neutral

lipids that do not bind CPPs, but otherwise identical in the number of oxidizable sites, do not (135). The fact that little binding is detected would then suggest that the binding sites available on the surface of RBCs, while important for TMR-CPP mediated lysis, are either few in numbers or not strongly associating with the TMR-CPP conjugates. Yet, these interactions are sufficient to permit membrane photo-oxidation and disruption.

Overall, our results highlight how changing the structure of a peptide while keeping ROS-generation yields constant can modulate and improve the photolytic activity of Fl-CPPs. Optimizing the photolytic activity of ROS generators with CPPs could in turn have several benefits. One can, for instance, envision how optimal compounds would achieve endosomal lysis at low light doses. This would then permit PCI protocols to be performed with a low cost irradiation set-up. In the context of *in vivo* experiments, PCI is currently limited by the fact that visible light does not penetrate tissues deeply. In principle, compounds that are active at low light doses could also facilitate PCI delivery deeper into tissues. In addition, as ROS can damage many different biomolecules in a cell, PCI agents that can trigger endosomal leakage at low ROS levels should lead to fewer undesirable off-target reactions. This might in turn be beneficial to the physiology and viability of cells. Our SAR studies suggest that optimization of the photolytic activity Fl-CPPs is a viable path toward solving these problems.

6.4 Materials and methods

Peptide synthesis reagents including amino acids were obtained from Novabiochem. Tiron, nitro blue tetrazolium (NBT), *p*-nitrosodimethylaniline (RNO), imidazole and Rose Bengal (RB) reagents were purchased from Sigma-Aldrich. Whole blood was ordered from the Gulf Coast Regional Blood Center (Houston, TX).

6.4.1 Solid phase peptide synthesis

The Fl-CPP conjugates TMR-TAT, eosin-TAT, TMR-R1, TMR-R3, TMR-R5, TMR-R7, TMR-R9, TMR-R11, TMR-R13, R9-K(TMR), K(TMR)-R9 and R4-K(TMR)-R5 were synthesized by SPPS synthesis (Fmoc chemistry). Rink amide MHBA resin was

used on a 0.72 mmol scale to synthesize the conjugates. The amino acids used for the making the peptide were Fmoc-Gly-OH, Fmoc-Arg(Pbf)-OH, Fmoc-Lys(Boc)-OH, Fmoc-Lys(Mtt)-OH, Fmoc-Gln-OH. Fluorophores used were 5(6)-carboxytetramethylrhodamine and 5(6)-carboxyeosin Y. Reactions were all carried out in a glass peptide synthesis vessel in the presence of N_2 gas at room temperature. First, the resin was treated with 20% piperidine in DMF to remove the Fmoc group (deprotection step). This step was carried out twice for 5 min and 15 min respectively with DMF washes after every reaction. Amino acids were then added to the resin (coupling step). Coupling reaction mixtures contained Fmoc-amino acid (2.88 mmol), HBTU (1.06 g, 2.80 mmol) and DIEA (1.25 mL, 7.2 mmol) in DMF for 4 hr. After every amino acid coupling, the resin was rinsed with DMF thoroughly and deprotected for Fmoc removal. For the preparation of TMR-Rn, TMR-TAT and eosin-TAT conjugates, peptides were first assembled using Fmoc-Gly-OH, Fmoc-Arg(Pbf)-OH, Fmoc-Lys(Boc)-OH, Fmoc-Gln-OH. The Fmoc-group on the N-terminal residue was then removed using a deprotection reaction while keeping intact the side chain protecting groups of the other residues. The fluorophores were coupled to the N-terminus of the peptides using a mixture of 5(6)-carboxy-tetramethylrhodamine or 5(6)-carboxyeosin Y (2.88 mmol), HBTU (1.06 g, 2.80 mmol) and DIEA (1.25 mL, 7.2 mmol) in DMF overnight. For R9-K(TMR), K(TMR)-R9 and R4-K(TMR)-R5, the amino acids Fmoc-Gly-OH, Fmoc-Arg(Pbf)-OH and Fmoc- Fmoc-Lys(Mtt)-OH were used for the peptide chain synthesis. The resin was then washed with DCM and treated with a solution containing 1% TFA and 1% triisopropylsilane in DCM (4 times) to remove the Mtt protecting group from the lysine side chain. The resin was rinsed with DMF. The fluorophore was then coupled to the lysine side chain using a mixture of 5(6)-carboxytetramethylrhodamine (2.88 mmol), HBTU (1.06 g, 2.80 mmol) and DIEA (1.25 mL, 7.2 mmol) in DMF overnight. The Fmoc on the N-terminal amino acid was then removed by a deprotection reaction.

Following assembly of the conjugates, the resin was treated with a reaction mixture containing TFA (95%), H_2O (2.5%) and triisopropylsilane (2.5%) for 2 h. This

reaction causes simultaneous removal of the side chain deprotection groups on all amino acid residues and cleavage of the Fl-CPP conjugate from the resin. Crude Fl-CPPs in the TFA solution were then subjected to a cold anhydrous Et_2O washes to obtain precipitates of Fl-CPP conjugates. The crude peptides were then solubilized in acetonitrile and lyophilized. The conjugates were purified by semi-preparative HPLC and their identity was confirmed by MALDI-TOF analysis. Pure Fl-CPPs were lyophilized and then dissolved in water to obtain a 1 mM stock solution. Concentrations of Fl-CPPs were calculated by measuring the absorbance of the TMR (ε = 91,500 $M^{-1}cm^{-1}$)(obtained from Molecular probes) or eosin (ε = 83,000 $M^{-1}cm^{-1}$)(283) at 556 nm and 525 nm respectively. Working solutions were made by diluting the Fl-CPP stocks in PBS.

Analytical results: TMR-TAT; calculated mass: 1865.07 Da, observed mass: 1865.94 Da; TMR-R1; calculated mass: 642.29 Da, observed mass: 642.61 Da; TMR-R3; calculated mass: 954.49 Da, observed mass: 955.51 Da; TMR-R5; calculated mass: 1266.70 Da, observed mass: 1267.74 Da; TMR-R7; calculated mass: 1578.90 Da, observed mass: 1579.99 Da; TMR-R9; calculated mass: 1891.10 Da, observed mass: 1892.96 Da; TMR-R11; calculated mass: 2203.30 Da, observed mass: 2204.82 Da; TMR-R13; calculated mass: 2515.50 Da, observed mass: 2516.95 Da; eosin-TAT; calculated mass: 2121.61 Da, observed mass: 2126.95 Da; R9-K(TMR); calculated mass: 2020.21 Da, observed mass: 2021.32 Da ; K(TMR)-R9; calculated mass: 2020.21 Da, observed mass: 2022.23 Da; R4-K(TMR)-R5; calculated mass: 2020.21 Da , observed mass: 2020.24 Da.

6.4.2 Photohemolysis assay

Whole blood was centrifuged for 15 min at 1500 g to separate the erythrocytes from other blood components. Erythrocyte pellet was resuspended in PBS and centrifuged (4 times) to remove plasma and the buffy coat completely. Equal volume of PBS was added to the erythrocyte pellet to obtain a 50% stock of RBCs. Fl-CPPs (2 μM) and a working solution of erythrocytes (0.1% in PBS) were then mixed in PBS and added to a 384-well plate. Cells were then incubated for 15 min and allowed to settle to the bottom of the dish prior to imaging. Following incubation, the sample was irradiated

using green light (560 nm) on the microscope (RFP channel, Ex = 560±20 nm / Em= 630±35 nm) at periodic intervals. Images were captured after each irradiation using time-lapse imaging using Slidebook 4.2 software. Using bright field images, the number of lysed cells was counted after each irradiation. Lysed RBCs on bright field appear as transparent ghosts (no hemoglobin inside cells) while intact RBCs have a dark contrast due to the presence of hemoglobin. For each Fl-CPP conjugate, a photohemolysis plot was generated. A minimum of 300 cells were analyzed for each Fl-CPP. Data represents the average lysis from 3 experiments. The corresponding standard deviations have also been shown.

6.4.3 Microscopy imaging

Samples on a 384-well dish were placed on a temperature controlled stage at 37 °C, on an inverted epifluorescence microscope (Model IX81, Olympus, Center Valley, PA). Imaging was performed using a Rolera-MGI Plus back-illuminated EMCCD camera (Qimaging, Surrey, BC, Canada). Images were captures at bright field and using the RFP filter set (Ex = 560±20 nm / Em= 630±35 nm). The light source used was a 100W mercury lamp (Leeds Precision Instruments # L202 Osram). Light passes through filter cubes and the 100X objective prior to being incident on the sample. The amount of light transmitted to the sample was controlled using neutral density filters (ND 1, 2, 3 and 4 correspond to 100, 25, 12.5 and 5% transmittance). Irradiances were measured using a monochromic photometer (model 840-c, Newport, Irvine, CA). At 100X, the irradiances is approximately 21 or 420 W/cm^2 with ND4 or ND1, respectively.

6.4.4 RNO assay to detect singlet oxygen production

A spectrophotometric RNO assay was performed to determine the production of singlet oxygen ($^1O_2$) from the TMR moiety of TMR-peptide conjugates upon light irradiation(242). The photosensitizer Rose Bengal (RB) has a reported $^1O_2$ quantum yield of 0.76 in aqueous solution(242). Since RB(284) has spectral properties that are comparable to TMR (Ex (max) = 550 nm, Em (max) = 580 nm)(285), RB was used as a positive control for the assay. The compounds *p*-nitrosodimethylaniline (RNO) (50 μM)

and imidazole (10 μM) were mixed with RB or TMR-CPPs in PBS on a 96-well plate and then irradiated using a halogen lamp set-up. First, a peroxide intermediate is formed upon reaction of $^1O_2$ with imidazole. Reaction of the chromophore RNO with the intermediate results in bleaching(249). As a result, there is a loss of absorbance of RNO at 450 nm wavelength which is used to determine the rate of production of $^1O_2$ (242). In order to ensure that both RB and TMR-CPPs absorb the same amount of light, the concentration of all compound was a adjusted such that their absorbance was 0.9 at 556 nm prior to irradiation(131). Upon irradiation, the decrease in the absorbance of RNO at 450 nm was recorded at periodic intervals using a plate reader.

6.4.5 Detection of superoxide formation using NBT method

A photometric assay that uses nitro blue tetrazolium (NBT) was performed to monitor the formation of superoxide (O_2^-) by TMR-CPPs(257, 277, 275). Eosin Y is a photosensitizer that produces superoxide radicals upon light irradiation(258). Hence, eosin-TAT was used as a positive control for this assay (conjugation of eosin Y to TAT was performed to improve the solubility of eosin Y in water). Singlet oxygen produced during the irradiation of the TMR-CPPs does not interfere with the NBT assay(257). NBT (80 μM), NADH (10 mM) and EDTA (1 mM) were mixed with TMR-CPPs (10 μM) in PBS buffer(286). The samples were then irradiated using the halogen lamp set-up. NBT gets reduced upon reaction with superoxide radicals and forms an insoluble purple compound formazan(257). Following irradiation, samples were diluted 5-fold in DMSO and absorbance at 600 nm was measured. The contribution of TMR or eosin to absorbance at 600 nm was negligible.

7. CONCLUSIONS

Fluorophore-cell penetrating peptides (Fl-CPPs) such as TMR-TAT are internalized into live mammalian cells through an endocytic route of uptake. In section 1, I observed that exposure of Fl-CPPs that were entrapped in endocytic vesicles to moderate doses of light caused release of the Fl-CPPs into the cells' cytosolic space. Interestingly, this endosomal release of Fl-CPPs was accompanied by loss of plasma membrane integrity, membrane blebbing effects and cell death. Through my study, I aimed to understand the mechanisms behind light mediated endosomal release of Fl-CPPs and the mechanism(s) behind cell death mediated by Fl-CPP endosomal release. Fl-CPPs caused photodamage of the plasma membrane even when applied extracellularly and also photolysed red blood cell membranes. Using red blood cells as an experimental membrane model, it was observed that TMR alone, TAT alone or TMR and TAT mixed together did not cause photolysis. Also, TMR-TAT mediated photolytic damage was inhibited in the presence of hydrophobic singlet oxygen quenchers but not hydrophilic ones. This suggested that Fl-CPP photolysis activity required conjugation of fluorophore to the CPP and might involve production of singlet oxygen within the hydrophobic environment of cell membranes. Fl-CPPs thus are potential photolytic agents however the cell death problems associated with their endocytic release posed as a limitation for their application as tools for PCI. Thus, the mechanism(s) behind Fl-CPP mediated changes in cell physiology and cell death was explored so that optimal and efficient cell delivery technologies can be developed. It was observed that release of TMR-TAT upon endosomolysis caused a rapid increase in the cytosolic calcium ion concentration. Further experiments revealed that TMR-TAT co-localized with endocytic vesicles containing calcium prior to irradiation and that PCI lead to release of endosomal contents. The calcium release into the cytosol was followed by accumulation of calcium in the mitochondria and subsequently caused cell death. Presence of Ruthenium red and cyclosporin A, inhibitors of calcium import to mitochondria and the mitochondrial permeability pore inhibited TMR-TAT mediated cell death. These results suggested that

PCI of Fl-CPPs caused an imbalance in cellular calcium homeostasis and that the import of calcium to mitochondria was a causative factor of the cell death. In section 4, experiments to delve deeper into the mechanistic aspects of Fl-CPP release from endosomes were performed using red blood cells as a model system. It was observed that Fl-CPPs such as TMR-TAT and TMR-R9 promoted photohemolysis by formation of singlet oxygen in the membrane vicinity while TMR-K9 showed significantly lower photolytic activity. In addition, unlabeled TAT and R9 enhanced the photolytic activity of the membrane bound photosensitizer Rose Bengal *in trans*. This suggested that CPPs specifically rich in arginine residues possess a latent membrane lytic activity of their own and participate in the destabilization of photo-oxidized membranes. These results therefore led to the conclusion that CPPs and singlet oxygen generators act synergistically to destroy membranes upon irradiation. In section 5, large unilamellar vesicles (LUVs), a simplified model of endosomes, synthesized from lipids of desired concentrations were used to probe the molecular level mechanisms of Fl-CPP photolysis. The binding of Fl-CPPs to LUVs was tested. It was observed that TMR-TAT and TMR-R9 bind to negatively charged lipids, bringing the fluorophore into close proximity of the lipid membrane. Upon light irradiation, Fl-CPPs produced singlet oxygen and superoxide radicals in the membrane vicinity, resulting in oxidation of the membrane. Fl-CPPs also caused aggregation of photo-oxidized membranes and arginine residues were required for this activity. Thus, CPPs played the dual role of targeting fluorophores to membranes and also destabilize photosensitized membranes. It was also evident that lipids are a target of the Fl-CPP mediated photolytic activity.

REFERENCES

1. Brooks, H., Lebleu, B. and Vives, E. (2005) Tat peptide-mediated cellular delivery: back to basics. *Adv Drug Deliv Rev* **57,** 559-77.

2. Heitz, F., Morris, M. C. and Divita, G. (2009) Twenty years of cell-penetrating peptides: from molecular mechanisms to therapeutics. *Br J Pharmacol* **157,** 195-206.

3. Nakase, I., Takeuchi, T., Tanaka, G. and Futaki, S. (2008) Methodological and cellular aspects that govern the internalization mechanisms of arginine-rich cell-penetrating peptides. *Adv Drug Deliv Rev* **60,** 598-607.

4. Green, M. and Loewenstein, P. M. (1988) Autonomous functional domains of chemically synthesized human immunodeficiency virus tat trans-activator protein. *Cell* **55,** 1179-88.

5. Frankel, A. D. and Pabo, C. O. (1988) Cellular uptake of the tat protein from human immunodeficiency virus. *Cell* **55,** 1189-93.

6. Vives, E., Brodin, P. and Lebleu, B. (1997) A truncated HIV-1 Tat protein basic domain rapidly translocates through the plasma membrane and accumulates in the cell nucleus. *J Biol Chem* **272,** 16010-7.

7. Mann, D. A. and Frankel, A. D. (1991) Endocytosis and targeting of exogenous HIV-1 Tat protein. *EMBO J* **10,** 1733-9.

8. Fawell, S., Seery, J., Daikh, Y., Moore, C., Chen, L. L., et al. (1994) Tat-mediated delivery of heterologous proteins into cells. *Proc Natl Acad Sci U S A* **91,** 664-8.

9. Langel, U. l. (2007) *Handbook of cell-penetrating peptides.* CRC/Taylor & Francis, Boca Raton, FL.

10. Kamide, K., Nakakubo, H., Uno, S. and Fukamizu, A. (2010) Isolation of novel cell-penetrating peptides from a random peptide library using in vitro virus and their modifications. *Int J Mol Med* **25,** 41-51.

11. Wender, P. A., Mitchell, D. J., Pattabiraman, K., Pelkey, E. T., Steinman, L., et al. (2000) The design, synthesis, and evaluation of molecules that enable or enhance cellular uptake: peptoid molecular transporters. *Proc Natl Acad Sci U S A* **97,** 13003-8.

12. Futaki, S., Suzuki, T., Ohashi, W., Yagami, T., Tanaka, S., et al. (2001) Arginine-rich peptides. An abundant source of membrane-permeable peptides having potential as carriers for intracellular protein delivery. *J Biol Chem* **276,** 5836-40.

13. Deshayes, S., Morris, M. C., Divita, G. and Heitz, F. (2006) Interactions of amphipathic CPPs with model membranes. *Biochim Biophys Acta-Biomembranes* **1758,** 328-335.

14. Morris, M. C., Depollier, J., Mery, J., Heitz, F. and Divita, G. (2001) A peptide carrier for the delivery of biologically active proteins into mammalian cells. *Nat Biotechnol* **19,** 1173-6.

15. Lorents, A., Kodavali, P. K., Oskolkov, N., Langel, Ü., Hällbrink, M., et al. (2012) Cell-penetrating Peptides Split into Two Groups Based on Modulation of Intracellular Calcium Concentration. *J Biol Chem* **287,** 16880-16889.

16. Torchilin, V. P. (2008) Cell penetrating peptide-modified pharmaceutical nanocarriers for intracellular drug and gene delivery. *Biopolymers* **90,** 604-10.

17. Jones, S. W., Christison, R., Bundell, K., Voyce, C. J., Brockbank, S. M., et al. (2005) Characterisation of cell-penetrating peptide-mediated peptide delivery. *Br J Pharmacol* **145,** 1093-102.

18. Schwarze, S. R., Ho, A., Vocero-Akbani, A. and Dowdy, S. F. (1999) In vivo protein transduction: delivery of a biologically active protein into the mouse. *Science* **285,** 1569-72.

19. Allinquant, B., Hantraye, P., Mailleux, P., Moya, K., Bouillot, C., et al. (1995) Downregulation of amyloid precursor protein inhibits neurite outgrowth in vitro. *J Cell Biology* **128,** 919-927.

20. Kato, D., Miyazawa, K., Ruas, M., Starborg, M., Wada, I., et al. (1998) Features of replicative senescence induced by direct addition of antennapedia-p16INK4A fusion protein to human diploid fibroblasts. *FEBS Letters* **427,** 203-208.

21. Nagahara, H., Vocero-Akbani, A. M., Snyder, E. L., Ho, A., Latham, D. G., et al. (1998) Transduction of full-length TAT fusion proteins into mammalian cells: TAT-p27Kip1 induces cell migration. *Nat Med* **4,** 1449-1452.

22. Eguchi, A. and Dowdy, S. F. (2009) siRNA delivery using peptide transduction domains. *Trends in Pharmacological Sci* **30,** 341-345.

23. Morris, M. C., Deshayes, S., Heitz, F. and Divita, G. (2008) Cell-penetrating peptides: from molecular mechanisms to therapeutics. *Biol Cell* **100,** 201-17.

24. Hatakeyama, H., Ito, E., Akita, H., Oishi, M., Nagasaki, Y., et al. (2009) A pH-sensitive fusogenic peptide facilitates endosomal escape and greatly enhances the gene silencing of siRNA-containing nanoparticles in vitro and in vivo. *J Control Release* **139,** 127-132.

25. Endoh, T. and Ohtsuki, T. (2010) Cellular siRNA delivery using TatU1A and photo-induced RNA interference. *Methods Mol Biol* **623,** 271-81.

26. Kim, W. J., Christensen, L. V., Jo, S., Yockman, J. W., Jeong, J. H., et al. (2006) Cholesteryl oligoarginine delivering vascular endothelial growth factor siRNA effectively inhibits tumor growth in colon adenocarcinoma. *Mol Ther* **14,** 343-50.

27. Nguyen, Q. N., Chavli, R. V., Marques, J. T., Conrad, P. G., Jr., Wang, D., et al. (2006) Light controllable siRNAs regulate gene suppression and phenotypes in cells. *Biochim Biophys Acta* **1758,** 394-403.

28. Zeineddine, D., Papadimou, E., Chebli, K., Gineste, M., Liu, J., et al. (2006) Oct-3/4 dose dependently regulates specification of embryonic stem cells toward a cardiac lineage and early heart development. *Dev Cell* **11,** 535-46.

29. Kumar, P., Wu, H., McBride, J. L., Jung, K. E., Kim, M. H., et al. (2007) Transvascular delivery of small interfering RNA to the central nervous system. *Nature* **448,** 39-43.

30. Ezzat, K., Andaloussi, S. E., Zaghloul, E. M., Lehto, T., Lindberg, S., et al. (2011) PepFect 14, a novel cell-penetrating peptide for oligonucleotide delivery in solution and as solid formulation. *Nucleic Acids Res* **39,** 5284-98.

31. Trabulo, S. C., A.L.; Mano, M.; De Lima, M.C.P. (2010) Cell-Penetrating Peptides—Mechanisms of Cellular Uptake and Generation of Delivery Systems. *Pharmaceuticals* **3,** 961-993.

32. Vives, E., Richard, J. P., Rispal, C. and Lebleu, B. (2003) TAT peptide internalization: seeking the mechanism of entry. *Curr Protein Pept Sci* **4,** 125-32.

33. Lundberg, M., Wikstrom, S. and Johansson, M. (2003) Cell surface adherence and endocytosis of protein transduction domains. *Mol Ther* **8,** 143-50.

34. Richard, J. P., Melikov, K., Vives, E., Ramos, C., Verbeure, B., et al. (2003) Cell-penetrating peptides. A reevaluation of the mechanism of cellular uptake. *J Biol Chem* **278,** 585-90.

35. Derossi, D., Joliot, A. H., Chassaing, G. and Prochiantz, A. (1994) The third helix of the Antennapedia homeodomain translocates through biological membranes. *J Biol Chem* **269,** 10444-50.

36. Duchardt, F., Fotin-Mleczek, M., Schwarz, H., Fischer, R. and Brock, R. (2007) A comprehensive model for the cellular uptake of cationic cell-penetrating peptides. *Traffic* **8,** 848-66.

37. Vives, E., Schmidt, J. and Pelegrin, A. (2008) Cell-penetrating and cell-targeting peptides in drug delivery. *Biochim Biophys Acta* **1786,** 126-38.

38. Derossi, D., Calvet, S., Trembleau, A., Brunissen, A., Chassaing, G., et al. (1996) Cell internalization of the third helix of the Antennapedia homeodomain is receptor-independent. *J Biol Chem* **271,** 18188-18193.

39. Ferrari, M. E., Nguyen, C. M., Zelphati, O., Tsai, Y. and Felgner, P. L. (1998) Analytical methods for the characterization of cationic lipid-nucleic acid complexes. *Hum Gene Ther* **9,** 341-51.

40. Fittipaldi, A., Ferrari, A., Zoppe, M., Arcangeli, C., Pellegrini, V., et al. (2003) Cell membrane lipid rafts mediate caveolar endocytosis of HIV-1 Tat fusion proteins. *J Biol Chem* **278,** 34141-9.

41. Richard, J. P., Melikov, K., Brooks, H., Prevot, P., Lebleu, B., et al. (2005) Cellular uptake of unconjugated TAT peptide involves clathrin-dependent endocytosis and heparan sulfate receptors. *J Biol Chem* **280,** 15300-6.

42. Kaplan, I. M., Wadia, J. S. and Dowdy, S. F. (2005) Cationic TAT peptide transduction domain enters cells by macropinocytosis. *J Control Release* **102,** 247-253.

43. Wadia, J. S., Stan, R. V. and Dowdy, S. F. (2004) Transducible TAT-HA fusogenic peptide enhances escape of TAT-fusion proteins after lipid raft macropinocytosis. *Nat. Med.* **10,** 310-5.

44. Belting, M. (2003) Heparan sulfate proteoglycan as a plasma membrane carrier. *Trends Biochem Sci* **28,** 145-51.

45. Palm-Apergi, C., Lorents, A., Padari, K., Pooga, M. and Hallbrink, M. (2009) The membrane repair response masks membrane disturbances caused by cell-penetrating peptide uptake. *FASEB J* **23,** 214-23.

46. Delaroche, D., Cantrelle, F. X., Subra, F., Van Heijenoort, C., Guittet, E., et al. (2010) Cell-penetrating peptides with intracellular actin-remodeling activity in malignant fibroblasts. *J Biol Chem* **285,** 7712-21.

47. Berlose, J.-P., Convert, O., Derossi, D., Brunissen, A. and Chassaing, G. (1996) Conformational and associative behaviours of the third helix of Antennapedia homeodomain in membrane-mimetic environments. *Eur J Biochemistry* **242,** 372-386.

48. Pouny, Y., Rapaport, D., Mor, A., Nicolas, P. and Shai, Y. (1992) Interaction of antimicrobial dermaseptin and its fluorescently labeled analogues with phospholipid membranes. *Biochemistry* **31,** 12416-23.

49. Shai, Y. (1999) Mechanism of the binding, insertion and destabilization of phospholipid bilayer membranes by alpha-helical antimicrobial and cell non-selective membrane-lytic peptides. *Biochim Biophys Acta* **1462,** 55-70.

50. Matsuzaki, K., Sugishita, K. and Miyajima, K. (1999) Interactions of an antimicrobial peptide, magainin 2, with lipopolysaccharide-containing liposomes as a model for outer membranes of Gram-negative bacteria. *FEBS Lett* **449,** 221-4.

51. Lundberg, P. and Langel, Ü. (2003) A brief introduction to cell-penetrating peptides. *J Mol Recogn* **16,** 227-233.

52. Yang, L., Harroun, T. A., Weiss, T. M., Ding, L. and Huang, H. W. (2001) Barrel-stave model or toroidal model? A case study on melittin pores. *Biophys J* **81,** 1475-85.

53. Melo, M. N., Ferre, R. and Castanho, M. A. (2009) Antimicrobial peptides: linking partition, activity and high membrane-bound concentrations. *Nat Rev Microbiol* **7,** 245-50.

54. Conner, S. D. and Schmid, S. L. (2003) Regulated portals of entry into the cell. *Nature* **422,** 37-44.

55. Mayor, S. and Pagano, R. E. (2007) Pathways of clathrin-independent endocytosis. *Nat Rev Mol Cell Biol* **8,** 603-12.

56. Fischer, R., Fotin-Mleczek, M., Hufnagel, H. and Brock, R. (2005) Break on through to the other side-biophysics and cell biology shed light on cell-penetrating peptides. *Chembiochem* **6,** 2126-42.

57. Nakase, I., Niwa, M., Takeuchi, T., Sonomura, K., Kawabata, N., et al. (2004) Cellular uptake of arginine-rich peptides: roles for macropinocytosis and actin rearrangement. *Mol Ther* **10,** 1011-22.

58. Gump, J. M., June, R. K. and Dowdy, S. F. (2010) Revised role of glycosaminoglycans in TAT protein transduction domain-mediated cellular transduction. *J Biol Chem* **285,** 1500-7.

59. Jones, A. T. (2008) Gateways and tools for drug delivery: endocytic pathways and the cellular dynamics of cell penetrating peptides. *Int J Pharm* **354,** 34-8.

60. Lundin, P., Johansson, H., Guterstam, P., Holm, T., Hansen, M., et al. (2008) Distinct uptake routes of cell-penetrating peptide conjugates. *Bioconjug Chem* **19,** 2535-42.

61. Fuchs, S. M. and Raines, R. T. (2004) Pathway for polyarginine entry into mammalian cells. *Biochemistry* **43,** 2438-2444.

62. Al-Taei, S., Penning, N. A., Simpson, J. C., Futaki, S., Takeuchi, T., et al. (2005) Intracellular traffic and fate of protein transduction domains HIV-1 TAT peptide and octaarginine. Implications for their utilization as drug delivery vectors. *Bioconjug Chem* **17,** 90-100.

63. Nishi, K. and Saigo, K. (2007) Cellular internalization of green fluorescent protein fused with herpes simplex virus protein VP22 via a lipid raft-mediated endocytic pathway independent of caveolae and Rho Family GTPases but dependent on dynamin and Arf6. *J Biol Chem* **282,** 27503-27517.

64. Gillmeister, M. P., Betenbaugh, M. J. and Fishman, P. S. (2011) Cellular trafficking and photochemical internalization of cell penetrating peptide linked cargo proteins: a dual fluorescent labeling study. *Bioconjug Chem* **22,** 556-566.

65. Turner, J. J., Arzumanov, A. A. and Gait, M. J. (2005) Synthesis, cellular uptake and HIV-1 Tat-dependent trans-activation inhibition activity of oligonucleotide analogues disulphide-conjugated to cell-penetrating peptides. *Nucleic Acids Research* **33,** 27-42.

66. El-Sayed, A., Futaki, S. and Harashima, H. (2009) Delivery of macromolecules using arginine-rich cell-penetrating peptides: ways to overcome endosomal entrapment. *The AAPS J* **11,** 13-22.

67. Mitchell, D. J., Kim, D. T., Steinman, L., Fathman, C. G. and Rothbard, J. B. (2000) Polyarginine enters cells more efficiently than other polycationic homopolymers. *J Pept Res* **56,** 318-25.

68. Wender, P. A., Galliher, W. C., Goun, E. A., Jones, L. R. and Pillow, T. H. (2008) The design of guanidinium-rich transporters and their internalization mechanisms. *Adv Drug Deliv Rev* **60,** 452-72.

69. Poon, G. M. and Gariépy, J. (2007) Cell-surface proteoglycans as molecular portals for cationic peptide and polymer entry into cells. *Biochem Soc Trans* **35,** 788-793.

70. Nakase, I., Tadokoro, A., Kawabata, N., Takeuchi, T., Katoh, H., et al. (2006) Interaction of arginine-rich peptides with membrane-associated proteoglycans is

crucial for induction of actin organization and macropinocytosis†. *Biochemistry* **46,** 492-501.

71. Mishra, A., Lai, G. H., Schmidt, N. W., Sun, V. Z., Rodriguez, A. R., et al. (2011) Translocation of HIV TAT peptide and analogues induced by multiplexed membrane and cytoskeletal interactions. *Proc Natl Acad Sci U S A* **108,** 16883-16888.

72. El-Andaloussi, S., Johansson, H. J., Lundberg, P. and Langel, U. (2006) Induction of splice correction by cell-penetrating peptide nucleic acids. *J Gene Med* **8,** 1262-73.

73. Sorkin, A. and Von Zastrow, M. (2002) Signal transduction and endocytosis: close encounters of many kinds. *Nat Rev Mol Cell Biol* **3,** 600-14.

74. Forgac, M. (2007) Vacuolar ATPases: rotary proton pumps in physiology and pathophysiology. *Nat Rev Mol Cell Biol* **8,** 917-29.

75. Scott, C. C. and Gruenberg, J. (2011) Ion flux and the function of endosomes and lysosomes: pH is just the start: the flux of ions across endosomal membranes influences endosome function not only through regulation of the luminal pH. *Bioessays* **33,** 103-10.

76. Casey, J. R., Grinstein, S. and Orlowski, J. (2010) Sensors and regulators of intracellular pH. *Nat Rev Mol Cell Biol* **11,** 50-61.

77. Gillmeister, M. P., Betenbaugh, M. J. and Fishman, P. S. (2011) Cellular trafficking and photochemical internalization of cell penetrating peptide linked cargo proteins: a dual fluorescent labeling study. *Bioconjug Chem* **22,** 556-66.

78. Appelbaum, Jacob S., LaRochelle, Jonathan R., Smith, Betsy A., Balkin, Daniel M., Holub, Justin M., et al. (2012) Arginine topology controls escape of minimally cationic proteins from early endosomes to the cytoplasm. *Chemistry & Biology* **19,** 819-830.

79. Burlina, F., Sagan, S., Bolbach, G. and Chassaing, G. (2006) A direct approach to quantification of the cellular uptake of cell-penetrating peptides using MALDI-TOF mass spectrometry. *Nat. Protocols* **1,** 200-205.

80. Paramelle, D., Subra, G., Vezenkov, L. L., Maynadier, M., André, C., et al. (2010) A straightforward approach for cellular-uptake quantification. *Angewandte Chemie International Edition* **49,** 8240-8243.

81. Walrant, A., Correia, I., Jiao, C.-Y., Lequin, O., Bent, E. H., et al. (2011) Different membrane behaviour and cellular uptake of three basic arginine-rich peptides. *Biochim Biophys Acta - Biomembranes* **1808,** 382-393.

82. Alves, I. D., Bechara, C., Walrant, A., Zaltsman, Y., Jiao, C.-Y., et al. (2011) Relationships between membrane binding, affinity and cell internalization efficacy of a cell-penetrating peptide: penetratin as a case study. *PLoS ONE* **6,** e24096.

83. Takeuchi, T., Kosuge, M., Tadokoro, A., Sugiura, Y., Nishi, M., et al. (2006) Direct and rapid cytosolic delivery using cell-penetrating peptides mediated by pyrenebutyrate. *ACS Chemical Biology* **1,** 299-303.

84. Medintz, I. L., Pons, T., Delehanty, J. B., Susumu, K., Brunel, F. M., et al. (2008) Intracellular delivery of quantum dot−protein cargos mediated by cell penetrating peptides. *Bioconjug Chem* **19,** 1785-1795.

85. Pan, C., Lu, B., Chen, H. and Bishop, C. (2010) Reprogramming human fibroblasts using HIV-1 TAT recombinant proteins OCT4, SOX2, KLF4 and c-MYC. *Mol Biol Reports* **37,** 2117-2124.

86. Loison, F., Nizard, P., Sourisseau, T., Le Goff, P., Debure, L., et al. (2005) A ubiquitin-based assay for the cytosolic uptake of protein transduction domains. *Mol Ther* **11,** 205-214.

87. Herce, H. D. and Garcia, A. E. (2007) Molecular dynamics simulations suggest a mechanism for translocation of the HIV-1 TAT peptide across lipid membranes. *Proc Natl Acad Sci U S A* **104,** 20805-10.

88. Thorén, P. E. G., Persson, D., Esbjörner, E. K., Goksör, M., Lincoln, P., et al. (2004) Membrane binding and translocation of cell-penetrating peptides. *Biochemistry* **43,** 3471-3489.

89. Tiriveedhi, V. and Butko, P. (2007) A Fluorescence Spectroscopy Study on the Interactions of the TAT-PTD peptide with model lipid membranes. *Biochemistry* **46,** 3888-3895.

90. Leventis, P. A. and Grinstein, S. (2010) The distribution and function of phosphatidylserine in cellular membranes. *Annual Review of Biophysics* **39,** 407-427.

91. Kay, J. G. and Grinstein, S. (2011) Sensing phosphatidylserine in cellular membranes. *Sensors (Basel)* **11,** 1744-55.

92. Ruzza, P., Biondi, B., Marchiani, A., Antolini, N. and Calderan, A. (2010) Cell-penetrating peptides: a comparative study on lipid affinity and cargo delivery properties. *Pharmaceuticals* **3,** 1045-1062.

93. Lee, Y. J., Johnson, G. and Pellois, J. P. (2010) Modeling of the endosomolytic activity of HA2-TAT peptides with red blood cells and ghosts. *Biochemistry* **49,** 7854-66.

94. Cahill, K. (2009) Molecular electroporation and the transduction of oligoarginines. *Physical Biology* **7,** 1-14.

95. Tünnemann, G., Ter-Avetisyan, G., Martin, R. M., Stöckl, M., Herrmann, A., et al. (2008) Live-cell analysis of cell penetration ability and toxicity of oligo-arginines. *J Peptide Sci* **14,** 469-476.

96. Bernfield, M., Götte, M., Park, P. W., Reizes, O., Fitzgerald, M. L., et al. (1999) Functions of cell surface heparan sulfate proteoglycans. *Ann Rev Biochem* **68,** 729-777.

97. Rothe, R., Liguori, L., Villegas-Mendez, A., Marques, B., Grunwald, D., et al. (2010) Characterization of the cell-penetrating properties of the epstein-barr virus ZEBRA trans-activator. *J Biol Chem* **285,** 20224-20233.

98. Fuchs, S. M. and Raines, R. T. (2004) Pathway for polyarginine entry into mammalian cells. *Biochemistry* **43,** 2438-44.

99. Tyagi, M., Rusnati, M., Presta, M. and Giacca, M. (2001) Internalization of HIV-1 Tat requires cell surface heparan sulfate proteoglycans. *J Biol Chem* **276,** 3254-3261.

100. Ziegler, A. (2008) Thermodynamic studies and binding mechanisms of cell-penetrating peptides with lipids and glycosaminoglycans. *Adv Drug Deliv Rev* **60,** 580-97.

101. Magzoub, M., Kilk, K., Eriksson, L. E. G. r., Langel, ú. and Gr√§slund, A. (2001) Interaction and structure induction of cell-penetrating peptides in the presence of phospholipid vesicles. *Biochim Biophys Acta - Biomembranes* **1512,** 77-89.

102. Kobayashi, T., Startchev, K., Whitney, A. J. and Gruenberg, J. (2001) Localization of lysobisphosphatidic acid-rich memmbrane domains in late endosomes. *Biol Chem* **382,** 483-485.

103. Matsuo, H., Chevallier, J., Mayran, N., Le Blanc, I., Ferguson, C., et al. (2004) Role of LBPA and Alix in multivesicular liposome formation and endosome organization. *Science* **303,** 531-534.

104. Yang, S. T., Zaitseva, E., Chernomordik, L. V. and Melikov, K. (2010) Cell-penetrating peptide induces leaky fusion of liposomes containing late endosome-specific anionic lipid. *Biophys J* **99,** 2525-33.

105. Koppelhus, U., Awasthi, S. K., Zachar, V., Holst, H. U., Ebbesen, P., et al. (2002) Cell-dependent differential cellular uptake of PNA, peptides, and PNA-peptide conjugates. *Antisense Nucleic Acid Drug Dev* **12,** 51-63.

106. Kramer, S. D. and Wunderli-Allenspach, H. (2003) No entry for TAT(44-57) into liposomes and intact MDCK cells: novel approach to study membrane permeation of cell-penetrating peptides. *Biochim Biophys Acta* **1609,** 161-9.

107. Zhang, X., Wan, L., Pooyan, S., Su, Y., Gardner, C. R., et al. (2004) Quantitative assessment of the cell penetrating properties of RI-Tat-9: evidence for a cell type-specific barrier at the plasma membrane of epithelial cells. *Mol Pharm* **1,** 145-55.

108. Caron, N. J., Torrente, Y., Camirand, G., Bujold, M., Chapdelaine, P., et al. (2001) Intracellular delivery of a Tat-eGFP fusion protein into muscle cells. *Mol Ther* **3,** 310-8.

109. Xia, H., Mao, Q. and Davidson, B. L. (2001) The HIV Tat protein transduction domain improves the biodistribution of beta-glucuronidase expressed from recombinant viral vectors. *Nat Biotechnol* **19,** 640-4.

110. Tseng, Y. L., Liu, J. J. and Hong, R. L. (2002) Translocation of liposomes into cancer cells by cell-penetrating peptides penetratin and tat: a kinetic and efficacy study. *Mol Pharmacol* **62,** 864-72.

111. Berg, K., Selbo, P. K., Prasmickaite, L., Tjelle, T. E., Sandvig, K., et al. (1999) Photochemical internalization: a novel technology for delivery of macromolecules into cytosol. *Cancer Res* **59,** 1180-3.

112. Berg, K., Weyergang, A., Prasmickaite, L., Bonsted, A., Hogset, A., et al. (2010) Photochemical internalization (PCI): a technology for drug delivery. *Methods Mol Biol* **635,** 133-45.

113. Kosuge, M., Takeuchi, T., Nakase, I., Jones, A. T. and Futaki, S. (2008) Cellular Internalization and distribution of arginine-rich peptides as a function of extracellular peptide concentration, serum, and plasma membrane associated proteoglycans. *Bioconjug Chem* **19,** 656-664.

114. Berg, K., Nordstrand, S., Selbo, P. K., Tran, D. T., Angell-Petersen, E., et al. (2011) Disulfonated tetraphenyl chlorin (TPCS2a), a novel photosensitizer developed

for clinical utilization of photochemical internalization. *Photochem Photobiol Sci* **10,** 1637-51.

115. Selbo, P. K., Weyergang, A., Bonsted, A., Bown, S. G. and Berg, K. (2006) Photochemical internalization of therapeutic macromolecular agents: a novel strategy to kill multidrug-resistant cancer cells. *J Pharmacol Exp Ther* **319,** 604-12.

116. Mathews, M. S., Blickenstaff, J. W., Shih, E. C., Zamora, G., Vo, V., et al. (2012) Photochemical internalization of bleomycin for glioma treatment. *J Biomed Opt* **17,** 058001.

117. Weyergang, A., Kaalhus, O. and Berg, K. (2008) Photodynamic therapy with an endocytically located photosensitizer cause a rapid activation of the mitogen-activated protein kinases extracellular signal-regulated kinase, p38, and c-Jun NH2 terminal kinase with opposing effects on cell survival. *Mol Cancer Ther* **7,** 1740-50.

118. Maiolo, J. R., 3rd, Ottinger, E. A. and Ferrer, M. (2004) Specific redistribution of cell-penetrating peptides from endosomes to the cytoplasm and nucleus upon laser illumination. *J Am Chem Soc* **126,** 15376-7.

119. Matsushita, M., Noguchi, H., Lu, Y. F., Tomizawa, K., Michiue, H., et al. (2004) Photo-acceleration of protein release from endosome in the protein transduction system. *FEBS Lett* **572,** 221-6.

120. Endoh, T., Sisido, M. and Ohtsuki, T. (2009) Spatial regulation of specific gene expression through photoactivation of RNAi. *J Control Release* **137,** 241-5.

121. Melikov, K. and Chernomordik, L. (2005) Arginine-rich cell penetrating peptides: from endosomal uptake to nuclear delivery. *Cellular Mol Life Sci* **62,** 2739-2749.

122. Choi, Y., McCarthy, J. R., Weissleder, R. and Tung, C. H. (2006) Conjugation of a photosensitizer to an oligoarginine-based cell-penetrating peptide increases the efficacy of photodynamic therapy. *ChemMedChem* **1,** 458-63.

123. Kasim, V., Miyagishi, M. and Taira, K. (2004) Control of siRNA expression using the Cre–loxP recombination system. *Nucleic Acids Research* **32,** e66-e66.

124. Wang, J. T., Giuntini, F., Eggleston, I. M., Bown, S. G. and MacRobert, A. J. (2012) Photochemical internalisation of a macromolecular protein toxin using a cell penetrating peptide-photosensitiser conjugate. *J Control Release* **157,** 305-13.

125. Barnett, E. M., Elangovan, B., Bullok, K. E. and Piwnica-Worms, D. (2006) Selective cell uptake of modified Tat peptide-fluorophore conjugates in rat retina in ex vivo and in vivo models. *Invest Ophthalmol Vis Sci* **47,** 2589-95.

126. Madani, F., Lindberg, S., Langel, U., Futaki, S. and Graslund, A. (2011) Mechanism of celullar uptake of cell-penetrating peptides. *J Biophysics* **2011**.

127. Grossweiner, L. I., Patel, A. S. and Grossweiner, J. B. (1982) Type I and Type II mechanisms in the photosensitized lysis of phosphatidylcholine liposomes by hematoporphyrin. *Photochem. Photobiol.* **36,** 159-167.

128. Dai, T., Fuchs, B. B., Coleman, J. J., Prates, R. A., Astrakas, C., et al. (2012) Concepts and principles of photodynamic therapy as an alternative antifungal discovery platform. *Front Microbiol* **3,** 120.

129. Valenzeno, D. P. (1987) Photomodification of biological-membranes with emphasis on singlet oxygen mechanisms. *Photochem Photobiol* **46,** 147-160.

130. Golding, P. S., King, T. A., Maddocks, L., Drucker, D. B. and Blinkhorn, A. S. (1998) Photosensitization of Staphylococcus aureus with malachite green isothiocyanate: inactivation efficiency and spectroscopic analysis. *J Photochem Photobiol B* **47,** 202-10.

131. Kochevar, I. E. and Redmond, R. W. (2000) Photosensitized production of singlet oxygen. *Methods Enzymol* **319,** 20-8.

132. Redmond, R. W. and Kochevar, I. E. (2006) Spatially resolved cellular responses to singlet oxygen. *Photochem Photobiol* **82,** 1178-86.

133. Srinivasan, D., Muthukrishnan, N., Johnson, G. A., Erazo-Oliveras, A., Lim, J., et al. (2011) Conjugation to the cell-penetrating peptide TAT potentiates the photodynamic effect of carboxytetramethylrhodamine. *PLoS ONE* **6,** e17732.

134. Muthukrishnan, N., Johnson, G., Erazo-Oliveras, A. and Pellois, J. P. (2012) Synergy between cell-penetrating peptides and singlet oxygen generators leads to efficient photolysis of membranes. *Photochem Photobiol*. **89**, 625-30.

135. Meerovich, I., Muthukrishnan, N., Johnson, G. A., Erazo-Oliveras, A. and Pellois, J. P. (2013) Photodamage of lipid bilayers by irradiation of a fluorescently labeled cell-penetrating peptide. *Biochim Biophys Acta*. **1840**, 507-15

136. Oliveira, S., Fretz, M. M., Hogset, A., Storm, G. and Schiffelers, R. M. (2007) Photochemical internalization enhances silencing of epidermal growth factor receptor through improved endosomal escape of siRNA. *Biochim Biophys Acta* **1768,** 1211-7.

137. Berg, K. and Moan, J. (1994) Lysosomes as photochemical targets. *Int J Cancer* **59,** 814-22.

138. Terman, A. and Kurz, T. (2013) Lysosomal iron, iron chelation, and cell death. *Antioxid Redox Signal* **18,** 888-98.

139. Allison, A. C., Magnus, I. A. and Young, M. R. (1966) Role of lysosomes and of cell membranes in photosensitization. *Nature* **209,** 874-8.

140. Gerasimenko, J. V., Tepikin, A. V., Petersen, O. H. and Gerasimenko, O. V. (1998) Calcium uptake via endocytosis with rapid release from acidifying endosomes. *Curr Biol* **8,** 1335-8.

141. Orrenius, S., Zhivotovsky, B. and Nicotera, P. (2003) Regulation of cell death: the calcium-apoptosis link. *Nat Rev Mol Cell Biol* **4,** 552-65.

142. Demaurex, N. and Distelhorst, C. (2003) Cell biology. Apoptosis--the calcium connection. *Science* **300,** 65-7.

143. Trump, B. F. and Berezesky, I. K. (1995) Calcium-mediated cell injury and cell death. *FASEB J* **9,** 219-28.

144. Fleckenstein, A., Janke, J., Doring, H. J. and Leder, O. (1974) Myocardial fiber necrosis due to intracellular Ca overload-a new principle in cardiac pathophysiology. *Recent Adv Stud Cardiac Struct Metab* **4,** 563-80.

145. Leonard, J. P. and Salpeter, M. M. (1979) Agonist-induced myopathy at the neuromuscular junction is mediated by calcium. *J Cell Biol* **82,** 811-9.

146. Schanne, F. A., Kane, A. B., Young, E. E. and Farber, J. L. (1979) Calcium dependence of toxic cell death: a final common pathway. *Science* **206,** 700-2.

147. Wyllie, A. H. (1980) Glucocorticoid-induced thymocyte apoptosis is associated with endogenous endonuclease activation. *Nature* **284,** 555-6.

148. Cohen, J. J. and Duke, R. C. (1984) Glucocorticoid activation of a calcium-dependent endonuclease in thymocyte nuclei leads to cell death. *J Immunol* **132,** 38-42.

149. McConkey, D. J., Nicotera, P., Hartzell, P., Bellomo, G., Wyllie, A. H., et al. (1989) Glucocorticoids activate a suicide process in thymocytes through an elevation of cytosolic Ca^{2+} concentration. *Arch Biochem Biophys* **269,** 365-70.

150. Ilinskaya, O. N., Dreyer, F., Mitkevich, V. A., Shaw, K. L., Pace, C. N., et al. (2002) Changing the net charge from negative to positive makes ribonuclease Sa cytotoxic. *Protein Sci* **11,** 2522-5.

151. Shaw, K. L., Grimsley, G. R., Yakovlev, G. I., Makarov, A. A. and Pace, C. N. (2001) The effect of net charge on the solubility, activity, and stability of ribonuclease Sa. *Protein Sci* **10,** 1206-15.

152. Berridge, M. J., Lipp, P. and Bootman, M. D. (2000) The versatility and universality of calcium signalling. *Nat Rev Mol Cell Biol* **1,** 11-21.

153. Kaufman, R. J. (2002) Orchestrating the unfolded protein response in health and disease. *J Clin Invest* **110,** 1389-98.

154. Ferri, K. F. and Kroemer, G. (2001) Organelle-specific initiation of cell death pathways. *Nat Cell Biol* **3,** E255-63.

155. Nakagawa, T., Zhu, H., Morishima, N., Li, E., Xu, J., et al. (2000) Caspase-12 mediates endoplasmic-reticulum-specific apoptosis and cytotoxicity by amyloid-beta. *Nature* **403,** 98-103.

156. Breckenridge, D. G., Stojanovic, M., Marcellus, R. C. and Shore, G. C. (2003) Caspase cleavage product of BAP31 induces mitochondrial fission through endoplasmic reticulum calcium signals, enhancing cytochrome c release to the cytosol. *J Cell Biol* **160,** 1115-27.

157. Frank, S., Gaume, B., Bergmann-Leitner, E. S., Leitner, W. W., Robert, E. G., et al. (2001) The role of dynamin-related protein 1, a mediator of mitochondrial fission, in apoptosis. *Dev Cell* **1,** 515-25.

158. Carafoli, E. (2002) Calcium signaling: a tale for all seasons. *Proc Natl Acad Sci U S A* **99,** 1115-22.

159. Baumgartner, H. K., Gerasimenko, J. V., Thorne, C., Ferdek, P., Pozzan, T., et al. (2009) Calcium elevation in mitochondria is the main Ca^{2+} requirement for mitochondrial permeability transition pore (mPTP) opening. *J Biol Chem* **284,** 20796-803.

160. Thor, H., Hartzell, P. and Orrenius, S. (1984) Potentiation of oxidative cell injury in hepatocytes which have accumulated Ca^{2+}. *J Biol Chem* **259,** 6612-5.

161. Rizzuto, R., Simpson, A. W., Brini, M. and Pozzan, T. (1992) Rapid changes of mitochondrial Ca^{2+} revealed by specifically targeted recombinant aequorin. *Nature* **358,** 325-7.

162. Rizzuto, R., Brini, M., Murgia, M. and Pozzan, T. (1993) Microdomains with high Ca^{2+} close to IP3-sensitive channels that are sensed by neighboring mitochondria. *Science* **262,** 744-7.

163. Hajnoczky, G., Robb-Gaspers, L. D., Seitz, M. B. and Thomas, A. P. (1995) Decoding of cytosolic calcium oscillations in the mitochondria. *Cell* **82,** 415-24.

164. Lemasters, J. J., Theruvath, T. P., Zhong, Z. and Nieminen, A. L. (2009) Mitochondrial calcium and the permeability transition in cell death. *Biochim Biophys Acta* **1787,** 1395-401.

165. Crompton, M. (1999) The mitochondrial permeability transition pore and its role in cell death. *Biochem J* **341 (Pt 2),** 233-49.

166. Halestrap, A. P., Kerr, P. M., Javadov, S. and Woodfield, K. Y. (1998) Elucidating the molecular mechanism of the permeability transition pore and its role in reperfusion injury of the heart. *Biochim Biophys Acta* **1366,** 79-94.

167. Crompton, M., Virji, S. and Ward, J. M. (1998) Cyclophilin-D binds strongly to complexes of the voltage-dependent anion channel and the adenine nucleotide translocase to form the permeability transition pore. *Eur J Biochem* **258,** 729-35.

168. Weis, M., Kass, G. E. and Orrenius, S. (1994) Further characterization of the events involved in mitochondrial Ca^{2+} release and pore formation by prooxidants. *Biochem Pharmacol* **47,** 2147-56.

169. Korge, P. and Weiss, J. N. (1999) Thapsigargin directly induces the mitochondrial permeability transition. *Eur J Biochem* **265,** 273-80.

170. Akao, Y., Maruyama, W., Shimizu, S., Yi, H., Nakagawa, Y., et al. (2002) Mitochondrial permeability transition mediates apoptosis induced by N-methyl(R)salsolinol, an endogenous neurotoxin, and is inhibited by Bcl-2 and rasagiline, N-propargyl-1(R)-aminoindan. *J Neurochem* **82,** 913-23.

171. Kidd, J. F., Pilkington, M. F., Schell, M. J., Fogarty, K. E., Skepper, J. N., et al. (2002) Paclitaxel affects cytosolic calcium signals by opening the mitochondrial permeability transition pore. *J Biol Chem* **277,** 6504-10.

172. Szabo, I. and Zoratti, M. (1991) The giant channel of the inner mitochondrial membrane is inhibited by cyclosporin A. *J Biol Chem* **266,** 3376-9.

173. Rossi, C. S., Vasington, F. D. and Carafoli, E. (1973) The effect of ruthenium red on the uptake and release of Ca 2+ by mitochondria. *Biochem Biophys Res Commun* **50,** 846-52.

174. Petronilli, V., Penzo, D., Scorrano, L., Bernardi, P. and Di Lisa, F. (2001) The mitochondrial permeability transition, release of cytochrome c and cell death. Correlation with the duration of pore openings in situ. *J Biol Chem* **276,** 12030-4.

175. Szalai, G., Krishnamurthy, R. and Hajnoczky, G. (1999) Apoptosis driven by IP(3)-linked mitochondrial calcium signals. *EMBO J* **18,** 6349-61.

176. Zhu, L., Ling, S., Yu, X. D., Venkatesh, L. K., Subramanian, T., et al. (1999) Modulation of mitochondrial Ca(2+) homeostasis by Bcl-2. *J Biol Chem* **274,** 33267-73.

177. Murphy, A. N., Bredesen, D. E., Cortopassi, G., Wang, E. and Fiskum, G. (1996) Bcl-2 potentiates the maximal calcium uptake capacity of neural cell mitochondria. *Proc Natl Acad Sci U S A* **93,** 9893-8.

178. Ott, M., Robertson, J. D., Gogvadze, V., Zhivotovsky, B. and Orrenius, S. (2002) Cytochrome c release from mitochondria proceeds by a two-step process. *Proc Natl Acad Sci U S A* **99,** 1259-63.

179. Petrosillo, G., Ruggiero, F. M., Pistolese, M. and Paradies, G. (2001) Reactive oxygen species generated from the mitochondrial electron transport chain induce cytochrome c dissociation from beef-heart submitochondrial particles via cardiolipin peroxidation. Possible role in the apoptosis. *FEBS Lett* **509,** 435-8.

180. Grijalba, M. T., Vercesi, A. E. and Schreier, S. (1999) Ca^{2+}-induced increased lipid packing and domain formation in submitochondrial particles. A possible early step in the mechanism of Ca^{2+}-stimulated generation of reactive oxygen species by the respiratory chain. *Biochemistry* **38,** 13279-87.

181. Jayaraman, T. and Marks, A. R. (2000) Calcineurin is downstream of the inositol 1,4,5-trisphosphate receptor in the apoptotic and cell growth pathways. *J Biol Chem* **275,** 6417-20.

182. Robertson, J. D., Orrenius, S. and Zhivotovsky, B. (2000) Review: nuclear events in apoptosis. *J Struct Biol* **129,** 346-58.

183. Liu, X., Li, P., Widlak, P., Zou, H., Luo, X., et al. (1998) The 40-kDa subunit of DNA fragmentation factor induces DNA fragmentation and chromatin condensation during apoptosis. *Proc Natl Acad Sci U S A* **95,** 8461-6.

184. Jones, D. P., McConkey, D. J., Nicotera, P. and Orrenius, S. (1989) Calcium-activated DNA fragmentation in rat liver nuclei. *J Biol Chem* **264,** 6398-403.

185. Kawane, K., Fukuyama, H., Kondoh, G., Takeda, J., Ohsawa, Y., et al. (2001) Requirement of DNase II for definitive erythropoiesis in the mouse fetal liver. *Science* **292,** 1546-9.

186. Gugliucci, A., Ranzato, L., Scorrano, L., Colonna, R., Petronilli, V., et al. (2002) Mitochondria are direct targets of the lipoxygenase inhibitor MK886. A strategy

for cell killing by combined treatment with MK886 and cyclooxygenase inhibitors. *J Biol Chem* **277,** 31789-95.

187. Muthukrishnan, N., Johnson, G. A., Lim, J., Simanek, E. E. and Pellois, J. P. (2012) TAT-mediated photochemical internalization results in cell killing by causing the release of calcium into the cytosol of cells. *Biochim Biophys Acta* **1820,** 1734-43.

188. Ruben, S., Perkins, A., Purcell, R., Joung, K., Sia, R., et al. (1989) Structural and functional characterization of human immunodeficiency virus tat protein. *J Virol* **63,** 1-8.

189. Wilson, P. D., Firestone, R. A. and Lenard, J. (1987) The role of lysosomal enzymes in killing of mammalian cells by the lysosomotropic detergent N-dodecylimidazole. *J Cell Biol* **104,** 1223-9.

190. Colin, F. C. and Schrier, S. L. (1991) Spontaneous endocytosis in human neonatal and adult red blood cells: comparison to drug-induced endocytosis and to receptor-mediated endocytosis. *Am J Hematol* **37,** 34-40.

191. Birchmeier, W., Lanz, J. H., Winterhalter, K. H. and Conrad, M. J. (1979) ATP-induced endocytosis in human erythrocyte ghosts. Characterization of the process and isolation of the endocytosed vesicles. *J Biol Chem* **254,** 9298-304.

192. Jay, A. W. and Rowlands, S. (1975) The stages of osmotic haemolysis. *J Physiol* **252,** 817-32.

193. Sheetz, M. P. and Singer, S. J. (1974) Biological membranes as bilayer couples. A molecular mechanism of drug-erythrocyte interactions. *Proc Natl Acad Sci U S A* **71,** 4457-61.

194. Evans, E. A. (1974) Bending resistance and chemically induced moments in membrane bilayers. *Biophys J* **14,** 923-31.

195. Davies, M. J. (2004) Reactive species formed on proteins exposed to singlet oxygen. *Photochem Photobiol Sci* **3,** 17-25.

196. Reyftmann, J. P., Kohen, E., Morliere, P., Santus, R., Kohen, C., et al. (1986) A microspectrofluorometric study of porphyrin-photosensitized single living cells--I. Membrane alterations. *Photochem Photobiol* **44,** 461-9.

197. Morliere, P., Moysan, A., Santus, R., Huppe, G., Maziere, J. C., et al. (1991) UVA-induced lipid peroxidation in cultured human fibroblasts. *Biochim Biophys Acta* **1084,** 261-8.

198. Ouedraogo, G. D. and Redmond, R. W. (2003) Secondary reactive oxygen species extend the range of photosensitization effects in cells: DNA damage produced via initial membrane photosensitization. *Photochem Photobiol* **77,** 192-203.

199. Eggeling, C., Widengren, J., Rigler, R. and Seidel, C. A. M. (1998) Photobleaching of fluorescent dyes under conditions used for single-molecule detection: Evidence of two-step photolysis. *Analytical Chemistry* **70,** 2651-2659.

200. Geissbuehler, M., Spielmann, T., Formey, A., Marki, I., Leutenegger, M., et al. (2010) Triplet imaging of oxygen consumption during the contraction of a single smooth muscle cell (A7r5). *Biophys J* **98,** 339-349.

201. Blum, A. and Grossweiner, L. I. (1985) Singlet oxygen generation by hematoporphyrin-IX, uroporphyrin-I and hematoporphyrin derivative at 546 nm in phosphate buffer and in the presence of egg phosphatidylcholine liposomes. *Photochem Photobiol* **41,** 27-32.

202. Nakase, I., Tadokoro, A., Kawabata, N., Takeuchi, T., Katoh, H., et al. (2007) Interaction of arginine-rich peptides with membrane-associated proteoglycans is crucial for induction of actin organization and macropinocytosis. *Biochemistry* **46,** 492-501.

203. Tyagi, M., Rusnati, M., Presta, M. and Giacca, M. (2001) Internalization of HIV-1 tat requires cell surface heparan sulfate proteoglycans. *J Biol Chem* **276,** 3254-61.

204. Console, S., Marty, C., Garcia-Echeverria, C., Schwendener, R. and Ballmer-Hofer, K. (2003) Antennapedia and HIV transactivator of transcription (TAT) "protein transduction domains" promote endocytosis of high molecular weight cargo upon binding to cell surface glycosaminoglycans. *J Biol Chem* **278,** 35109-14.

205. Poon, G. M. and Gariepy, J. (2007) Cell-surface proteoglycans as molecular portals for cationic peptide and polymer entry into cells. *Biochem Soc Trans* **35,** 788-93.

206. Drzeniek, Z., Stocker, G., Siebertz, B., Just, U., Schroeder, T., et al. (1999) Heparan sulfate proteoglycan expression is induced during early erythroid differentiation of multipotent hematopoietic stem cells. *Blood* **93,** 2884-97.

207. Vogt, A. M., Winter, G., Wahlgren, M. and Spillmann, D. (2004) Heparan sulphate identified on human erythrocytes: a Plasmodium falciparum receptor. *Biochem J* **381,** 593-7.

208. Ciobanasu, C., Harms, E., Tunnemann, G., Cardoso, M. C. and Kubitscheck, U. (2009) Cell-penetrating HIV1 TAT peptides float on model lipid bilayers. *Biochemistry* **48,** 4728-37.

209. Grossweiner, L. I. (1984) Membrane photosensitization by hematoporphyrin and hematoporphyrin derivative. *Prog Clin Biol Res* **170,** 391-404.

210. Eisenberg, W. C., Taylor, K. and Grossweiner, L. I. (1984) Lysis of egg phosphatidylcholine liposomes by singlet oxygen generated in the gas phase. *Photochem Photobiol* **40,** 55-8.

211. Doleiden, F. H., Fahrenholtz, S. R., Lamola, A. A. and Trozzolo, A. M. (1974) Reactivity of cholesterol and some fatty acids toward singlet oxygen. *Photochem Photobiol* **20,** 519-21.

212. Sevanian, A. and Hochstein, P. (1985) Mechanisms and consequences of lipid peroxidation in biological systems. *Annu Rev Nutr* **5,** 365-90.

213. Herce, H. D., Garcia, A. E., Litt, J., Kane, R. S., Martin, P., et al. (2009) Arginine-rich peptides destabilize the plasma membrane, consistent with a pore formation translocation mechanism of cell-penetrating peptides. *Biophys J* **97,** 1917-25.

214. Dolmans, D. E., Fukumura, D. and Jain, R. K. (2003) Photodynamic therapy for cancer. *Nat Rev Cancer* **3,** 380-7.

215. Brown, S. B., Brown, E. A. and Walker, I. (2004) The present and future role of photodynamic therapy in cancer treatment. *Lancet Oncol* **5,** 497-508.

216. Hong, S. B. and Lee, M. H. (2005) Topical aminolevulinic acid-photodynamic therapy for the treatment of acne vulgaris. *Photodermatol Photoimmunol Photomed* **21,** 322-5.

217. Schmidt-Erfurth, U., Miller, J. W., Sickenberg, M., Laqua, H., Barbazetto, I., et al. (1999) Photodynamic therapy with verteporfin for choroidal neovascularization caused by age-related macular degeneration: results of retreatments in a phase 1 and 2 study. *Arch Ophthalmol* **117,** 1177-87.

218. Bagdonas, S., Kirdaite, G., Streckyte, G., Graziene, V., Leonaviciene, L., et al. (2005) Spectroscopic study of ALA-induced endogenous porphyrins in arthritic knee tissues: targeting rheumatoid arthritis PDT. *Photochem Photobiol Sci* **4,** 497-502.

219. Bourre, L., Giuntini, F., Eggleston, I. M., Mosse, C. A., Macrobert, A. J., et al. (2010) Effective photoinactivation of Gram-positive and Gram-negative bacterial strains using an HIV-1 Tat peptide-porphyrin conjugate. *Photochem Photobiol Sci* **9,** 1613-20.

220. Sehgal, I., Sibrian-Vazquez, M. and Vicente, M. G. (2008) Photoinduced cytotoxicity and biodistribution of prostate cancer cell-targeted porphyrins. *J Med Chem* **51,** 6014-20.

221. Woods, L. K., Morgan, R. T., Quinn, L. A., Moore, G. E., Semple, T. U., et al. (1979) Comparison of four new cell lines from patients with adenocarcinoma of the ovary. *Cancer Res* **39,** 4449-59.

222. Lee, Y. J., Datta, S. and Pellois, J. P. (2008) Real-time fluorescence detection of protein transduction into live cells. *J Am Chem Soc* **130,** 2398-9.

223. Christensen, K. A., Myers, J. T. and Swanson, J. A. (2002) pH-dependent regulation of lysosomal calcium in macrophages. *J Cell Sci* **115,** 599-607.

224. Haller, T., Dietl, P., Deetjen, P. and Volkl, H. (1996) The lysosomal compartment as intracellular calcium store in MDCK cells: a possible involvement in InsP3-mediated Ca^{2+} release. *Cell Calcium* **19,** 157-65.

225. Grynkiewicz, G., Poenie, M. and Tsien, R. Y. (1985) A new generation of Ca^{2+} indicators with greatly improved fluorescence properties. *J Biol Chem* **260,** 3440-50.

226. Gee, K. R., Brown, K. A., Chen, W. N., Bishop-Stewart, J., Gray, D., et al. (2000) Chemical and physiological characterization of fluo-4 Ca(2+)-indicator dyes. *Cell Calcium* **27,** 97-106.

227. Gunter, T. E., Buntinas, L., Sparagna, G., Eliseev, R. and Gunter, K. (2000) Mitochondrial calcium transport: mechanisms and functions. *Cell Calcium* **28,** 285-96.

228. Reed, K. C. and Bygrave, F. L. (1974) The inhibition of mitochondrial calcium transport by lanthanides and ruthenium red. *Biochem J* **140,** 143-55.

229. Fournier, N., Ducet, G. and Crevat, A. (1987) Action of cyclosporine on mitochondrial calcium fluxes. *J Bioenerg Biomembr* **19,** 297-303.

230. Broekemeier, K. M., Dempsey, M. E. and Pfeiffer, D. R. (1989) Cyclosporin A is a potent inhibitor of the inner membrane permeability transition in liver mitochondria. *J Biol Chem* **264,** 7826-30.

231. van der Goot, F. G. and Gruenberg, J. (2006) Intra-endosomal membrane traffic. *Trends Cell Biol* **16,** 514-21.

232. Berg, K., Selbo, P. K., Weyergang, A., Dietze, A., Prasmickaite, L., et al. (2005) Porphyrin-related photosensitizers for cancer imaging and therapeutic applications. *J Microsc* **218,** 133-47.

233. Woodburn, K. W., Fan, Q., Miles, D. R., Kessel, D., Luo, Y., et al. (1997) Localization and efficacy analysis of the phototherapeutic lutetium texaphyrin (PCI-0123) in the murine EMT6 sarcoma model. *Photochem Photobiol* **65,** 410-5.

234. O'Connor, A. E., Gallagher, W. M. and Byrne, A. T. (2009) Porphyrin and nonporphyrin photosensitizers in oncology: preclinical and clinical advances in photodynamic therapy. *Photochem Photobiol* **85,** 1053-74.

235. Kruman, II and Mattson, M. P. (1999) Pivotal role of mitochondrial calcium uptake in neural cell apoptosis and necrosis. *J Neurochem* **72,** 529-40.

236. Lattanzio, F. A., Jr. (1990) The effects of pH and temperature on fluorescent calcium indicators as determined with Chelex-100 and EDTA buffer systems. *Biochem Biophys Res Commun* **171,** 102-8.

237. Bancel, F., Salmon, J. M., Vigo, J., Vo-Dinh, T. and Viallet, P. (1992) Investigation of noncalcium interactions of fura-2 by classical and synchronous fluorescence spectroscopy. *Anal Biochem* **204,** 231-8.

238. Alonso, M. T., Chamero, P., Villalobos, C. and Garcia-Sancho, J. (2003) Fura-2 antagonises calcium-induced calcium release. *Cell Calcium* **33,** 27-35.

239. Nascimento, F. D., Sancey, L., Pereira, A., Rome, C., Oliveira, V., et al. (2012) The natural cell-penetrating peptide crotamine targets tumor tissue in vivo and triggers a lethal calcium-dependent pathway in cultured cells. *Mol Pharm* **9,** 211-21.

240. Varkouhi, A. K., Scholte, M., Storm, G. and Haisma, H. J. (2011) Endosomal escape pathways for delivery of biologicals. *J Control Release* **151,** 220-8.

241. Ebright, Y. W., Chen, Y., Pendergrast, P. S. and Ebright, R. H. (1992) Incorporation of an EDTA-metal complex at a rationally selected site within a protein: application to EDTA-iron DNA affinity cleaving with catabolite gene activator protein (CAP) and Cro. *Biochemistry* **31,** 10664-70.

242. Kraljić, I. and Mohsni, S. E. (1978) A new method for the detection of singlet oxygen in aqueous solutions. *Photochem Photobiol* **28,** 577-581.

243. Kraljić, I. and Mohsni, S. E. (1978) A new method for the detection of singlet oxygen in aqueous solutions. *Photochem Photobiol* **28,** 577-581.

244. Redmond, R. W. and Gamlin, J. N. (1999) A compilation of singlet oxygen yields from biologically relevant molecules. *Photochem Photobiol* **70,** 391-475.

245. Bechinger, B. (2004) Structure and function of membrane-lytic peptides. *Critical Rev in Plant Sci* **23,** 271-292.

246. Jiao, C. Y., Delaroche, D., Burlina, F., Alves, I. D., Chassaing, G., et al. (2009) Translocation and endocytosis for cell-penetrating peptide internalization. *J Biol Chem* **284,** 33957-65.

247. Futaki, S., Goto, S., Suzuki, T., Nakase, I. and Sugiura, Y. (2003) Structural variety of membrane permeable peptides. *Curr Protein Pept Sci* **4,** 87-96.

248. Steck, T. L. (1974) The organization of proteins in the human red blood cell membrane. A review. *J Cell Biol* **62,** 1-19.

249. Kraljic, I. and Mohsni, S. E. (1978) New method for detection of singlet oxygen in aqueous-solutions. *Photochem Photobiol* **28,** 577-581.

250. Evans, W. H. and Hardison, W. G. (1985) Phospholipid, cholesterol, polypeptide and glycoprotein composition of hepatic endosome subfractions. *Biochem J* **232,** 33-6.

251. Guha, S., Rajani, M. and Padh, H. (2007) Identification and characterization of lipids from endosomes purified by electromagnetic chromatography. *Indian J Biochem Biophys* **44,** 443-9.

252. Goyal, G. C., Blum, A. and Grossweiner, L. I. (1983) Photosensitization of liposomal membranes by hematoporphyrin derivative. *Cancer Res.* **43,** 5826-5830.

253. Foote, C. S. (2008) Definition of Type I and Type II photosensitized oxidation. *Photochem Photobiol* **54,** 659.

254. Gandin, E., Lion, Y. and Vandevorst, A. (1983) Quantum yield of singlet oxygen production by xanthene derivatives. *Photochem Photobiol* **37,** 271-278.

255. Mathai, S., Smith, T. A. and Ghiggino, K. P. (2007) Singlet oxygen quantum yields of potential porphyrin-based photosensitisers for photodynamic therapy. *Photochem Photobiol Sci* **6,** 995-1002.

256. DeRosa, M. C. and Crutchley, R. J. (2002) Photosensitized singlet oxygen and its applications. *Coordination Chemistry Reviews* **233-234,** 351-371.

257. Tegos, G. P., Anbe, M., Yang, C., Demidova, T. N., Satti, M., et al. (2006) Protease-stable polycationic photosensitizer conjugates between polyethyleneimine and chlorin(e6) for broad-spectrum antimicrobial photoinactivation. *Antimicrob Agents Chemother* **50,** 1402-10.

258. Natera, J. E., Massada, W. A., Amat-Guerri, F. and García, N. A. (2011) Elementary processes in the eosin-sensitized photooxidation of 3,3′-diaminobenzidine for correlative fluorescence and electron microscopy. *J Photochem Photobiol A: Chemistry* **220,** 25-30.

259. Bors, W., Saran, M. and Michel, C. (1979) Pulse-radiolytic investigations of catechols and catecholamines II. Reactions of Tiron with oxygen radical species. *Biochim Biophys Acta - General Subjects* **582,** 537-542.

260. Tavares, A., Dias, S. R. S., Carvalho, C. M. B., Faustino, M. A. F., Tome, J. P. C., et al. (2011) Mechanisms of photodynamic inactivation of a Gram-negative recombinant bioluminescent bacterium by cationic porphyrins. *Photochemical & Photobiological Sci* **10**.

261. Aizenman, E. (1995) Modulation of N-methyl-d-aspartate receptors by hydroxyl radicals in rat cortical neurons in vitro. *Neurosci Letters* **189,** 57-59.

262. Girotti, A. W. (1998) Lipid hydroperoxide generation, turnover, and effector action in biological systems. *J Lipid Res* **39,** 1529-42.

263. Smith, L. L. and Hill, F. L. (1972) Detection of sterol hydroperoxides on thin-layer chromatoplates by means of the Wurster dyes. *J Chromatogr* **66,** 101-9.

264. Williams, S. L., Kirkpatrick, I. and Worrall, D. R. (2010) Electron transfer reactions in ternary systems on silica gel surfaces: evidence for radical cation diffusion. *Photochem Photobiol Sci* **9,** 937-41.

265. Kriska, T. and Girotti, A. W. (2004) Separation and quantitation of peroxidized phospholipids using high-performance thin-layer chromatography with tetramethyl-p-phenylenediamine detection. *Anal Biochem* **327,** 97-106.

266. Girotti, A. W. (2008) Translocation as a means of disseminating lipid hydroperoxide-induced oxidative damage and effector action. *Free Radical Biology & Medicine* **44,** 956-968.

267. Kobayashi, T., Stang, E., Fang, K. S., de Moerloose, P., Parton, R. G., et al. (1998) A lipid associated with the antiphospholipid syndrome regulates endosome structure and function. *Nature* **392,** 193-7.

268. Chen, B., Jiang, Y., Zeng, S., Yan, J., Li, X., et al. (2010) Endocytic sorting and recycling require membrane phosphatidylserine asymmetry maintained by TAT-1/CHAT-1. *PLoS Genet* **6,** e1001235.

269. Volinsky, R., Cwiklik, L., Jurkiewicz, P., Hof, M., Jungwirth, P., et al. (2011) Oxidized phosphatidylcholines facilitate phospholipid flip-flop in liposomes. *Biophys J* **101,** 1376-84.

270. Tamm, L. K. (1991) Membrane insertion and lateral mobility of synthetic amphiphilic signal peptides in lipid model membranes. *Biochim Biophys Acta* **1071,** 123-48.

271. Peitzsch, R. M. and McLaughlin, S. (1993) Binding of acylated peptides and fatty acids to phospholipid vesicles: pertinence to myristoylated proteins. *Biochemistry* **32,** 10436-43.

272. Ingersoll, C. M. and Strollo, C. M. (2007) Steady state fluorescence anisotropy to investigate flavonoids binding to proteins. *J Chemical Edu* **84,** 1313-1315.

273. Lakovicz, J. R. (2006) *Principles of Fluorescence Spectroscopy.* Springer, Baltimore MD.

274. Srinivasan, D., Muthukrishnan, N., Johnson, G. A., Erazo-Oliveras, A., Lim, J., et al. (2011) Conjugation to the cell-penetrating peptide TAT potentiates the photodynamic effect of carboxytetramethylrhodamine. *PLoS One* **6,** e17732.

275. Umezawa, N., Arakane, K., Ryu, A., Mashiko, S., Hirobe, M., et al. (1997) Participation of reactive oxygen species in phototoxicity induced by quinolone antibacterial agents. *Arch Biochem Biophys* **342,** 275-81.

276. Yamakoshi, Y., Umezawa, N., Ryu, A., Arakane, K., Miyata, N., et al. (2003) Active oxygen species generated from photoexcited fullerene (C60) as potential medicines: O2-* versus 1O2. *J Am Chem Soc* **125,** 12803-9.

277. Choi, H. S., Kim, J. W., Cha, Y. N. and Kim, C. (2006) A quantitative nitroblue tetrazolium assay for determining intracellular superoxide anion production in phagocytic cells. *J Immunoassay Immunochem* **27,** 31-44.

278. Bisby, R. H., Mead, C. and Morgan, C. G. (2000) Active uptake of drugs into photosensitive liposomes and rapid release on UV photolysis. *Photochem Photobiol* **72,** 57-61.

279. Van Bambeke, F., Kerkhofs, A., Schanck, A., Remacle, C., Sonveaux, E., et al. (2000) Biophysical studies and intracellular destabilization of pH-sensitive liposomes. *Lipids* **35,** 213-23.

280. Stewart, J. C. (1980) Colorimetric determination of phospholipids with ammonium ferrothiocyanate. *Anal Biochem* **104,** 10-4.

281. Connor, J., Gillum, K. and Schroit, A. J. (1990) Maintenance of lipid asymmetry in red blood cells and ghosts: effect of divalent cations and serum albumin on the transbilayer distribution of phosphatidylserine. *Biochim Biophys Acta* **1025,** 82-6.

282. Henriques, S. T. and Castanho, M. A. (2004) Consequences of nonlytic membrane perturbation to the translocation of the cell penetrating peptide pep-1 in lipidic vesicles. *Biochemistry* **43,** 9716-24.

283. Hulspas, R., Krijtenburg, P. J., Keij, J. F. and Bauman, J. G. (1993) Avidin-EITC: an alternative to avidin-FITC in confocal scanning laser microscopy. *J Histochem Cytochem* **41,** 1267-72.

284. Sugioka, K. and Nakano, M. (1976) A possible mechanism of the generation of singlet molecular oxygen in nadph-dependent microsomal lipid peroxidation. *Biochim Biophys Acta* **423,** 203-16.

285. Geisow, M. J. and Evans, W. H. (1984) pH in the endosome. Measurements during pinocytosis and receptor-mediated endocytosis. *Exp Cell Res* **150,** 36-46.

286. Seki, S., Flavahan, N. A., Smedira, N. G. and Murray, P. A. (1999) Superoxide anion scavengers restore NO-mediated pulmonary vasodilation after lung transplantation. *Am J Physiol* **276,** H42-6.